DEUTSCHES ELEKTRONEN-SYNCHROTRON DESY

DESY 77/38
June 1977

Physics with Large Electron-Proton Colliding Rings

by

C. H. Llewellyn-Smith
University of Oxford

B. H. Wiik
Deutsches Elektronen-Synchrotron DESY, Hamburg

NOTKESTRASSE 85 · 2 HAMBURG 52

To be sure that your preprints are promptly included in the
HIGH ENERGY PHYSICS INDEX ,
send them to the following address (if possible by air mail) :

DESY
Bibliothek
Notkestraße 85
2 Hamburg 52
Germany

PHYSICS WITH LARGE ELECTRON-PROTON COLLIDING RINGS

C.H.Llewellyn-Smith
Oxford University

B.H.Wiik
DESY

1. INTRODUCTION

During the last few years much effort has been devoted to the study of possible new accelerators and the physics which can be done with them. Large proton synchrotrons [1] and colliding e^+e^- [2], p-p [1,3] and $p\bar{p}$ [4] machines have received the most attention. Whereas the accelerator problems connected with e-p colliding beams have been much discussed [1,5,6], we feel that the physics which can be investigated with very large e-p rings merits further study.

At the time this study began, there seemed to be three natural ways to realize a large electron-proton colliding beam project in Europe:

I. Add an electron ring to an upgraded superconducting ISR which could just conceivably be pushed to 140 GeV, the electron energy being limited to 12 GeV by synchrotron radiation giving a centre-of-mass energy squared $s = 4 \times 12\ \text{GeV} \times 140\ \text{GeV} = 6720\ \text{GeV}^2$.

II. Add a 25 GeV electron ring as an option to the 400 GeV proton storage rings LSR now under study at CERN. This accelerator would be capable of reaching $s = 40'000\ \text{GeV}^2$.

III. Add a superconducting proton ring to PETRA. Such a facility would be capable of reaching s values on the order of $20'000\ \text{GeV}^2$.

During the course of this study, it has been shown [7] that it is possible to install a 25 GeV electron ring in the SPS tunnel and collide the electrons (positrons) in this ring with the protons in the main ring, producing a peak luminosity of $5 \times 10^{31}\ \text{cm}^{-2}\ \text{s}^{-1}$ at a relatively modest cost. A study group is now working on this project and will produce a detailed report on many of its aspects in due course [8]. Meanwhile, this report makes available cross-section estimates which demonstrate the great potential of large e-p rings. In making these estimates we have retained the limiting energies ($s = 6720\ \text{GeV}^2$ - option I and $s = 40'000\ \text{GeV}^2$ - option II) and assumed a luminosity of $10^{32}\ \text{cm}^{-2}\ \text{s}^{-1}$. We furthermore assumed that the electrons will be transversely polarized due to synchrotron radiation and that the transverse polarization can be rotated into a longitudinal polarization by a system of magnets located adjacent to the interaction region. Such magnet systems in conjunction with wiggler magnets make it possible to obtain electrons and positrons of both helicities over a

wide range of energies.

This report is organized as follows:
We first discuss deep inelastic electron scattering $e + p \to e' + X$ which proceeds both by the electromagnetic and the neutral weak current. We then turn to the reaction $e + p \to \nu + X$ which can be used to obtain information on the charged weak current. This is followed by a discussion of experiments using almost real incident photons. In the last section we discuss the production rates and the signatures for the intermediate vector bosons Z^o and $W^\pm$ and for new heavy leptons.

Any new facility should give access to a large unexplored kinematical region with sufficient luminosity to investigate what now seem to be the most profound problems in particle physics. With an electron-proton colliding beam facility one can attack questions such as:

- What is the structure of the weak interaction ?
- What mechanism, if any, will damp the rising weak cross section at high energy ?
- Do the intermediate vector bosons - $W^\pm$ and Z^o - exist ?
- How will the neutral current affect the scattering of charged leptons ?
- Are the weak and electromagnetic interactions different manifestations of a single force ?
- To what extent does the point-like behaviour of hadrons revealed by deep inelastic ν, μ and e experiments persist at higher energies ?
- Do scaling violations have the characteristic features expected if the strong interactions are described by a gauge theory ?
- Are there additional heavy leptons ?
- Are there further hadronic degrees of freedom beyond charm ?

Our investigations show that a large e-p machine could indeed provide answers to most of these questions as well as being an excellent tool for the study of other more mundane topics. The main results, summarized in the order in which they are discussed below in detail, are:

1) Measurement of $e + p \to e + X$ at momentum transfers of thousands of GeV^2 are feasible with large e-p rings. They will probe the nucleon at a new level and a study of scaling violations should reveal the structure of the strong interaction - in particular whether it is described by a gauge theory.

2) $e + p \to e + X$ is expected to be a fertile source for the associated production of new flavours according to current theories in which at large Q^2 and small x the nucleon behaves like the vacuum in $e^+ + e^- \to X$.

3) Study of the final states in electroproduction as a function of Q^2 should prove very interesting, e.g. it allows tests of the short range order concept.

4) The neutral current effects in $e + p \to e + X$ are easy to detect and will provide fundamental new information about the weak interaction. At the higher energy they are sensitive to the existence of the Z^o since they can be studied at $\sqrt{Q^2} \sim 75$ GeV; which is believed to be the mass scale of the neutral weak interaction. These studies could perhaps tell us whether several mass scales are involved, in which cases different effective couplings would exhibit different Q^2 dependence.

5) We find that the reaction $e + p \to \nu + X$ can be identified and measured. Data on this reaction will yield information on the charged weak current at values of $\sqrt{Q^2}$ comparable to or even larger than the natural mass scale of the charged weak current. Measurements with electrons and positrons of both helicities will reveal whether the weak interaction is damped by a single $W^\pm$ or whether a more complicated scheme involving many W's is needed. In particular measurements with e^-_R and e^+_L are very sensitive to additional W's. The charged weak current also permits us to probe for new flavours up to large masses.

6) Big e-p machines can be used to study photoproduction in great detail since they produce millions of events per day in which the photon has $Q^2 \leq M_\pi 2$.

If photons continue to behave like hadrons at high energy this allows the study of all conventional hadronic physics with the advantage that the beam is polarized and the Q^2 variation can be studied. In addition, photon beams are a copious source for the diffractive production of heavy vector mesons and the Primakoff effect gives a large production cross section for

all particles with a sizable coupling to two photons. Photoproduction will also extend the search for vector mesons with hidden new flavours up to a mass of around 40 GeV.

7) The cross sections for $W^{\pm}$ and Z^{o} production are disappointingly small, although both particles will give very clean and unique signatures. However, electron-proton collisions are very favourable for producing new heavy leptons. The large production rate and the fact that the signature is spectacular mean that a machine with $s = 40'000\ GeV^2$ ($6720\ GeV^2$) will be sensitive to new leptons with masses up to 100 GeV (30 GeV) or more.

Obviously, a large e-p machine is capable of answering many very interesting questions in the context of present orthodoxy. Given the large new kinematical region that it will open up, it is likely to reveal an even richer structure than we can imagine at present.

2. DEEP INELASTIC ELECTRON-PROTON SCATTERING

There are three obvious contributions to inclusive electro-production:

1) One photon exchange
2) Z^{o} exchange
3) Higher order photon exchange

Can these contributions be separated ? The leading term due to higher order photon exchange is of order $\pm \alpha/2\pi \ln^2 (Q^2/M^2)$, where the sign depends on the charge of the incident lepton and M might be the parton mass [9]. This term might be as big as 15% for $Q^2 \sim 10^4\ GeV^2$ (higher order terms are expected to be negligible even at these Q^2's). However, it can be removed by averaging the cross sections for electrons and positrons. Furthermore, its Q^2 dependence is quite different from that of the Z^{o} contribution which is expected to grow as Q^2. Measurements of $\sigma(e^{+}p) - \sigma(e^{-}p)$ at low values of Q^2 ($Q^2 \lesssim 100\ GeV^2$) where the weak effects are negligible can therefore be used to determine the size of two photon effects. The two photon effect at large Q^2 can then be obtained from these data using the $\ln^2\left(Q^2/m^2\right)$ dependence. The electromagnetic and weak currents can also be separated by measurements with longitudinally polarized electrons and positrons as discussed below in more detail.

2.1 One Photon Exchange Contribution

2.1.1 Inclusive Electroproduction

First we focus on the information which can be obtained from the one photon exchange diagram by studying the scattered electron only. The kinematic variables are defined in Fig. 1. We frequently employ the dimensionless variables $x = Q^2/2M_p \nu$ and $y = \nu/\nu_{max}$. Fig. 2 shows the longitudinal and transverse momentum of the scattered electron in the collision of a 25 GeV electron with a 400 GeV proton as a function of Q^2 and W.

Quite generally the one photon exchange cross section can be written in terms of two dimensionless structure functions $F_{1,2}(x, Q^2)$:

$$\frac{d\sigma}{dxdy} = \frac{4\pi\alpha^2}{s\,x^2y^2}\left\{(1-y)\,F_2(x, Q^2) + y^2 \times F_1(x, Q^2)\right\}$$

In agreement with existing data, we assume that the contribution of transverse virtual photons dominates the longitudinal contribution, to first approximation, as in spin 1/2 parton models, in which case $2x\,F_1 = F_2$. To get a first idea of possible counting rates we assume scaling i.e. that F_2 is a function of x only, so that the cross section at any energy can be evaluated in terms of existing data. In fact, we used the Barger and Phillips parton model form of the structure functions [10]. +) (We are forced to have recourse to some such model to discuss neutral currents in any case.) The resulting rates per day in bins of dxdy = 0.01 are shown in Figs. 3 and 4 for machines of $12 \times 140\ GeV^2$ and $25 \times 400\ GeV^2$ respectively.

It is clear that the rates are sufficiently large to exploit much of the available kinematic region provided the scattered electrons are identified and measured over a large solid angle. In fact, we see from Figs. 2, 3 and 4 that, because of the point-like nature of the interaction and the asymmetry between the electron and proton energies, the scattered electrons tend to emerge in the laboratory with high energy at rather large angles with respect to their direction of incidence.

+)This model is known to underestimate the cross section at small x even at the Q^2 values for which it is supposed to apply but it is quite satisfactory for orientation.

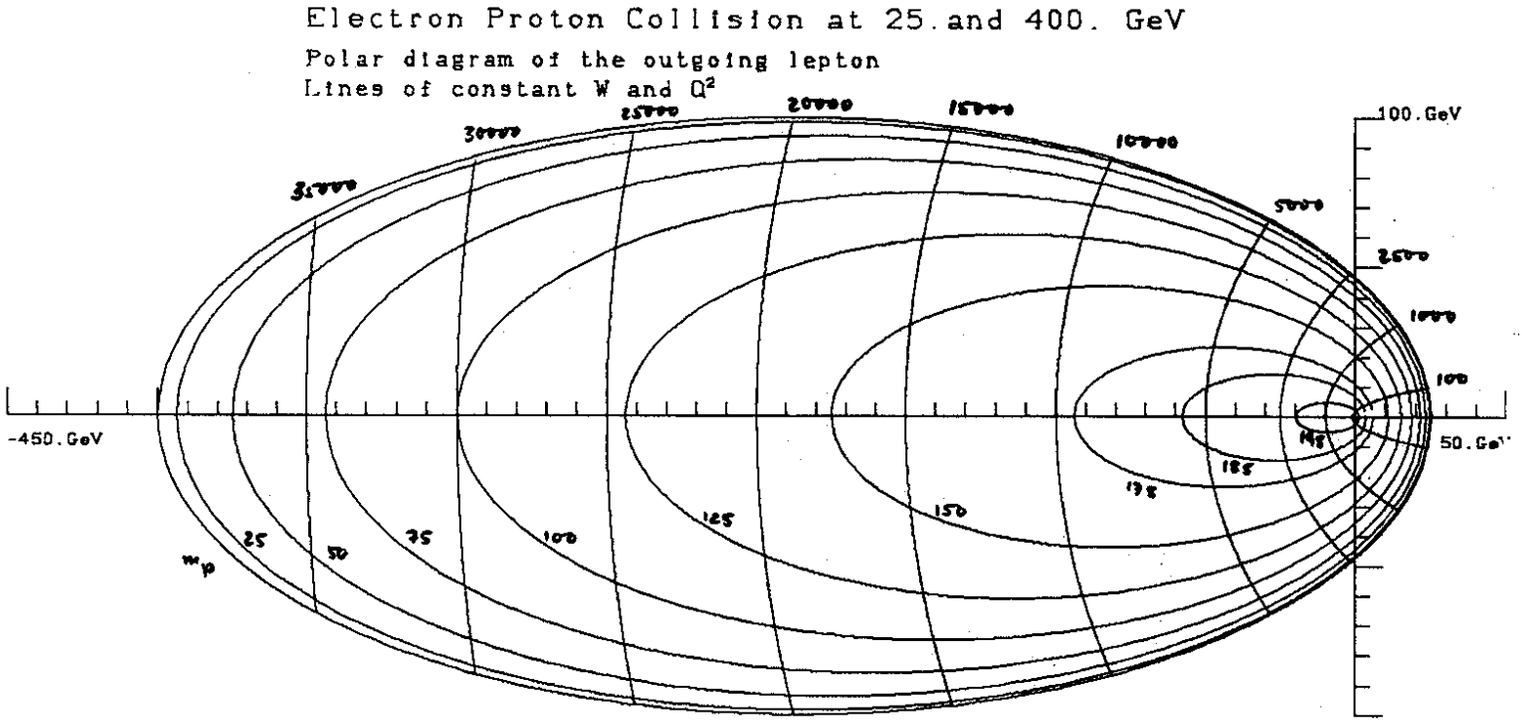

Fig. 2

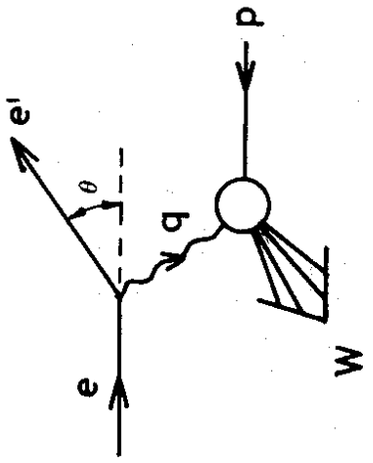

$$Q^2 = -q^2 = -(e-e')^2 = 4EE' \sin^2\theta/2$$

$$\nu = \frac{q \cdot p}{m_p} \approx \frac{2E_p\,(E - E'\cos^2\theta/2)}{m_p}$$

$$W^2 = 2\nu - Q^2 + m_p^2$$

Fig. 1

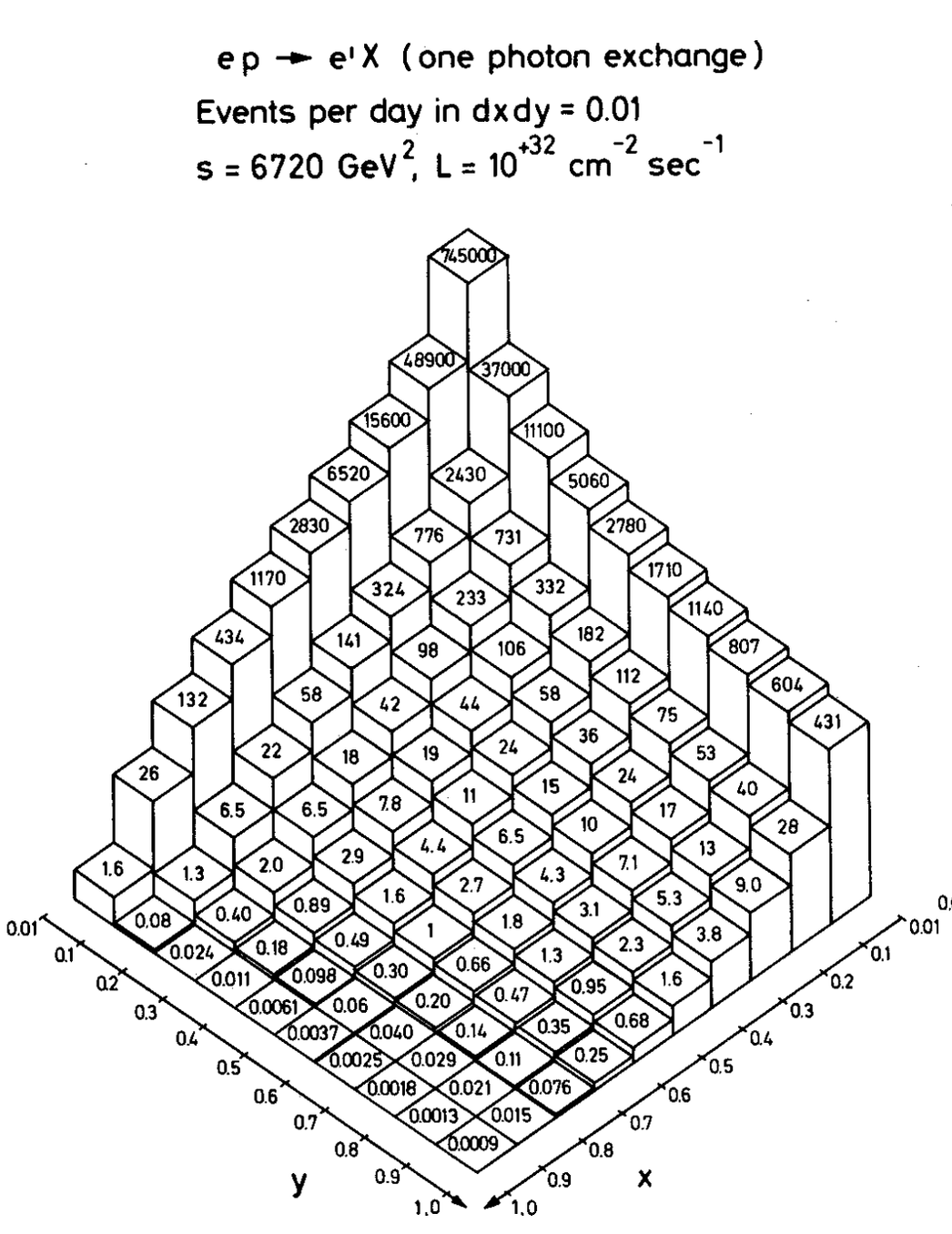
e p → e' X (one photon exchange)
Events per day in dxdy = 0.01
s = 6720 GeV², L = 10^+32 cm^-2 sec^-1
745000
48900
37000
15600
11100
6520
2430
5060
2830
776
731
2780
1170
324
233
332
1710
434
141
98
106
182
1140
132
58
42
44
58
112
807
26
22
18
19
24
36
75
604
6.5
6.5
7.8
11
15
24
53
431
1.6
1.3
2.0
2.9
4.4
6.5
10
17
40
0.08
0.40
0.89
1.6
2.7
4.3
7.1
13
28
0.024
0.18
0.49
1
1.8
3.1
5.3
9.0
0.011
0.098
0.30
0.66
1.3
2.3
3.8
0.0061
0.06
0.20
0.47
0.95
1.6
0.0037
0.040
0.14
0.35
0.68
0.0025
0.029
0.11
0.25
0.0018
0.021
0.076
0.0013
0.015
0.0009
0.01
0.1
0.2
0.3
0.4
0.5
0.6
0.7
0.8
0.9
1.0
y
x

Fig. 3

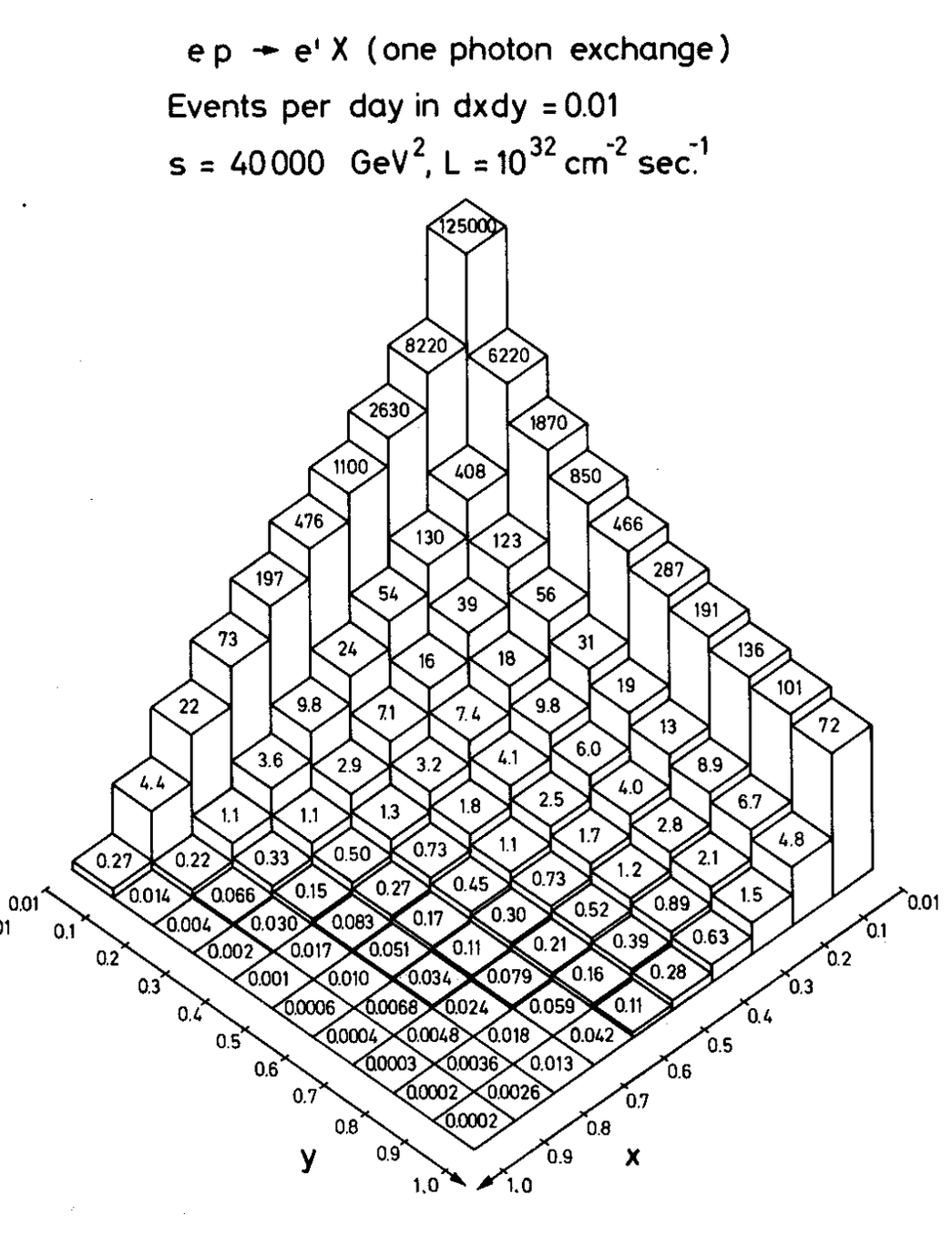
e p → e' X (one photon exchange)
Events per day in dxdy = 0.01
s = 40000 GeV², L = 10^32 cm^-2 sec.^-1
125000
8220
6220
2630
1870
1100
408
850
476
130
123
466
197
54
39
56
287
73
24
16
18
31
191
22
9.8
7.1
7.4
9.8
19
136
4.4
3.6
2.9
3.2
4.1
6.0
13
101
1.1
1.1
1.3
1.8
2.5
4.0
8.9
72
0.27
0.22
0.33
0.50
0.73
1.1
1.7
2.8
6.7
0.014
0.066
0.15
0.27
0.45
0.73
1.2
2.1
4.8
0.004
0.030
0.083
0.17
0.30
0.52
0.89
1.5
0.002
0.017
0.051
0.11
0.21
0.39
0.63
0.001
0.010
0.034
0.079
0.16
0.28
0.0006
0.0068
0.024
0.059
0.11
0.0004
0.0048
0.018
0.042
0.0003
0.0036
0.013
0.0002
0.0026
0.0002
0.01
0.1
0.2
0.3
0.4
0.5
0.6
0.7
0.8
0.9
1.0
y
x

Fig. 4

The rates are also plotted in Figs. 5 and 6 as a function of Q^2 and y. Since it seems feasible to construct a detector [+)] which covers all production angles within 10 mrad (5mrad) of the primary electron (proton) direction and nearly 2π in azimuth, the losses due to the angular cuts are negligible. Similarly, since the scattered electrons tend to have high energies and the background from photoproduction is strongly collimated along the beam directions, the loss due to a cut in electron energy should be quite small.

Tests of scaling can be carried out at fixed s by plotting the cross section as a function of y at constant x. No normalization is needed for this test since all the data are collected simultaneously. However, in order to measure F_1 and F_2 directly, data at different values of s are needed. In this case the luminosity can be obtained from a measurement of elastic electron proton scattering at low Q^2.

New phenomena might be expected to show up as a function of Q^2. It is therefore useful to consider rates as a function of $Q^2 (= xys)$. If scaling holds, the cross section for Q^2 greater than some minimum Q_o^2 scales thus

$$\sigma_{eN} (Q^2 > Q_o^2) = \frac{2.60 \times 10^{-31}}{s(GeV^2)} K^{eN} (Q_o^2/s) \text{ cm}^2$$

where

$$K^{eN} (Q_o^2/s) = \int_{Q^2 > Q_o^2} \int \frac{dxdy}{x^2 y^2} (1 - y + y^2/2) F_2^{eN}(x)$$

assuming $\sigma_L = 0$. Our model calculation of K^{eN} is shown in Figs. 7a and 7b. In Fig. 8 we show the expected number of events per day with $Q^2 > Q_o^2$ according to this model assuming $L = 10^{32}$ cm^{-2} s^{-1}. We see that the large machine might be able to study Q^2 beyond 15'000 GeV^2 and the small machine beyond 3'000 GeV^2.

+) Detailed consideration of the detector layout and background may be found elsewhere [8)].

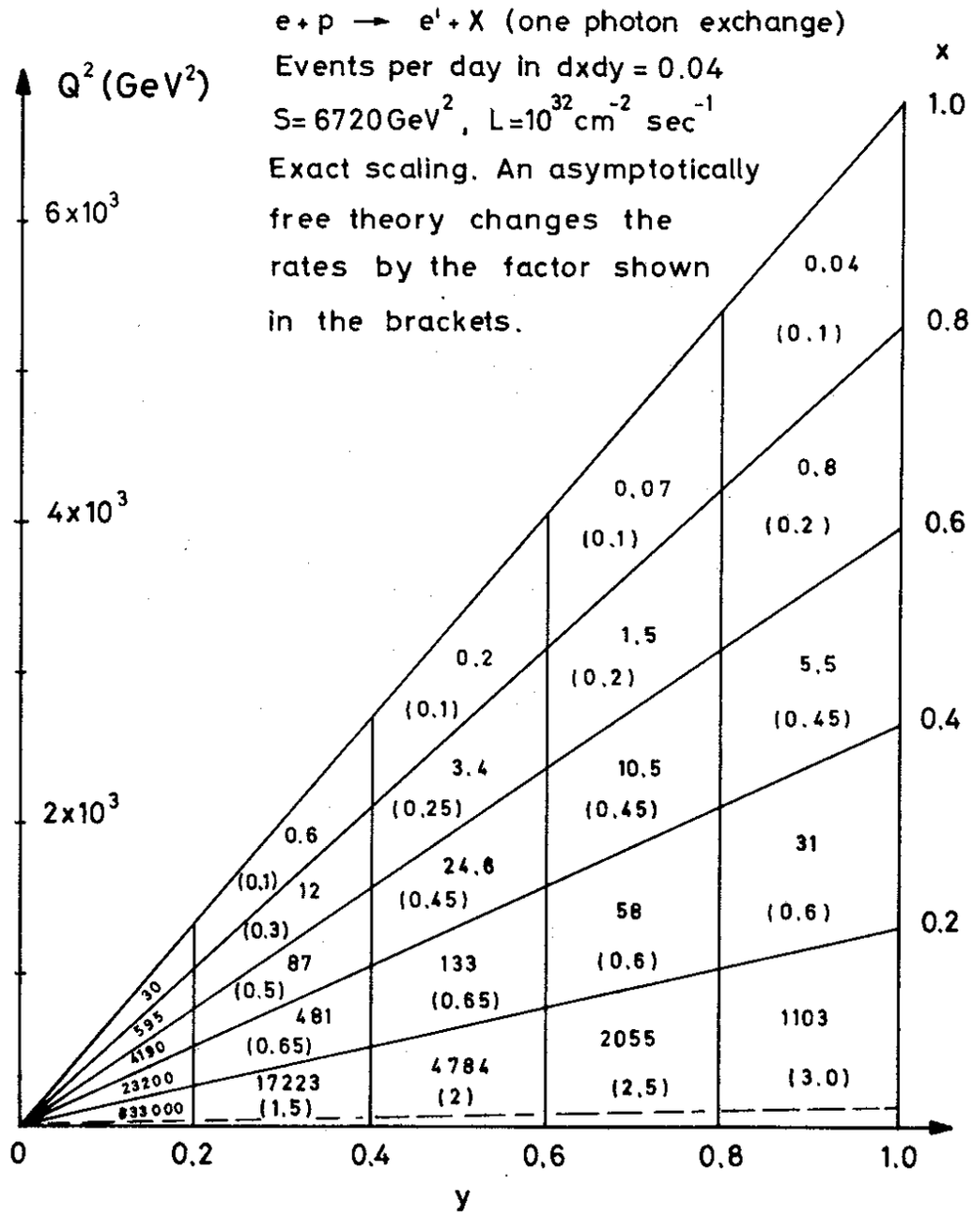

Fig.5

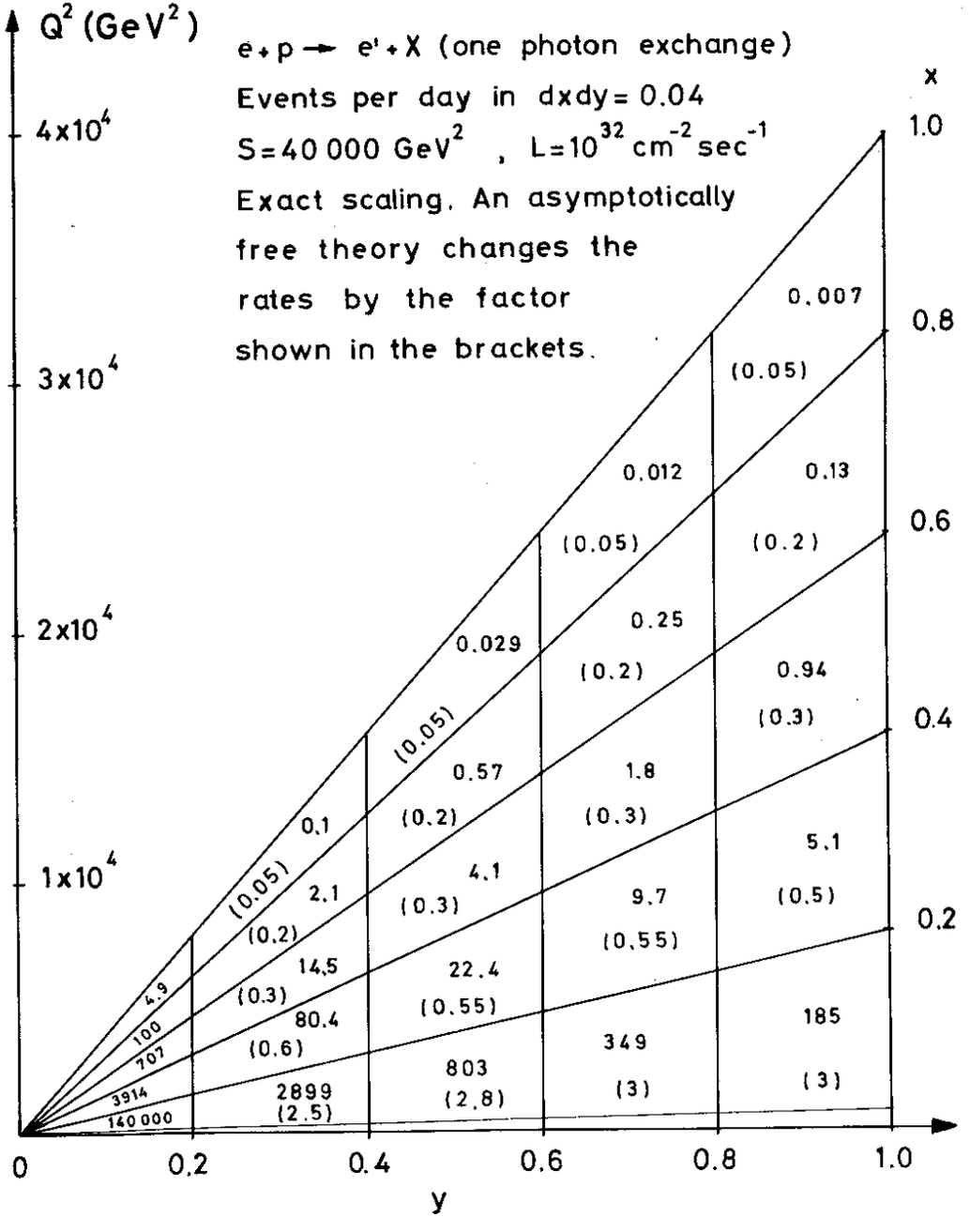
Q^2 (GeV^2)
e + p → e' + X (one photon exchange)
Events per day in dxdy = 0.04
S = 40 000 GeV^2 , L = 10^{32} cm^{-2} sec^{-1}
Exact scaling. An asymptotically free theory changes the rates by the factor shown in the brackets.
4x10^4
3x10^4
2x10^4
1x10^4
x
1.0
0.8
0.6
0.4
0.2
0
0.2
0.4
0.6
0.8
1.0
y
0.007
(0.05)
0.012
(0.05)
0.13
(0.2)
0.029
(0.05)
0.25
(0.2)
0.94
(0.3)
0.1
(0.05)
0.57
(0.2)
1.8
(0.3)
5.1
(0.5)
2.1
(0.2)
4.1
(0.3)
9.7
(0.55)
14.5
(0.3)
22.4
(0.55)
80.4
(0.6)
185
(3)
349
(3)
803
(2.8)
2899
(2.5)
4.9
100
707
3914
140 000

Fig. 6

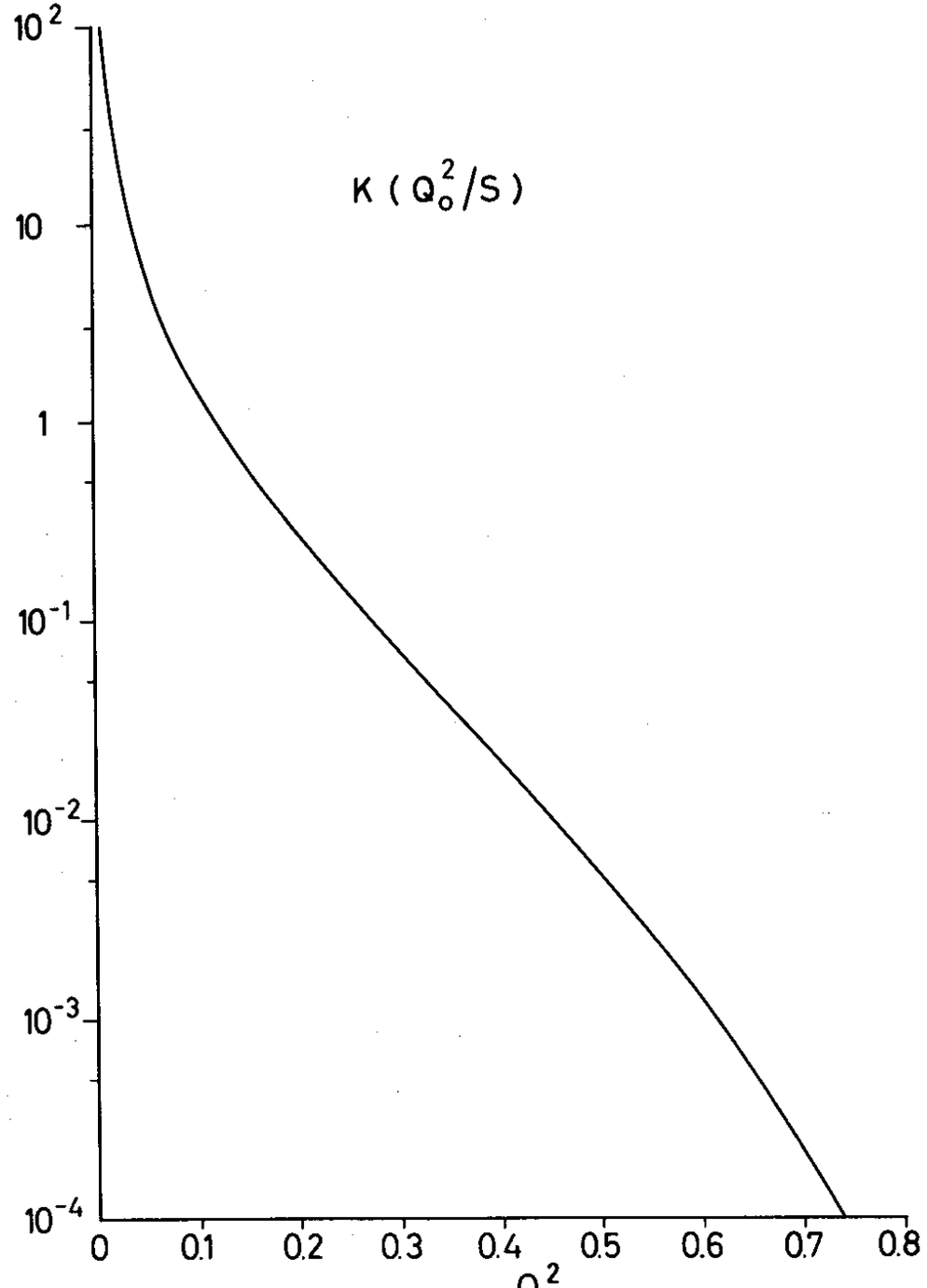
10^2
10
1
10^{-1}
10^{-2}
10^{-3}
10^{-4}
K (Q_o^2/S)
0
0.1
0.2
0.3
0.4
0.5
0.6
0.7
0.8
E = $\frac{Q_o^2}{S}$

Fig. 7a

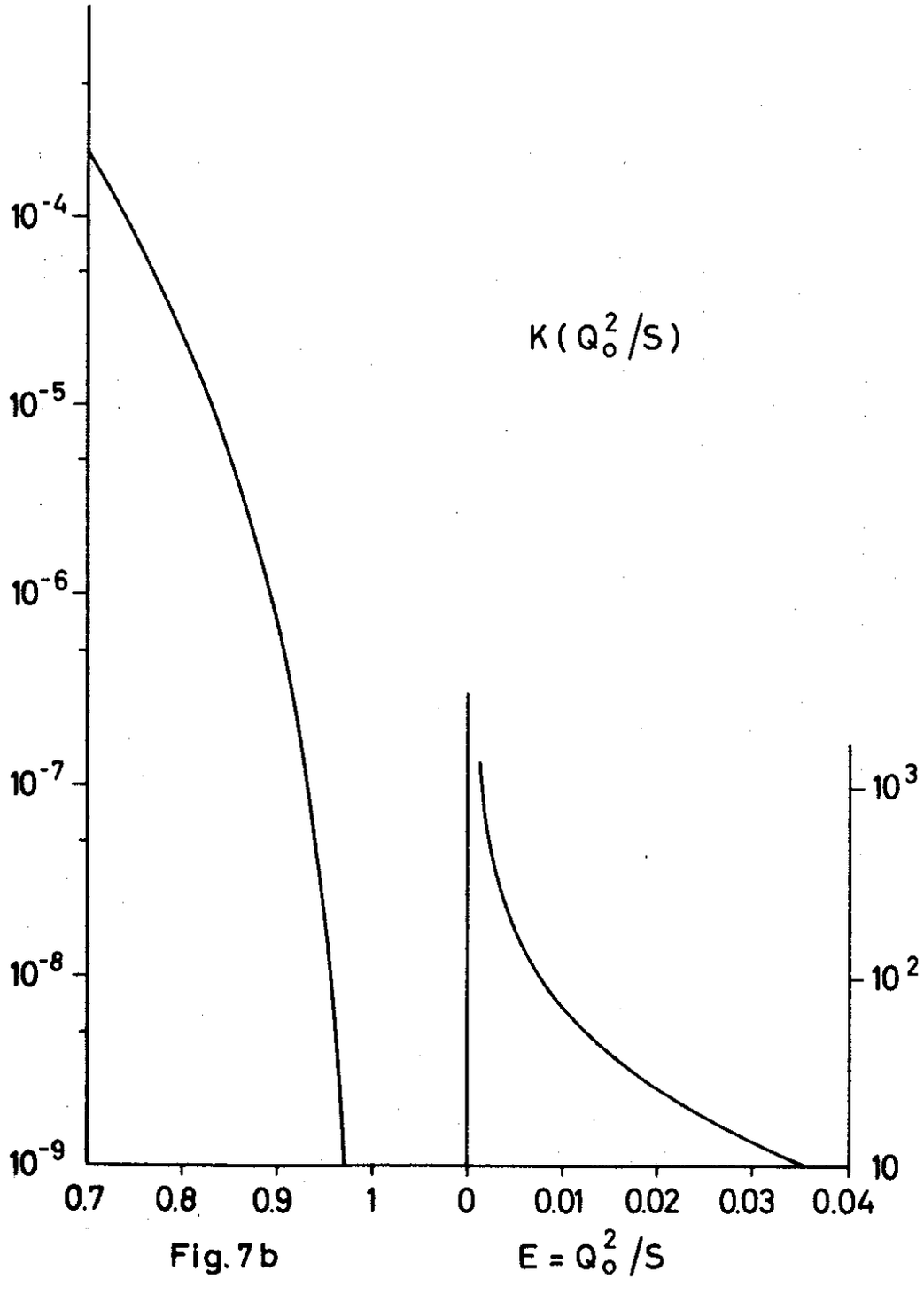
10^{-4}
10^{-5}
10^{-6}
10^{-7}
10^{-8}
10^{-9}
$K(Q_o^2/S)$
10^3
10^2
10
0.7
0.8
0.9
1
0
0.01
0.02
0.03
0.04
$E = Q_o^2/S$

Fig. 7b

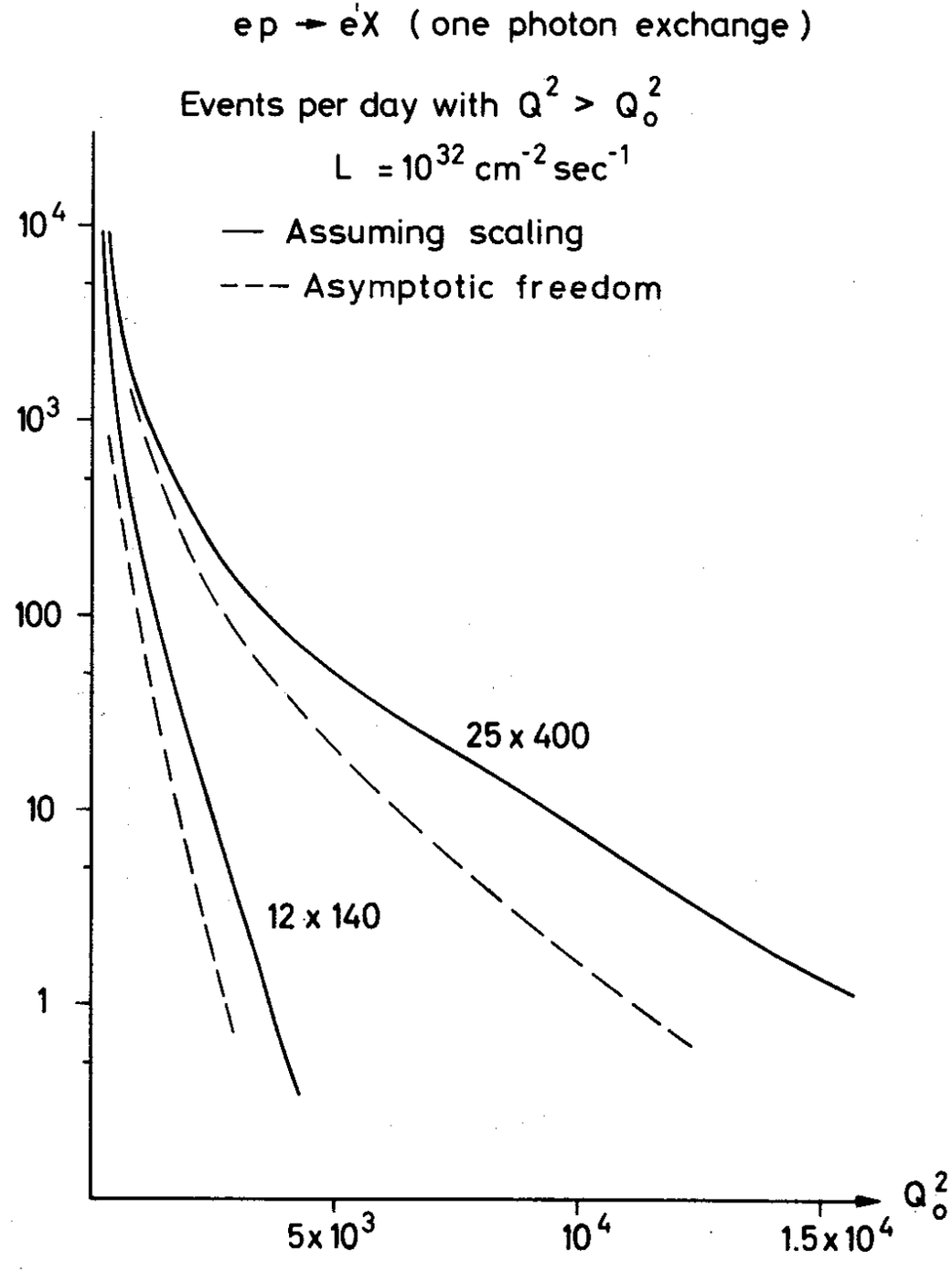
$ep \rightarrow e'X$ (one photon exchange)
Events per day with $Q^2 > Q_o^2$
$L = 10^{32}\,cm^{-2}\,sec^{-1}$
— Assuming scaling
--- Asymptotic freedom
10^4
10^3
100
10
1
25 x 400
12 x 140
5×10^3
10^4
1.5×10^4
Q_o^2

Fig. 8

What do we hope to learn from these measurements ? Large e-p rings will explore an enormous terra incognita where, a priori, almost anything might happen, as is illustrated by the table below which shows the behaviour of some ad-hoc functions normalized to

Table I – Possible Q^2 dependence of F_2

Q^2 (GeV)^2	2	30	100	2000	10^4
$\frac{1}{\sqrt{Q^2}}$ fm	0.15	0.04	0.02	0.004	0.002
$(\frac{\ln 8}{\ln 4Q^2})^{0.43}$	1	0.7	0.63	0.53	0.50
$(\frac{2}{Q^2})^{0.13}$	1	0.7	0.60	0.41	0.33
$(\frac{143}{141+Q^2})^2$	1	0.7	0.35	4.5×10^{-3}	2×10^{-4}
$(\frac{132}{130+Q^2})^2 \cdot \exp\frac{Q^2-2}{1000}$	1	0.7	0.36	0.03	3.7

The logarithmic function is that which controls the area under the valence quark distributions according to asymptotic freedom (assuming 4 flavours and $\alpha_s(1\ \text{GeV}^2) = 1.1$). The other functions are chosen to behave in the same way between $Q^2 = 2\ \text{GeV}^2$ and $30\ \text{GeV}^2$.

---

behave in the same way in the region we know. In fact, the investigation of how Bjorken scaling is broken or whether it becomes exact at very high energy is of fundamental importance for the understanding of the nature of strong interactions because [11]:

1) Exact scaling is impossible if the strong forces are described by a conventional field theory.

2) The form of scale breaking provides basic information about the nature

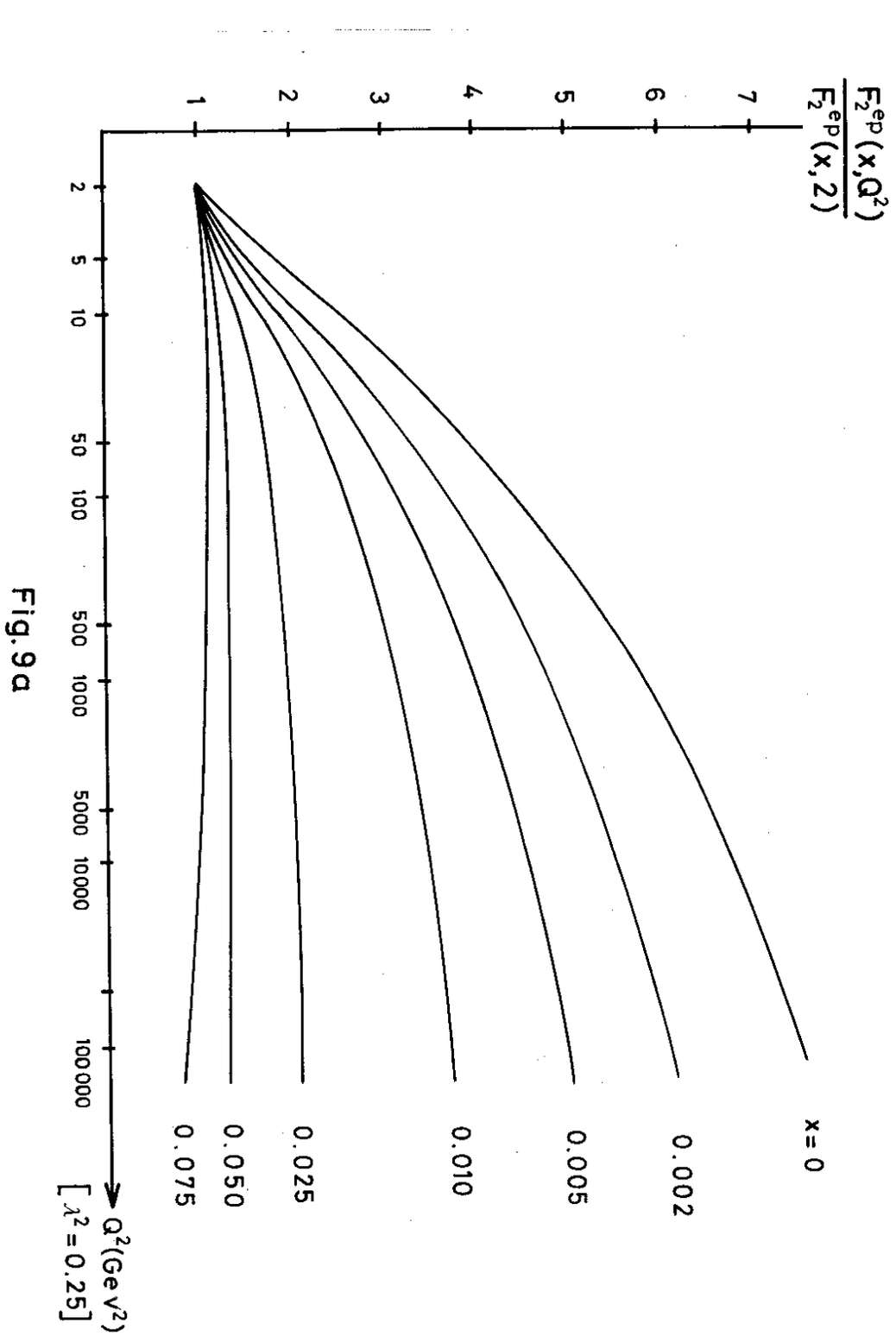

Fig. 9a

of the field theory. If, and only if, it is a gauge theory, the moments of the structure functions ($\int x^n F_2(x, Q^2)\, dx$) will behave as $(\ln Q^2)^{-\gamma_n}$ where the γ_n can be calculated exactly, given the number of flavours. In non-gauge field theories the moments may behave as $(Q^2)^{-a_n}$ where the a_n cannot be calculated.

A detailed discussion of how the behaviour of moments translates into behaviour of structure functions may be found in ref. 12 and references therein.

The scaling violations now observed at FNAL [13] and SLAC [14] are consistent with the pattern anticipated by gauge theories.

The results of one calculation [12] of the scale breaking effects expected in an asymptotically free gauge theory, which is currently the best candidate for a model of the strong interactions, are shown +) in Figs. 5, 6, 8, 9a and 9b. Several important remarks should be made about these predictions:

a) The cross section is substantially increased by scaling violations at small x. The only really radical reduction occurs for $x \gtrsim 0.5$ where the rate is anyway rather small due to the photon propagator.

b) The effects of asymtotic freedom are most prominent at relatively modest Q^2 ($\lesssim$ 1000 GeV^2) after which the structure functions vary extremely slowly (unless the coupling constant is much less than is currently believed). This does <u>not</u> mean that it is sufficient to investigate modest Q^2 to test asymptotic freedom; very large Q^2 is needed to see whether the Q^2 variation indeed slows down dramatically without stopping altogether. If these predictions are correct, it will be very fortunate because it means that scaling violations will be extremely gentle in the region where we hope to see propagator effects in the weak interaction (conversely in the region of more rapid variation, where we hope to parameterize the behaviour, weak effects will not confuse the issue).

c) Although judiciously chosen power of Q^2 can mimic logs over an enormous Q^2 range (see table above), the fact that the expected powers of the log can be calculated for each moment in gauge theories should make it possible to differentiate them from other field theories. In this context, information on neutron structure functions would be especially interesting since they would allow particularly clean tests of asymptotic freedom; it is therefore interesting to note that a machine like the SPS can in principle accelerate

+) An asymtotically free theory changes the rates listed in Figs. 5 and 6 by the factor shown in the bracket. In the lowest x-bin this factor is evaluated for $0.02 < x < 0.2$.

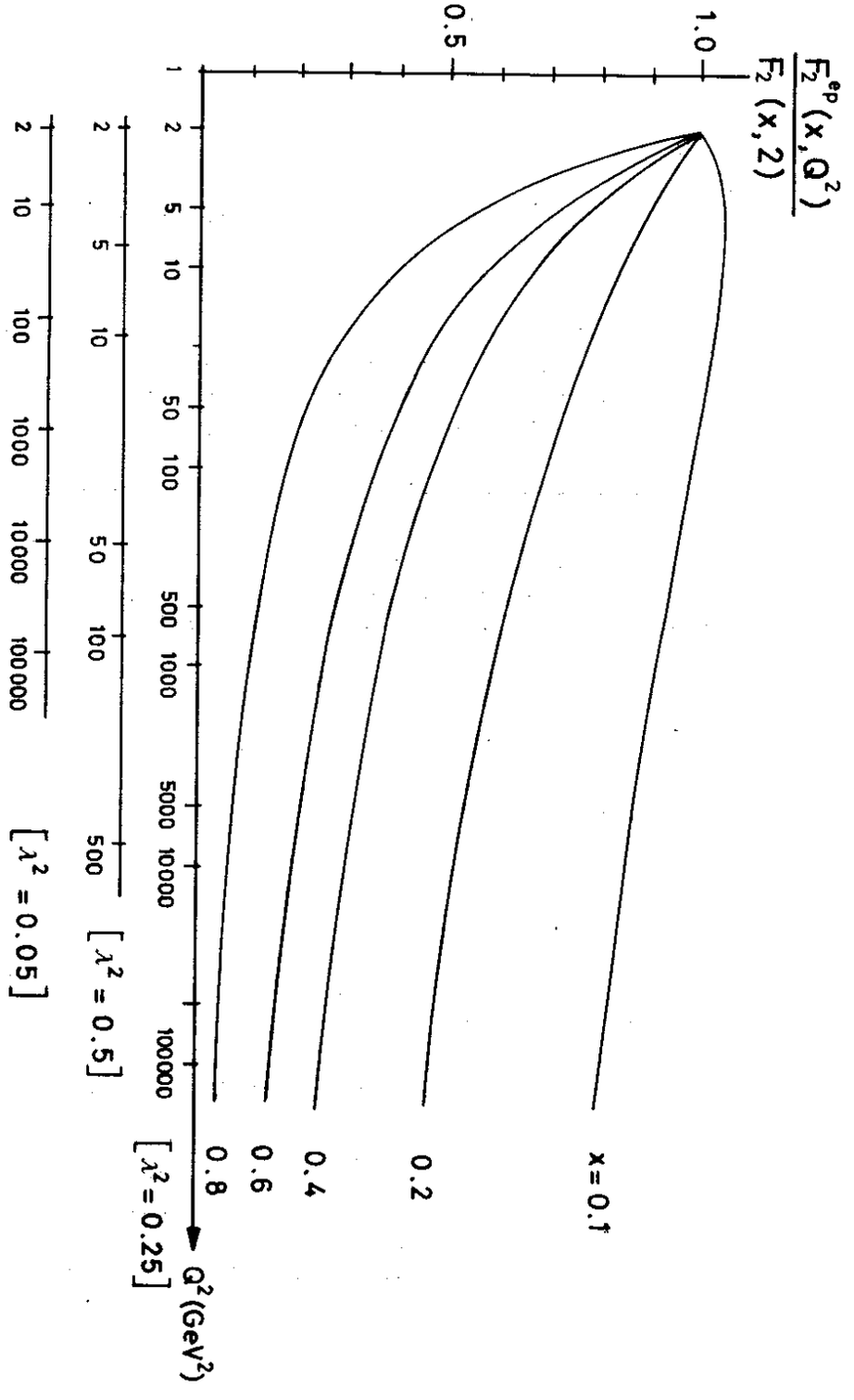

Fig. 9 b

deuterons [15].

3) Large violations of scaling could provide evidence for new phenomena e.g. a large new threshold.

It is clear that a measurement of the inclusive electron cross section will provide basic information about the nature of the strong interaction. More detailed information can be obtained by studying final states in coincidence with the scattered electron.

2. 1. 2 Final States in Electroproduction

All the available data on deep inelastic lepton hadron scattering is well described by a simple parton [5] model (suitably modified to incorporate the effects of asymptotic freedom). In this picture the virtual photon interacts with a light parton which carries a well defined fraction x of the proton's momentum and has a small transverse momentum. After the collision, the struck parton materializes into a jet of hadrons at large angles while the spectator partons give rise to a jet along the initial proton direction. Both jets are well separated from the scattered electron +), as shown schematically in Fig. 10. It is important to realize that the momentum of the "current fragmentation" jet ($x \vec{p}_p + \vec{q}$) is completely determined in terms of the electron variables which determine x and $\vec{q}$; this is shown in Fig. 11. Explicitly the angle θ_H (Fig. 10) at which the hadrons from the current jet emerges is related to ν and Q^2. Lines of constant θ_H in the ν/Q^2 plane are shown in Figs. 12 and 13.

If this picture is valid, then the hadrons belonging to the current jet are well separated from both the scattered electrons and the hadrons in the proton jet and should be readily detected.

+) Extrapolating the present data on deep inelastic lepton scattering to high energies lead to very well defined current jet with most of the hadrons within a narrow cone with a opening angle of a few degrees around the jet axis. A detailed discussion can be found in ref. 8.

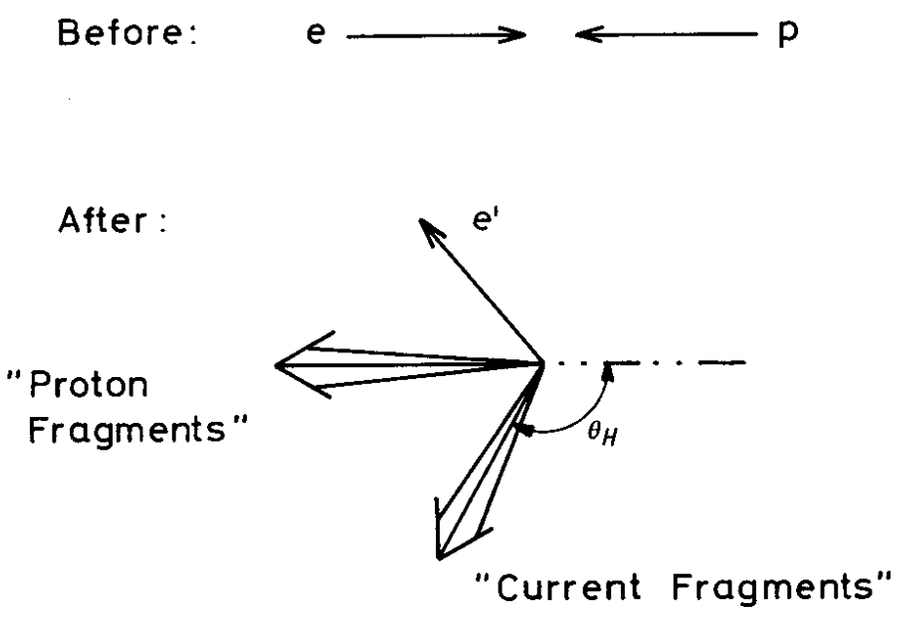

Fig. 10

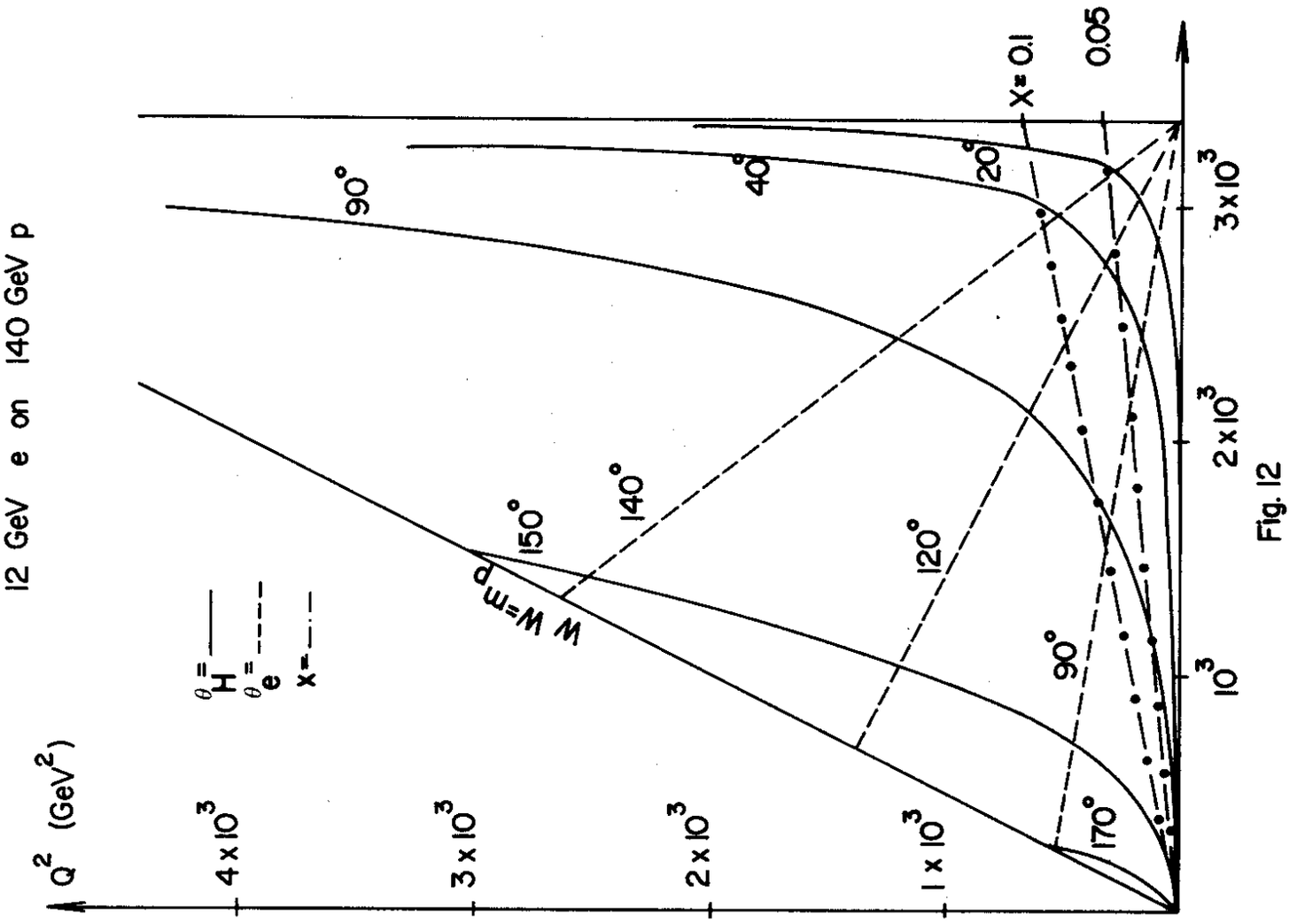
12 GeV e on 140 GeV p
X= 0.1
0.05
90°
40°
20°
3x10^3
2x10^3
10^3
150°
140°
120°
90°
170°
W W=m p
θ H =
θ e =
x =
Q^2 (GeV^2)
4x10^3
3x10^3
2x10^3
1x10^3

Fig. 12

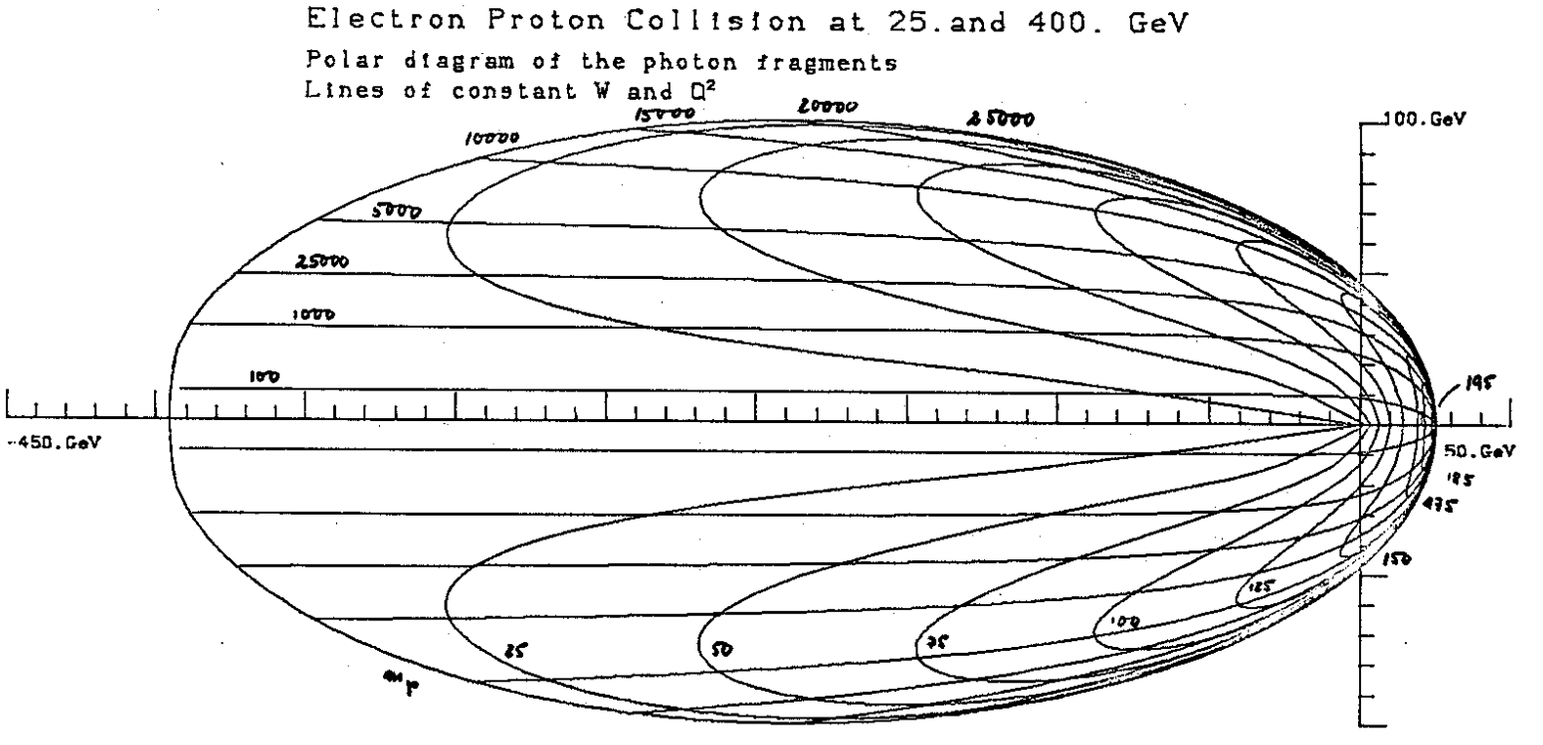
Electron Proton Collision at 25. and 400. GeV
Polar diagram of the photon fragments
Lines of constant W and Q²
100.GeV
-450.GeV
50.GeV
10000
15000
20000
25000
5000
2500
1000
100
195
185
175
150
125
100
75
50
35
25

Fig. 11

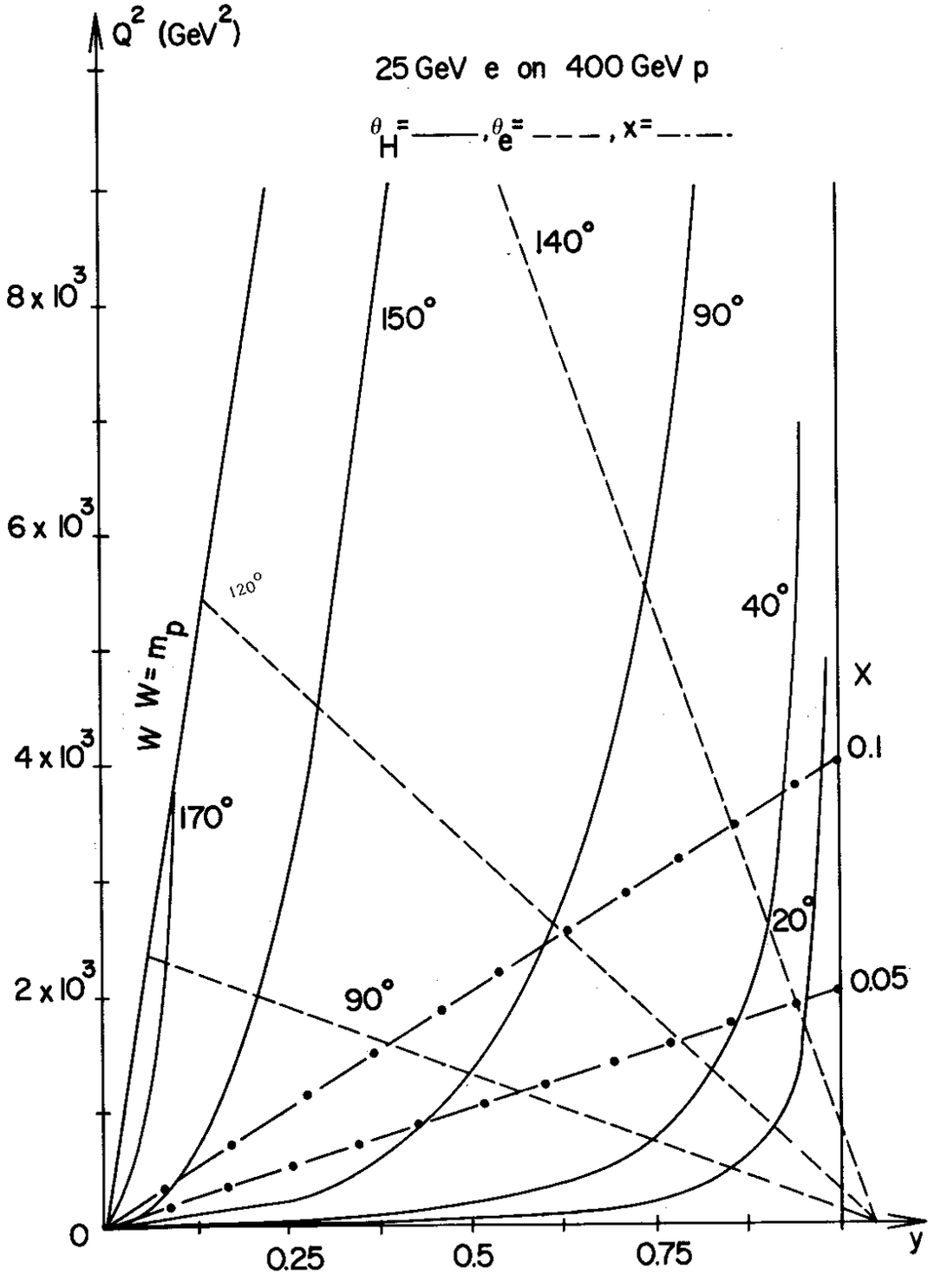

Fig. 13

More model calculations, now under way [8], will show whether it is possible to detect the proton fragments. We now turn to more specific predictions which illustrate the great interest of studying the final states.

2. 1. 3 Inclusive Hadron Electroproduction

The distribution of secondaries in virtual photon scattering provides an opportunity to study the effects of varying the mass of one of the incident particles. In particular it can be used to study the concept of short range order, frequently invoked in discussions of ISR data. Is this concept correct, in which case changes of Q^2 in $\gamma^*(Q^2) + P \to H + \ldots$ would only influence $\langle P_T \rangle_H$, particle composition etc. in the quark fragmentation region ?

Current thinking suggests the possibility of the somewhat richer structure [17], illustrated in Fig. 14, the hadronic plateau being similar to that observed in ISR collisions and the current plateau to the presumed plateau in e^+e^- reactions. To test such ideas it is necessary to be able to vary $\ln(Q^2)$ by a substantial factor in a region where of order 10 units of rapidity are available. A very large machine is needed to do this, as may be seen by calculating the rapidity range as a function of Q^2 or s:

$s(Q^2)$ GeV^2	:	50	100	500	10^3	5×10^3	10^4
$\ln \frac{s(Q^2)}{M_p^2}$	:	4	4.7	6.3	7.0	8.6	9.3

Of course, the whole two-jet picture may break down at high energies. This would be rather surprising since the jet structure is basically a kinematical effect. However, even according to current conventional wisdom corrections to this simple picture are expected. As discussed by Floratos [18], the struck parton may occasionally radiate a hard gluon at a large angle giving rise to events with a three-jet structure at the level of 10^{-4} of the total cross section.

2. 1. 4 Production of New Flavours

Electroproduction is likely to be a very fertile source of associated production of new flavours. An energetic, large Q^2 photon which strikes a quark with a new

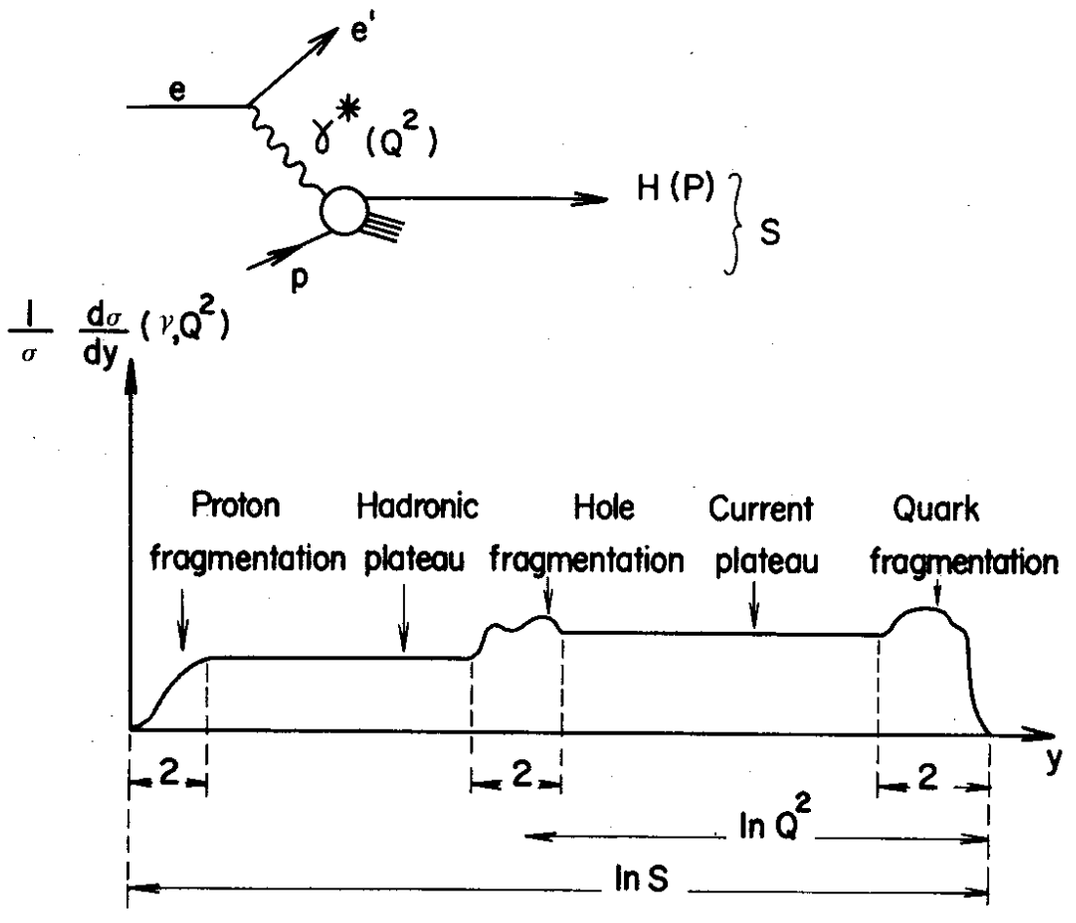

Fig. 14

flavour can displace it to a distant region of rapidity from that occupied by its antiquark partner, so that the system is likely to evolve into a final state containing new flavours. According to asymptotic freedom, the sea of quark-antiquark pairs within the nucleon appears bigger and richer in new flavours with increasing Q^2. At very high Q^2 the low x-region is expected to become democratically populated with a given fraction of the proton's momentum shared equally among all flavours. Asymptotically quarks of a given flavour and their corresponding antiquarks together carry a fraction $3/(3m+16)$ of the proton's momentum, where m is the number of flavours.

Sensible estimates of how the contribution of new heavy quarks grows with Q^2 requires a detailed knowledge of how to make mass corrections to the formulae derived from asymptotic freedom, which is at present a contentious issue. If we ignore these factors and use the asymptotic formulae starting with no quarks of a given flavour, they will grow rapidly as is shown in Fig. 15 for the case of charm [12].

To obtain estimates, we have adopted the following procedure [19]:

1) New flavour distribution are generated using the asymptotic formulae, starting from zero at $Q^2 = 2\ GeV^2$. (In fact, we used the charmed quark distributions in a 4 quark model; new flavours in other models grow in almost the same way.)

2) The contribution to νW_2 is calculated assuming charge 2/3. It is then suppressed by a "Q^2 threshold factor"

$$\frac{Q^2}{Q^2 + (2M_t)^2}$$

suggested by generalized vector dominance, M_t being the quark mass.

3) An absolute cut $Q^2 > Q_{min}^2$ is used where we have chosen $Q_{min}^2 = M_t^2$, $(2M_t)^2$ and $2(2M_t)^2$. (There is also a cut $W > 2M_t$).

The results are shown in Table II. The rates are of course very dependent on the choice of Q_{min}^2. It could be argued that no Q_{min}^2 cut is needed, all mass effects being included in the "Q^2 threshold factor". We feel that this is overly optimistic but that equating Q_{min}^2 with M_t^2 may be justified. In this case reasonable rates can be obtained for $M_t \lesssim 25$ GeV.

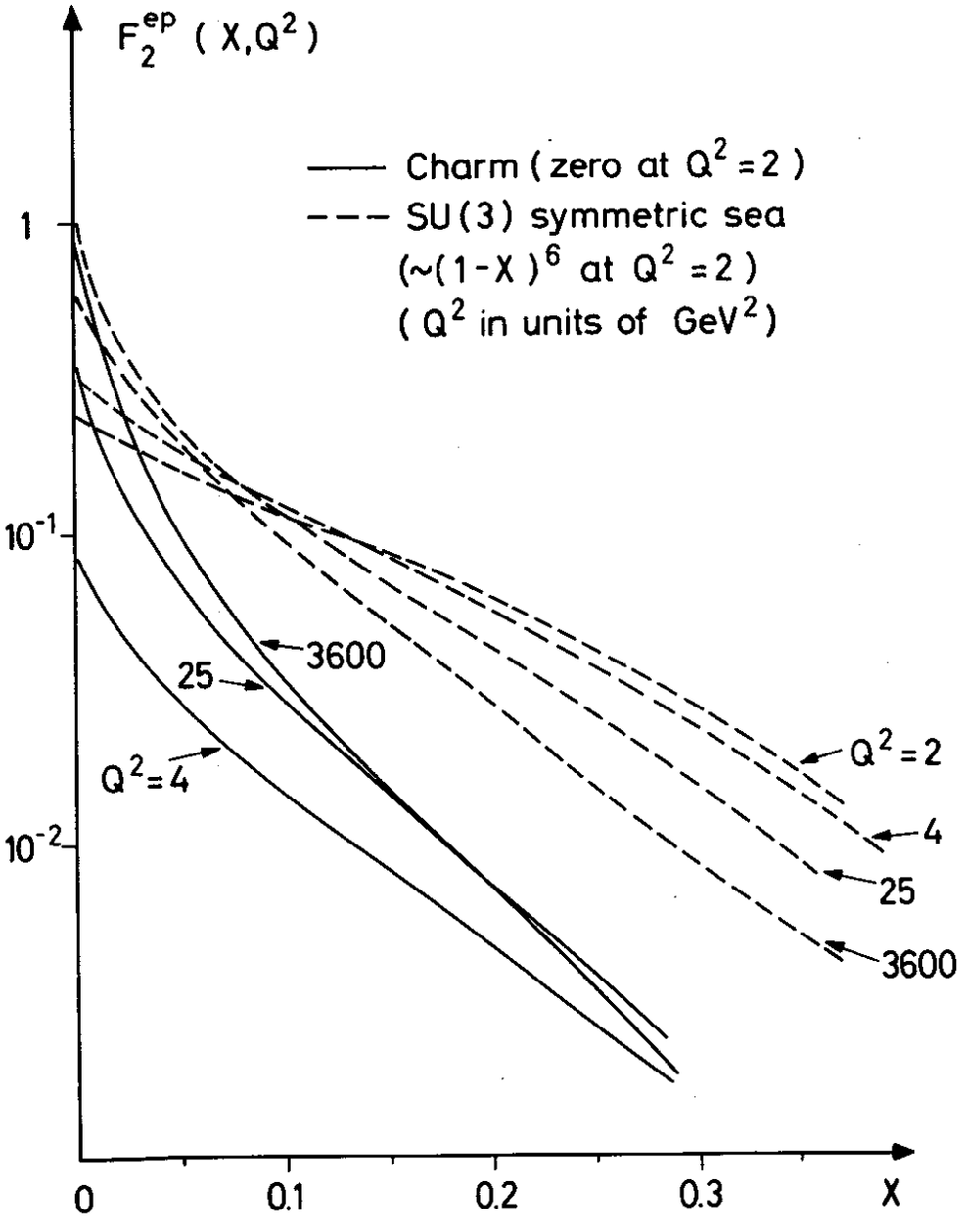

Fig. 15

Can these hadrons with new flavours also be detected ? Since they are produced at small x (x < 0.1), Figs. 12 and 13 show that the scattered electron in general emerges in the forward direction well separated from the direction of the current jet containing one of the new hadrons. There is always a large azimuthal angle between the electron and the current jet. The current jet and hence the new hadron tends to come at large angles ((γ^* + x p) is nearly at rest) with rather low momenta and is hence well separated both from the scattered electron and the proton jet and therefore accessible to analysis. (The second new hadron will probably travel at small angles with respect to the proton beam).

The production of new flavours will give rise to a step in the inclusive electron yield as a function of ν. Note that at low x a large fraction of the proton's momentum is carried by "new" quarks (if they exist) leading to a favourable signal to background ratio. The flavoured hadron will mainly decay into mixed lepton hadron final states or hadrons only. The signature for the first decay is anomalous dilepton production. The purely hadronic decay modes can be identified from effective mass plots obtained by identifying the particles in the final state and measuring their momentum. Such spectroscopy seems feasible since the particles emerge at large angles with low momenta and the ratio of flavoured to non-flavoured events seems to be on the order of several percent.

Table II

Number of e + p → e + X events/day (for L = 10^{32} cm^{-2} s^{-1}) in which scattering occurs on a quark with a new flavour (leading to associated production) for quark charge 2/3 and mass M_t and $Q^2 > Q_{min}^2$ (according to assumptions discussed in the text). The number in brakets () are the numbers of events off the old (u, d, s and c) quarks. Q^2 and s in in units of GeV^2.

	Q_{min}^2	s = 6720	27000	40000
M_t = 5 GeV	25	5500 (10^5)	15000 ($\gtrsim 10^5$)	18000 ($\gtrsim 10^5$)
	100	550 ($\gtrsim 10^4$	3400 (2×10^4)	4600 (2×10^4)
	200	180 (4000)	1200	1600
M_t = 10 GeV	100	370 ($\gtrsim 10^4$)	1600 (2×10^4)	2200 (2×10^4)
	400	17 (900)	220 (5000)	350 (5000)
	800	2.3 (200)	45 (900)	82 (900)
M_t = 25 GeV	625	1.7 (400)	33 (1500)	57 (1500)
	2500	- (2)	1 (70)	2.8 (130)
	5000	-	0.06 (9)	0.3 (20)
M_t = 50 GeV	2500	-	0.2 (70)	0.4 (130)
	10000	-	-	-

2. 2. 1 The Neutral Weak Current Contribution

Inclusive electron scattering at very large Q^2 provides a way to obtain new information about the coupling of the neutral current to leptons and hadrons. The combinations of coupling constants measured in various experiments +) are listed symbolically in Table III.

Table III

Experiment	Quantity measured
$\nu + N \to \nu + X$	$\lvert g_\nu \cdot g_{hadron}\rvert^2$
$\nu + e \to \nu + e$	$\lvert g_\nu \cdot g_e\rvert^2$ $(Q^2 \gtrsim 0)$
$e^+ + e^- \to \mu^+ + \mu^-$	$e^2\lvert g_e \cdot g_\mu\rvert + \ldots$
$e^+ + e^- \to$ hadrons	$e^2\lvert g_e \cdot g_{hadrons}\rvert + \ldots$
$e + p \to e + X$	$e^2\lvert g_e \cdot h_{hadrons}\rvert + \ldots$

Measurements of inclusive electron scattering are needed to untangle the couplings and will therefore not have lost their importance by the time a large e–p machine is built, although $\nu + N \to \nu + X$, $e^+ + e^- \to \mu^+ + \mu^-$ and $e^+ + e^- \to$ hadrons will be much better studied by then.

+) Atomic experiment measure $g_e^A \cdot g_{hadron}^V$ at $Q^2 = 0$. This in no way pre-empts e + p → e + ... experiments since:

a) We wish to know the Q^2 dependence of the couplings.

b) Atomic experiments measure coherent combinations of couplings to constituents; e + p → e + ... measures incoherent combinations.

c) Atomic experiments only measure one V - A combination. Zero parity violation in atomic physics does not imply zero parity violation in e + p → e + X.

d) The uncertainties of interpretation are quite different.

However, the most important information will come from a measurement of the various coupling constants as a function of Q^2. In fact, present machines [+)] are only sensitive to the coupling constants at values of $\sqrt{Q^2}$ which are small compared to the probably mass scale of the weak interactions currently assumed to be around $\sqrt{(75\ \mathrm{GeV})^2}$. How these couplings change with Q^2 is a completely open question. If several mass scales (several Z^o's) are involved different effective couplings could have dramatically different Q^2 dependence.

The weak effects may be parameterized quite generally in terms of three new weak-electromagnetic interference structure functions (F_i^I) and three purely weak structure functions (F_i^{wk}). Assume there is only one Z^o whose coupling to the electron is defined as

$$\sqrt{\frac{G_F M_Z^2}{2}}\ Z^\lambda\ \bar{e}\ \gamma_\lambda \left[g_L \frac{(1-\gamma_5)}{2} + g_R \frac{(1+\gamma_5)}{2} \right] e \quad .$$

In this case the cross section may be written as [20)]

$$\left(\frac{d^2\sigma}{dxdy}\right)_\eta = \left(\frac{d^2\sigma}{dxdy}\right)_{e.m.} \left\{ 1 + \frac{\sqrt{2}\, G_F\, Q^2\, M_Z^2}{e^2(Q^2+M_Z^2)}\ g_\eta\ \frac{(1-y)\,F_2^I + y^2 \times F_1^I - \xi_\eta\, y(1-y/2)}{(1-y)\,F_2 + y^2 \times F_1} \right.$$

$$\left. + \frac{G_F^2\, s}{8\pi}\ \frac{M_Z^4\, g_\eta^2}{(Q^2+M_Z^2)} \left[(1-y)\,F_2^{wk} + y^2 \times F_1^{wk} - \xi_\eta\, y(1-y/2) \times F_3^{wk} \right] \right\} \rho \quad .$$

where η labels the projectile (e^-_L, e^+_R etc.) the F's being the same in all cases. g_η and ξ_η are determined thus

+) Experiments at PETRA and PEP will greatly increase our knowledge of the leptonic couplings of the Z^o but the energy will probably not be quite high enough to detect propagator effects. We assume here that the current is (axial) vector in nature, although this is not yet fully established. S, P and T contributions flip the electron helicity and therefore do not interfere with the electromagnetic term in the approximation $m_e = 0$. Hence they would not be seen at PETRA and PEP but might be revealed by an e-p machine sensitive to the purely weak term.

Particle	Polarization	g_η	ξ_η
e^-	L	g_L	+ 1
e^-	R	g_R	- 1
e^+	R	g_L	- 1
e^+	L	g_R	+ 1

If there are several Z^o's, their contributions to the interference term simply add but the purely weak term is more complex.

Low energy data show that the neutral weak structure functions F_i^{wk} and F_i are of the same order, so the "interference structure functions" F_i^I are likely to be comparable (they are bounded by a Schwartz inequality), and that g_η is probably of order one. This leads to the following order of magnitude estimates (which are borne out in the model calculations described below):

1) Relative to the purely electromagnetic contribution the interference term is likely to be of order $\frac{G M_Z^2 \sqrt{2}\, Q^2}{e^2(Q^2+M_Z^2)} \sim 1.5 \times 10^{-4}\, Q^2(\mathrm{GeV}^2)$ for $Q^2 \ll M_Z^2$. This is illustrated in Fig. 16.

2) The purely weak term is of relative order $\frac{1}{4}\left[\frac{\sqrt{2}\, G\, M_Z^2\, Q^2}{e^2(Q^2+M_Z^2)}\right]^2$.

In the (unlikely) event that $M_Z = \infty$, it will overtake the electromagnetic contribution for $Q^2 \gtrsim 5000\ (\mathrm{GeV})^2$ and this will lead to an apparent large violation of scaling at large Q^2. This is illustrated [+)] in Fig. 17, where we assumed scaling and took

$$\left.\frac{d\sigma^{ep\to e+..}}{dxdy}\right|_{\substack{\text{pure}\\ \text{weak}}} = \frac{G^2 s}{8\pi} F_2^{em}(x)$$

+) This estimate is approximately reproduced by taking the Weinberg model couplings below with $M_Z \to \infty$. Assuming $g_e = g_\nu$, we expect

$$\sigma(e+p \to e+X)\Big|_{\substack{\text{pure}\\ \text{weak}}} = \frac{\sigma(\nu+N \to \nu+X)}{\sigma(\nu+N \to \mu+X)}\ \sigma(e+N \to \nu+X)$$

$$= \frac{1}{2}\ \frac{\sigma(\nu+N\to\nu+X)}{\sigma(\nu+N\to\mu+X)}\ \sigma(e_L+N\to\nu+X) \simeq \frac{1}{10}\ \sigma(e_L+N\to\nu+X)$$

Our estimate of $\sigma(e_L^-+N \to \nu+X)$ below is indeed about 10 times the weak term in Fig. 17.

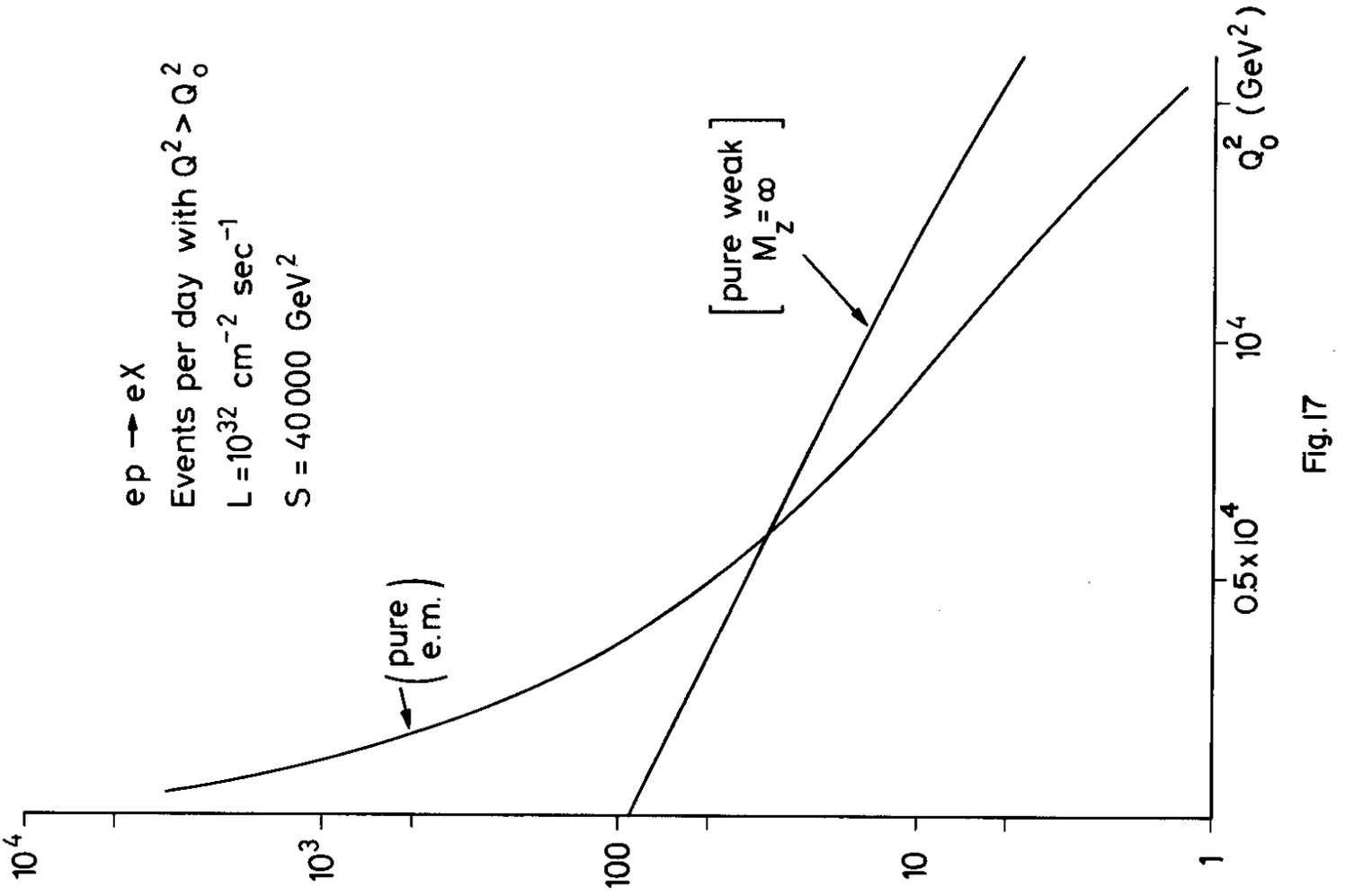

Fig. 17

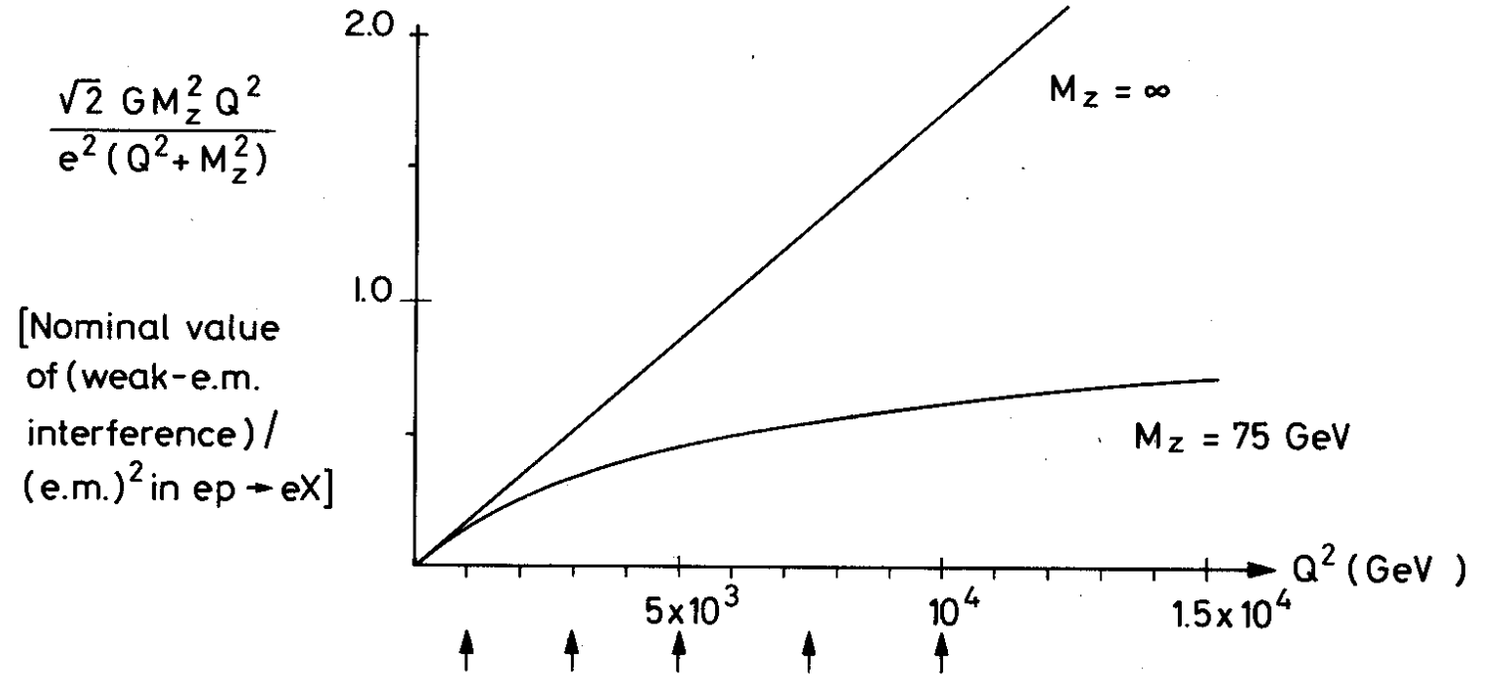

Events per day above Q^2(GeV^2)						
	200	3				12 x 140
	1500	150	50	15	8	25 x 400

Fig. 16

These estimates are of course fraught with uncertainty but they indicate that a big e-p machine may be sensitive to M_Z.

There are three clear signatures for weak effects:

1) Parity violation $\sigma(e_L^-) \neq \sigma(e_R^-)$; $\sigma(e_L^+ \neq \sigma(e_R^+)$ which cannot arise in any other way. This will occur even if $g_L = g_R$, as suggested by recent atomic experiments [+], provided F_3^I and or F_3^{wk} are non-zero, as required if $\sigma(\nu + N \to \nu + N) \neq \sigma(\bar{\nu} + N \to \bar{\nu} + N)$, as seems to be the case. To make this point clear it is instructive to rewrite the terms in curly brackets {} in the general formulae above in the following symbolic way(assuming $\sigma_L = 0$)

$$\{\}_{e_L^-} = 1 + \frac{\chi g_L}{q + \bar{q}} \left[G_V(q + \bar{q}) - f(y)\, G_A(q - \bar{q})\right]$$

$$\{\}_{e_L^+} = 1 + \frac{\chi g_R}{q + \bar{q}} \left[G_V(q + \bar{q}) - f(y)\, G_A(q - \bar{q})\right]$$

$$\{\}_{e_R^-} = 1 + \frac{\chi g_R}{q + \bar{q}} \left[G_V(q + \bar{q}) + f(y)\, G_A(q - \bar{q})\right]$$

$$\{\}_{e_R^+} = 1 + \frac{\chi g_L}{q + \bar{q}} \left[G_V(q + \bar{q}) + f(y)\, G_A(q - \bar{q})\right]$$

where $\chi \sim \frac{G_F M_Z^2 Q^2}{Q^2 + M_Z^2}$ and $f(y) = \frac{1 - (1 - y)^2}{1 + (1 - y)^2}$.

$q(\bar{q})$ represent quark (antiquark) distributions and $G_{V,A}$ represent the Z^o-quark couplings. These formulae show explicitly that parity is violated even if $g_L = g_R$ provided $G_A \neq 0$ since the interference of the γ and Z^o to hadron couplings is parity violating.

2) "C violation" ($\sigma_{e_{L,R}^-} \neq \sigma_{e_{L,R}^+}$) will only occur if $g_L \neq g_R$.
This effect is also produced by two photon contributions but they have a quite different Q^2 dependence and will not grow as large.

+) Note that C and P violating effects will be absent in $e^+ + e^- \to \mu^+ + \mu^-$ if $g_L^\mu = g_R^\mu$ and $g_L^e = g_R^e$.

3) The F_3 terms introduce a characteristic y dependence which is not allowed in the one photon exchange approximation (two photon effects will not produce the same characteristic y dependence); if $\sigma_L = 0$, F_3 adds a $1 - (1 - y)^2$ dependence to the usual $1 + (1 - y)^2$ form.

In principle the sensitivity to the sign and polarization of the beam and the characteristic Q^2 and y dependence can be used to separate the electromagnetic and the different weak contributions. This may actually prove quite easy in practice given constraints on g_L and g_R which will be available from other experiments.

To obtain a quantitative idea of the possible asymmetries we turn to the Weinberg model which we use in conjunction with a very naive valence parton model in which the u and d quarks are assumed to have the same x distribution. This gives [20]

$$\left(\frac{d\sigma}{dxdy}\right)_\eta = \left(\frac{d\sigma}{dxdy}\right)_{e.m.} \left\{ 1 + \frac{\sqrt{2}\, G\, Q^2\, M_Z^2\, g_\eta}{e^2 (Q^2 + M_Z^2)} \left[A^I + \xi_\eta\, B^I\, f(y)\right] + \frac{G^2 Q^4}{2e^4} \frac{M_Z^4\, g_\eta^2}{(Q^2 + M_Z^2)^2} \left[A^{wk} + \xi_\eta\, B^{wk}\, g(y)\right] \right\}$$

In the Weinberg model [+]

$$g_R = 2\sqrt{2} \sin^2\theta_W,\quad g_L = \sqrt{2}\,(-1 + 2 \sin^2\theta_W)$$

$$M_Z = \frac{73\ \text{GeV}}{|\sin 2\theta_W|}$$

+) For a neutron target:
$A^I = \sqrt{2}(2 \sin^2\theta_W - 1)$, $B^I = -\sqrt{2}$
$A^{wk} = 1/2\left[16 \sin^4\theta_W - 16 \sin^2\theta_W + 9\right]$
$B^{wk} = 1/2\left[-16 \sin^2\theta_W + 9\right]$

$$A^I = \frac{\sqrt{2}}{6}\,(12\sin^2\theta_W - 5),\quad B^I = -\frac{5\sqrt{2}}{6}$$

$$A^{wk} = 1/3\left[24\sin^4\theta_W - 20\sin^2\theta_W + 9\right]$$

$$B^{wk} = 1/2\left[-20\sin^2\theta_W + 9\right]$$

With $\sin^2\theta_W = 0.38$ we obtain

$$\left(\frac{d\sigma}{dxdy}\right)_\eta = \left(\frac{d\sigma}{dxdy}\right)_{e.m.}\left\{1 + g_\eta\left(\frac{Q^2}{Q^2+M_Z^2}\right)\left[-0.10 - 1.18\,\xi_\eta\, f(y)\right] + g_\eta^2\left(\frac{Q^2}{Q^2+M_Z^2}\right)^2\left[0.41 + 0.12\,\xi_\eta\, f(y)\right]\right\}$$

where

M_Z = 75.2 GeV

g_R = 1.07 GeV

g_L = -0.34 GeV

Some of the numbers are quite sensitive to the Weinberg angle, e.g. with $\sin^2\theta_W = 0.3$, A^I changes by almost a factor of four. They are of course also very sensitive to the model, e.g. if we suppose that e_R^- belongs to a weak doublet together with a heavy neutral electron, the only change is that now $g_R = g_L = \sqrt{2}(-1 + 2\sin^2\theta_W)$. In this case, there is no parity violation in atomic physics (or in $e^+ + e^- \to \mu^+ + \mu^-$ if $g_R^\mu = g_L^\mu$) but there is in $e + p \to e + X$, although the cross sections differ from those predicted by the standard model. It would be interesting to study other models, especially ones with several Z^o's whose interplay would lead to violent Q^2 dependence in the effective couplings.

In Figs. 18 - 21 we show $\frac{d\sigma(x,y)}{[d\sigma(x,y)]_{e.m.}}$ in two cases:

a) The simple Weinberg model above with $\sin^2\theta_W = 0.38$.

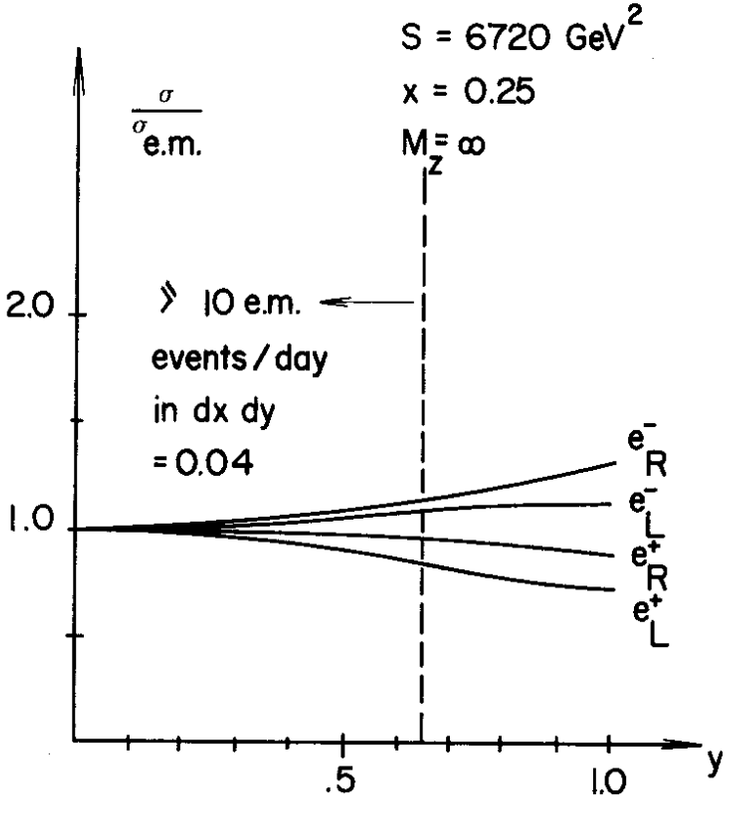

Fig. 18

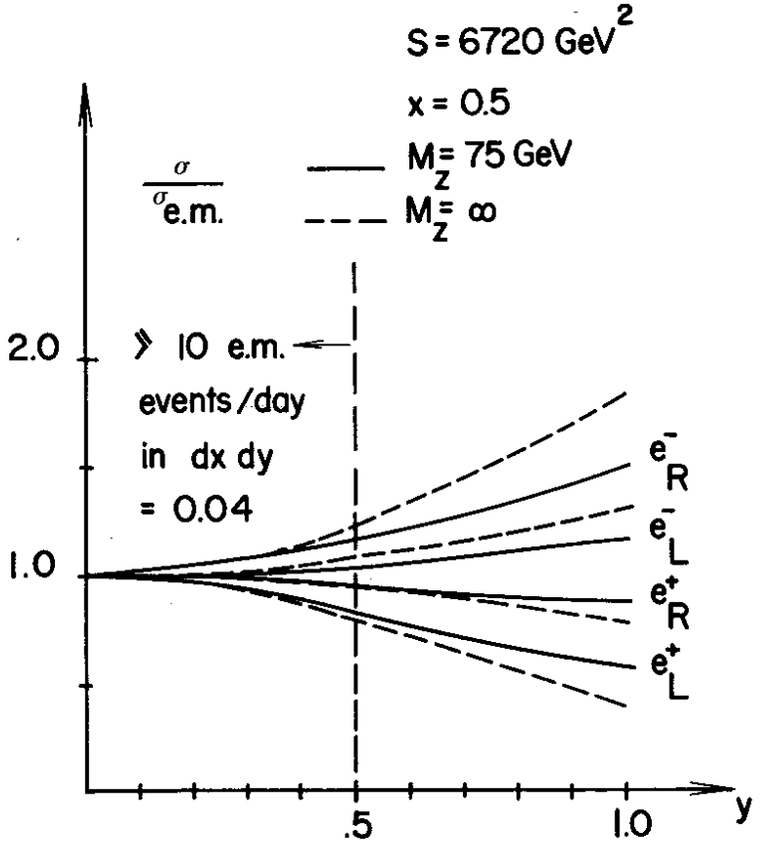
S = 6720 GeV²
x = 0.5
σ / σe.m.
M_Z = 75 GeV
M_Z = ∞
2.0
1.0
» 10 e.m.
events / day
in dx dy
= 0.04
e⁻R
e⁻L
e⁺R
e⁺L
.5
1.0
y

Fig. 19

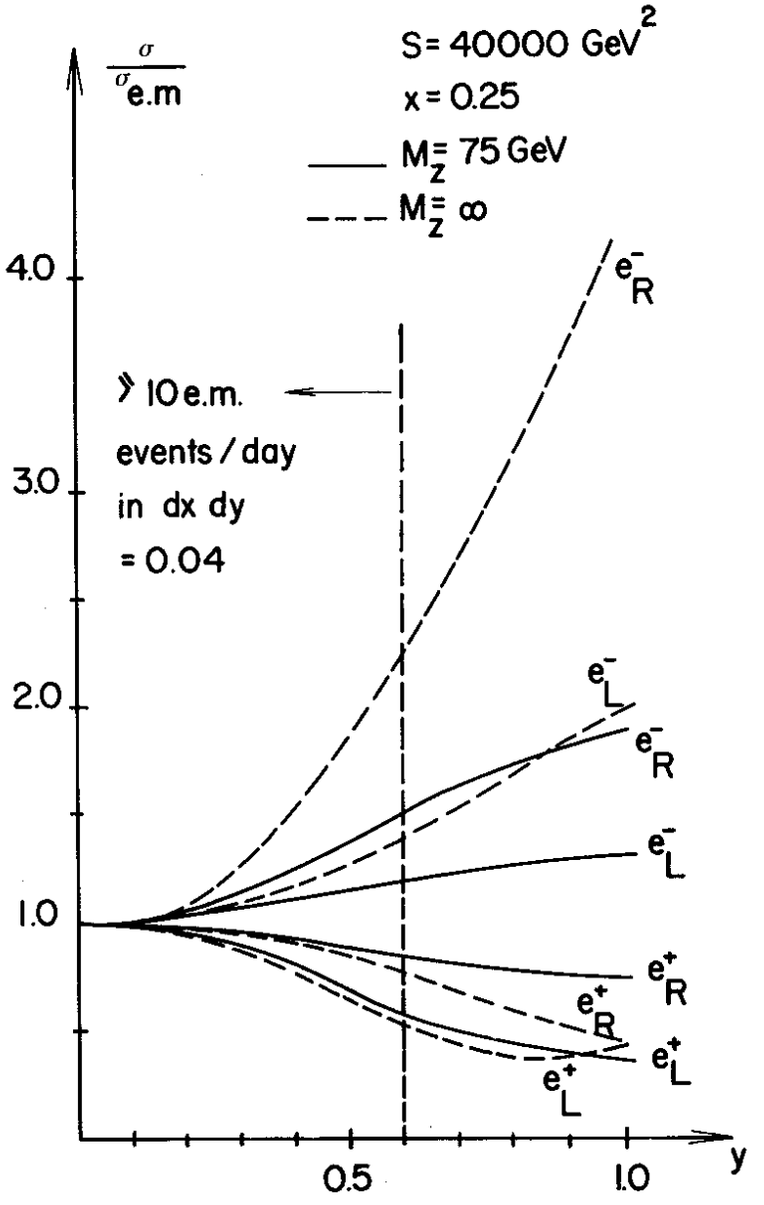
S = 40000 GeV²
x = 0.25
σ / σe.m
M_Z = 75 GeV
M_Z = ∞
4.0
3.0
2.0
1.0
» 10 e.m.
events / day
in dx dy
= 0.04
e⁻R
e⁻L
e⁻R
e⁻L
e⁺R
e⁺R
e⁺L
e⁺L
0.5
1.0
y

Fig. 20

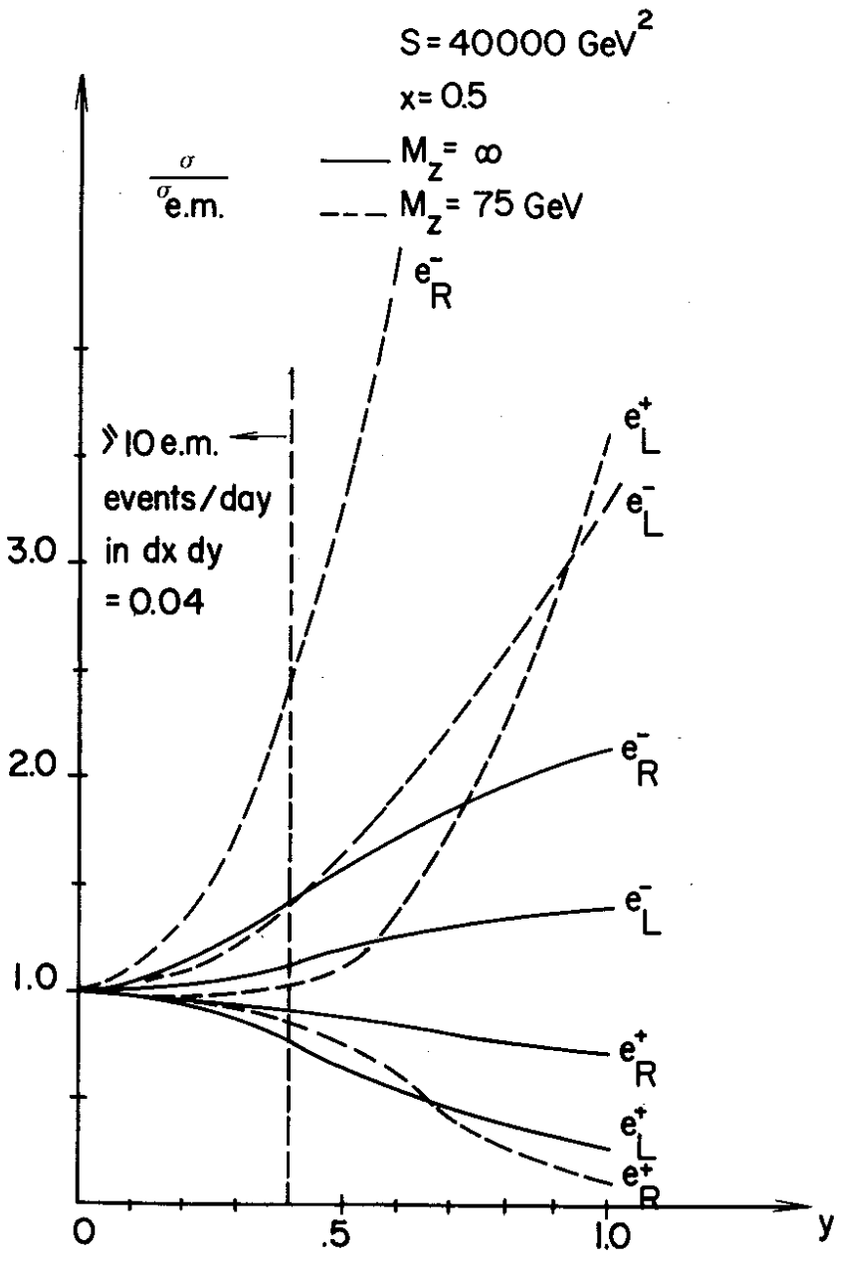

Fig. 21

b) The same model except that $\frac{Q^2}{Q^2 + M_Z^2}$ is replaced by $\frac{Q^2}{(75\ \text{GeV})^2}$; this equivalent to studying a model with $M_Z = \infty$ but the same effective couplings at $Q^2 = 0$.

These figures bear out the order of magnitude estimates above. They show that weak effects should be measurable at either s = 6720 GeV^2 or 40'000 GeV^2 and that a large machine is sensitive to the mass of the Z^o. In fact, the energy dependence of the asymmetries is clearly sensitive to M_Z in a region where there is an appreciable rate. Furthermore, the pattern of asymmetries is seen to be sensitive to M_Z. If M_Z = 75 GeV, the pure weak term is of minor importance in the region where there is an apreciable rate and the pattern does not change greatly, although the values of asymmetries are scaled up, on going from one energy to another. With $M_Z = \infty$, however, the pure weak term dominates at large Q^2 and produces a different pattern of asymmetries than the interference term does.

In fact, it is probably the case that the asymmetries can be measured best at modest Q^2 where they are small but the counting rate is high. Study of the Q^2 dependence can then reveal the Z^o unless substantial reduction of the rates by unexpectedly large scaling violations occurs.

3. MEASUREMENTS OF THE CHARGED WEAK CURRENT

High energy electron-proton colliding rings make it possible to probe the charged weak current at values of Q^2 which are comparable or even larger than the natural mass scale of the weak interaction. Measurements with left-handed electrons and right-handed positrons are sensitive to propagator effects and to new currents (new flavours) at the hadron vertex, whereas measurements with right-handed electrons and left-handed positrons are sensitive to modifications at the lepton vertex (new $W^{\pm}$'s).

In this chapter we first discuss the rates assuming scaling and a pointlike interaction. We then estimate how these rates are modified in an asymptotically free theory and evaluate the sensitivity of the experiments to intermediate vector bosons of mass between 60 GeV and 150 GeV.

The process e + p → ν + X can only be identified and ν and Q^2 determined by observing the hadronic final state X. We first discuss the information which can be obtained from a measurement of the total cross section only and then the additional information which can be gained by measuring the cross section as a function of x and y. Whereas it seems rather straightforward to identify the reaction e + p → ν + X, as discussed below, a measurement of this reaction as a function of x and y is obviously much more difficult.

The weak cross section is given in terms of three structure functions $F_{1,2,3}$ by

$$\frac{d^2\sigma^{ep\to\nu X}}{dxdy} = \frac{G^2 s}{2\pi}\left[(1-y)F_2 + y^2 \times F_1 - y\,(1-\frac{1}{2}y) \times F_3\right]$$

This formula applies to a left-handed electron with $F_i^{\nu n}$ and a right-handed positron with $F_i^{\nu p}$. The cross section for right-handed electrons and left-handed positrons vanishes identically according to the conventional theory of weak interactions.

The distribution of the events in the x y plane were computed assuming a point coupling and scaling with the parton distributions taken from the model of Barger and Phillips [10]. The numbers of events a day in bins dxdy = $(0.1)^2$ are plotted in Figs. 22 – 25 assuming a luminosity of 10^{32} cm^{-2} s^{-1}. The large difference in rate between the electron and the positron cross section arises as follows: $e^+ + p \to \bar{\nu} + X$ loses almost a factor of three because of the assumed dominance of left-handed quarks and another factor of almost 2 because W^+ couples to d quarks and W^- to u quarks and there is nearly twice as many u quarks. However, this may be a large underestimate of the $e_R^+ + p$ cross section relative to the $e_L^- + p$ cross section; asymptotic freedom tends to equalize the various quarks species and new flavours with right-handed couplings will lead to a large increase in the cross section for $e_R^+ + p$.

Assuming scaling, the cross section for events with Q^2 above a certain limit Q_o^2 can be written as

$$\sigma(Q^2 > Q_o^2)_{e_L^-, e_R^+} = 0.80 \cdot s(\mathrm{GeV}^2) \cdot H_{\pm}\,(Q_o^2/s) \cdot 10^{-38}\ \mathrm{cm}^2$$

with

$e_L^- p \to \nu X$

Events per day in dxdy = 0.01

$S = 6720\ \mathrm{GeV}^2$, $L = 10^{32}\ \mathrm{cm}^{-2}\ \mathrm{sec}^{-1}$

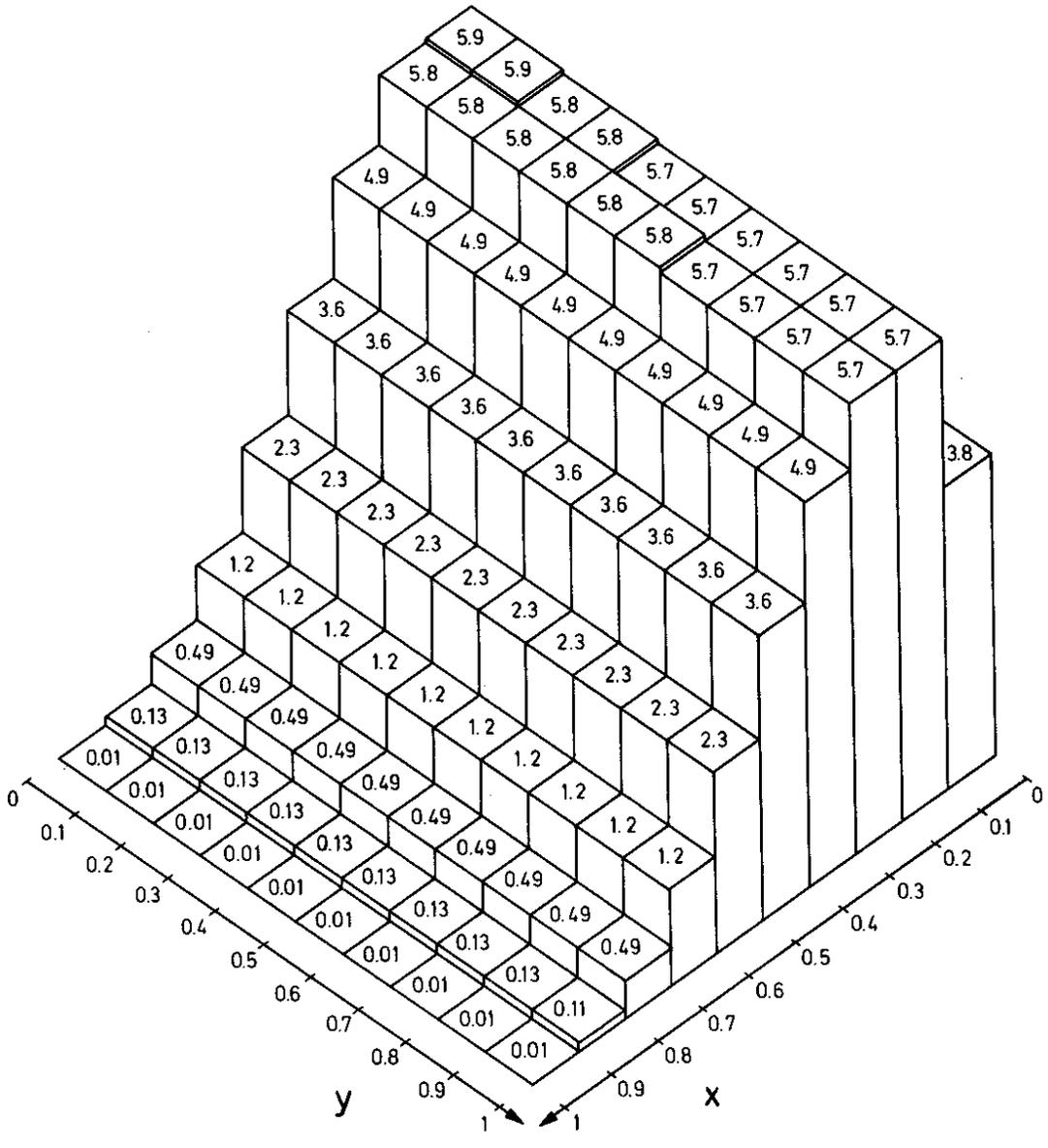

Fig. 22

$e^+ p \to \bar{\nu} X$

Events per day in $dx\,dy = 0.01$

$S = 6720\ GeV^2$, $L = 10^{32}\ cm^{-2}\,sec^{-1}$

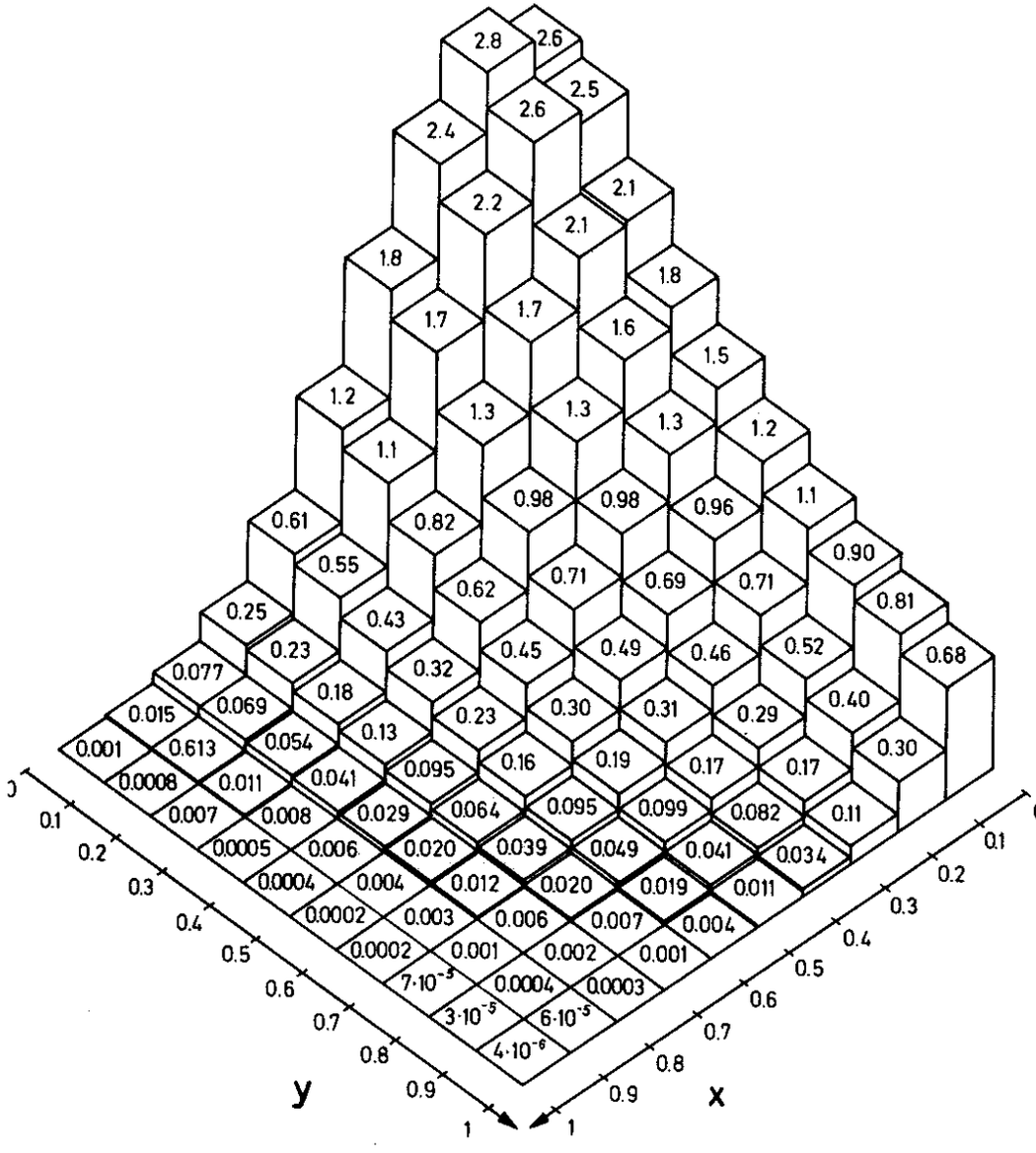

Fig. 23

$e_L^- p \to \nu X$

Events per day in $dx\,dy = 0.01$

$S = 40000\ GeV^2$, $L = 10^{32}\ cm^{-2}\,sec^{-1}$

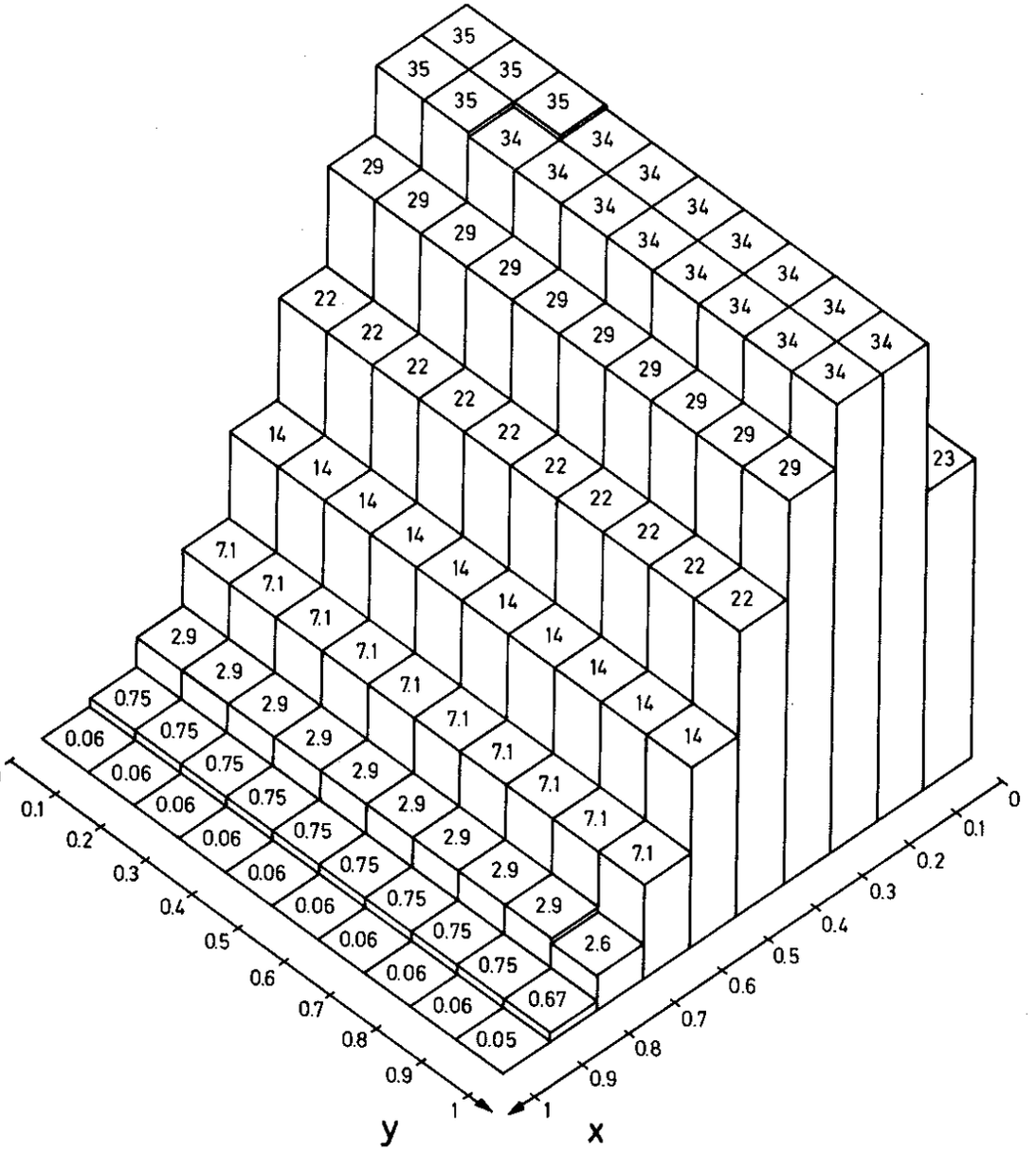

Fig.24

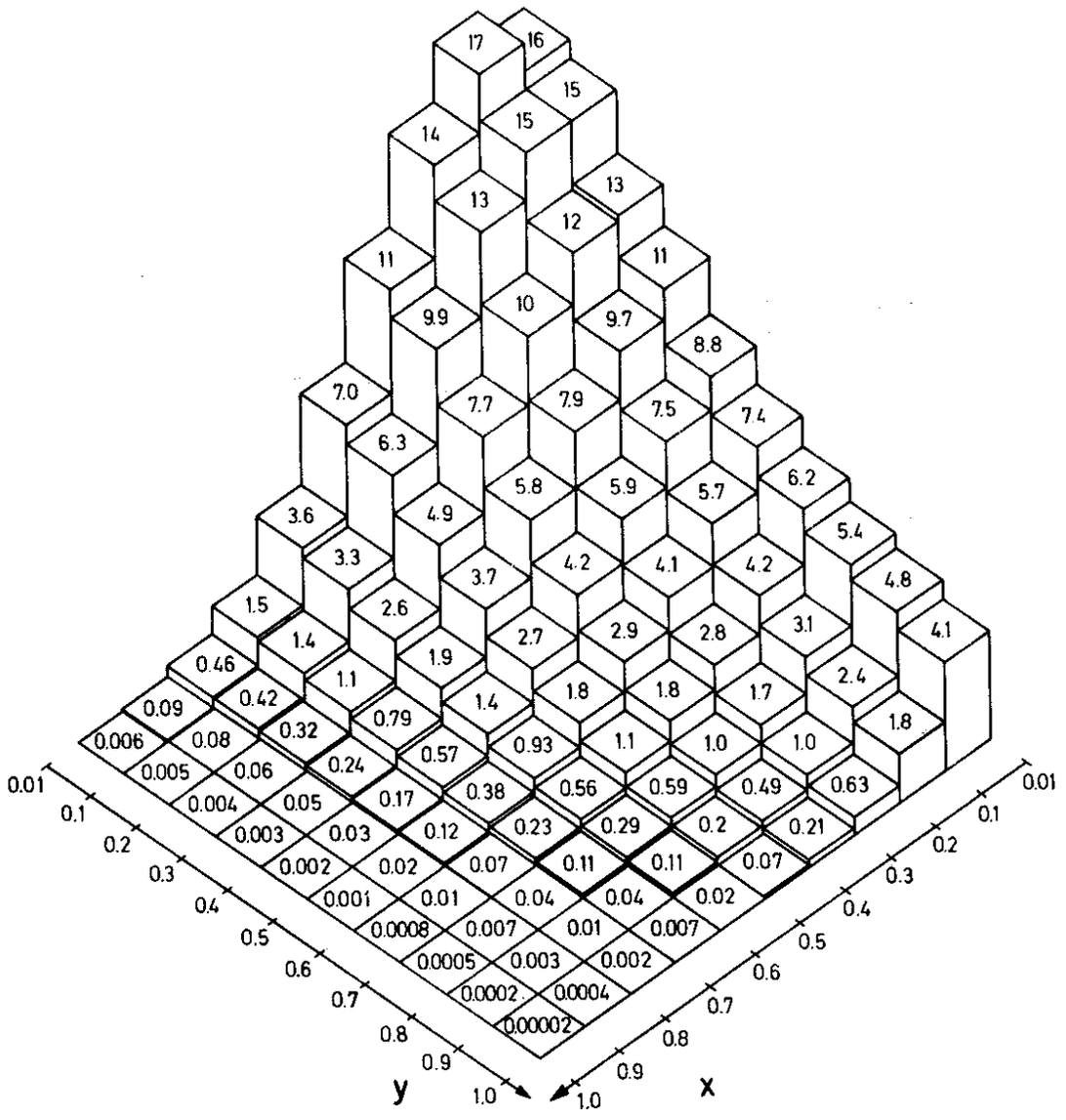

Fig. 25

$$H_{\pm} = \int_{Q^2>Q_o^2} \int dxdy \left[(1 - y + y^2/2) F_2^{\nu p(n)} \mp (y - y^2/2) F_3^{\nu p(n)} \right]$$

and $\sigma_L = 0$. The functions $H_{\pm}$ were calculated using the quark distribution function listed by Barger and Phillips [10] and the results are plotted in Figs. 26 and 27. These functions are used to construct the rate of events with $Q^2 > Q_o^2$ as a function of Q_o^2. These rates are plotted in Figs. 28 and 29 and they show that the charged weak current can be probed for values of Q^2 up to 25'000 GeV^2 with option II and 4'000 GeV^2 with option I. This is of course only true if the assumptions - scaling and a point coupling - remain valid. However, scaling is expected to be violated and the corresponding reduction in rate has been evaluated in an asymptotically free gauge theory [12]. The results of these calculations are also plotted in Figs. 28 and 29. The rates for e_L^- + p are reduced by about a factor of 6 at large values of Q^2 - however, the rates are still sufficient to explore the cross section for values of Q^2 beyond 15'000 GeV^2. The rates for e_R^+ + p are decreased less since the number of antiquarks is increasing (see Figs. 31 and 32).

The deviation from a point coupling will also lead to a reduction in rate and this damping is just the effect we want to study. In current models the weak interaction is damped by assigning a finite mass to the intermediate vector boson - a popular value of the mass is M_W = 62 GeV. The modifications of the cross section due to an intermediate vector boson of mass 62 GeV are also shown in Figs. 28 and 29. The effects are large - the rates are reduced by a factor of 30 at $Q^2 \simeq$ 15'000 GeV^2. An intermediate vector boson of mass 150 GeV reduces the rate by a factor of 3 at the same Q^2. Propagator effects and scaling effects can be separated by comparing e + p → e + X and e + p → ν x X since scaling violations are expected to modify both reactions in a similar manner.

The weak reaction e + p → ν + X is presumably kinematically similar to the electromagnetic (neutral weak) prosess e + p → e + X. The kinematics of the latter process are shown in Figs. 1, 2, 10, 11, 12 and 13. The weak current interacts with a parton which carries the appropriate fraction of momentum x. The struck parton materializes as a jet of hadrons at large angles; the transverse momentum of this jet with respect to the beam axis is balanced by the

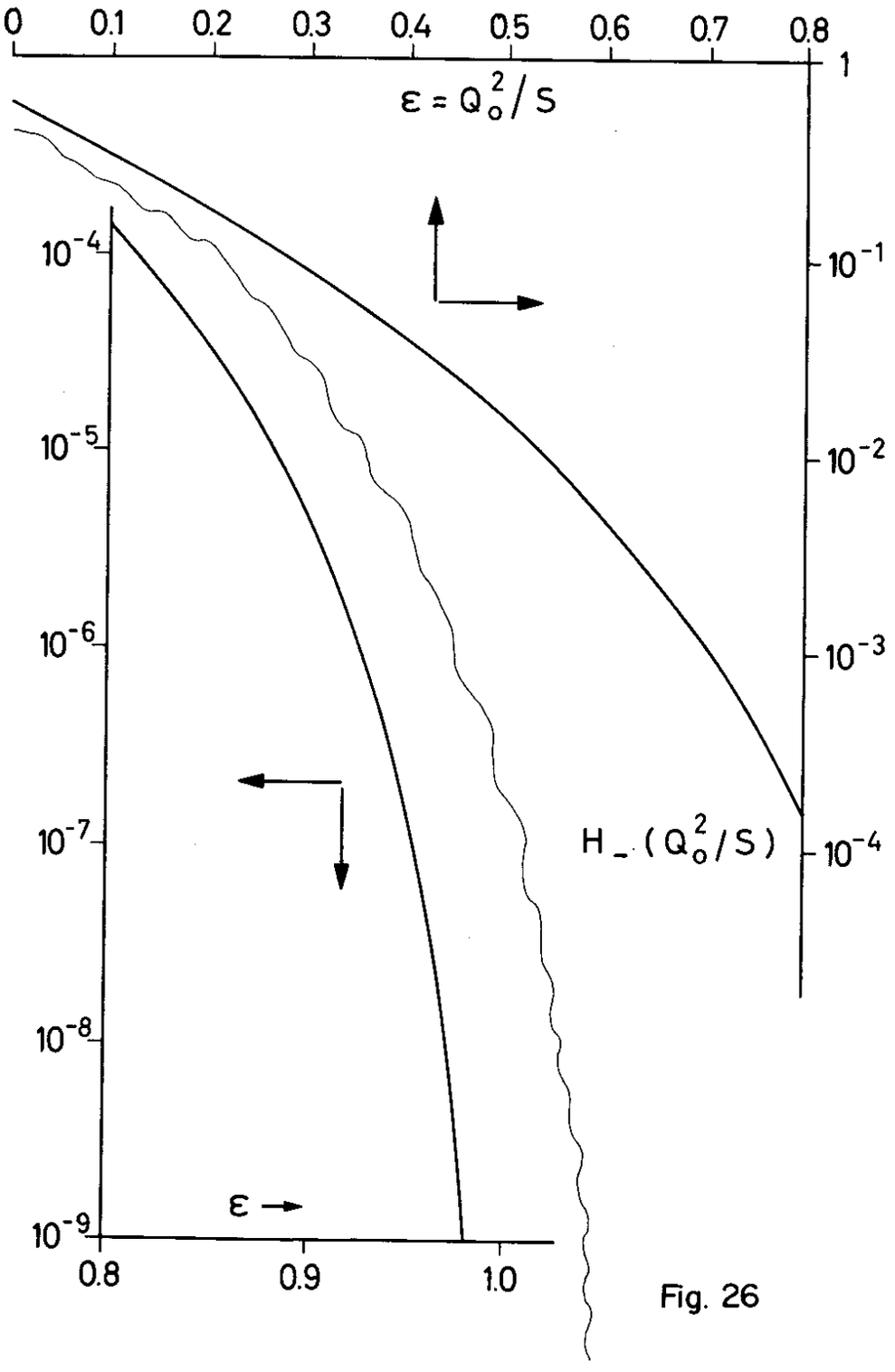
0 0.1 0.2 0.3 0.4 0.5 0.6 0.7 0.8 1
$\varepsilon = Q_o^2/S$
10^{-4} 10^{-5} 10^{-6} 10^{-7} 10^{-8} 10^{-9}
10^{-1} 10^{-2} 10^{-3} 10^{-4}
$H_-(Q_o^2/S)$
$\varepsilon \rightarrow$
0.8 0.9 1.0

Fig. 26

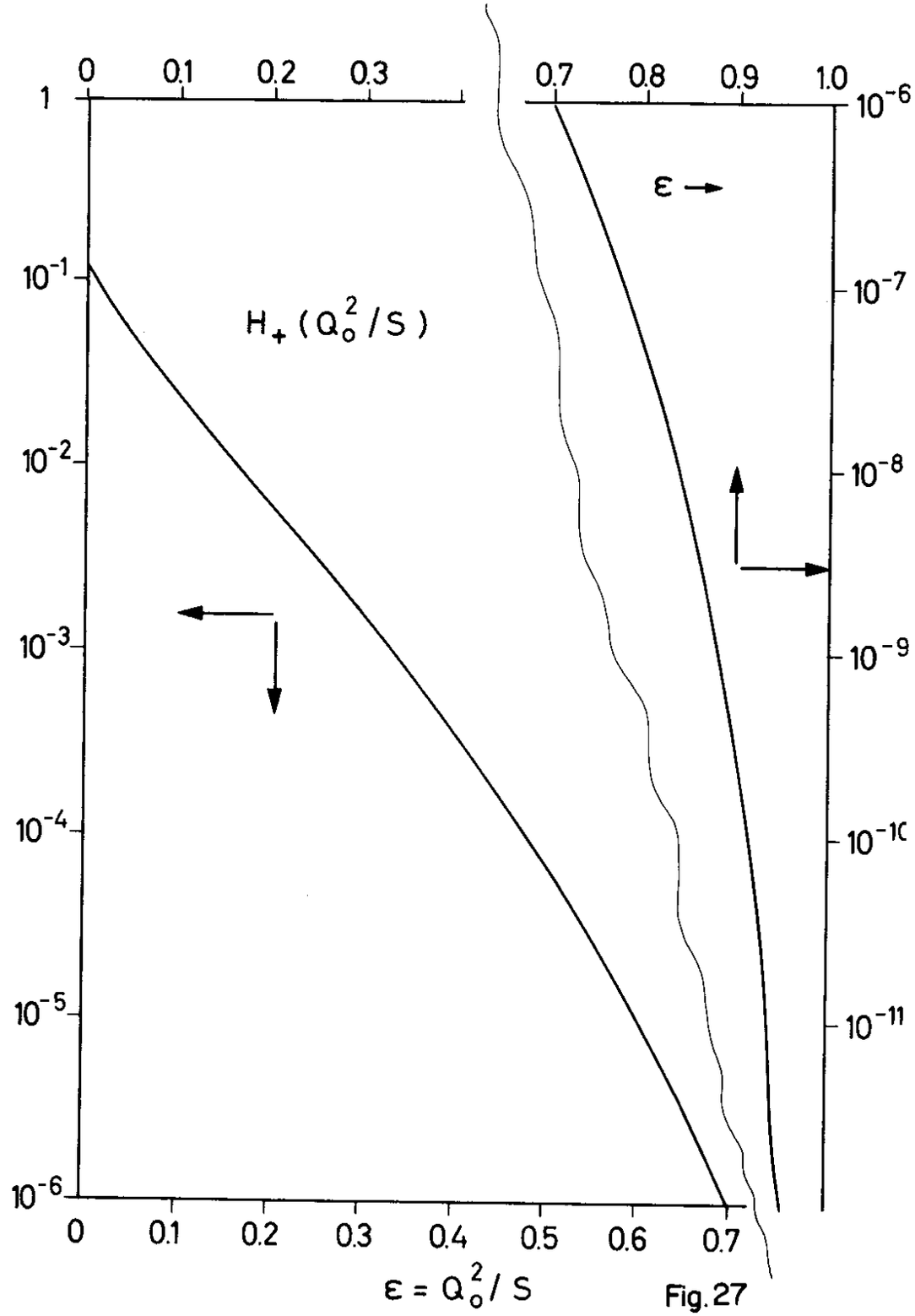
1 0 0.1 0.2 0.3
0.7 0.8 0.9 1.0
10^{-1} 10^{-2} 10^{-3} 10^{-4} 10^{-5} 10^{-6}
10^{-6} 10^{-7} 10^{-8} 10^{-9} 10^{-10} 10^{-11}
$H_+(Q_o^2/S)$
$\varepsilon \rightarrow$
0 0.1 0.2 0.3 0.4 0.5 0.6 0.7
$\varepsilon = Q_o^2/S$

Fig. 27

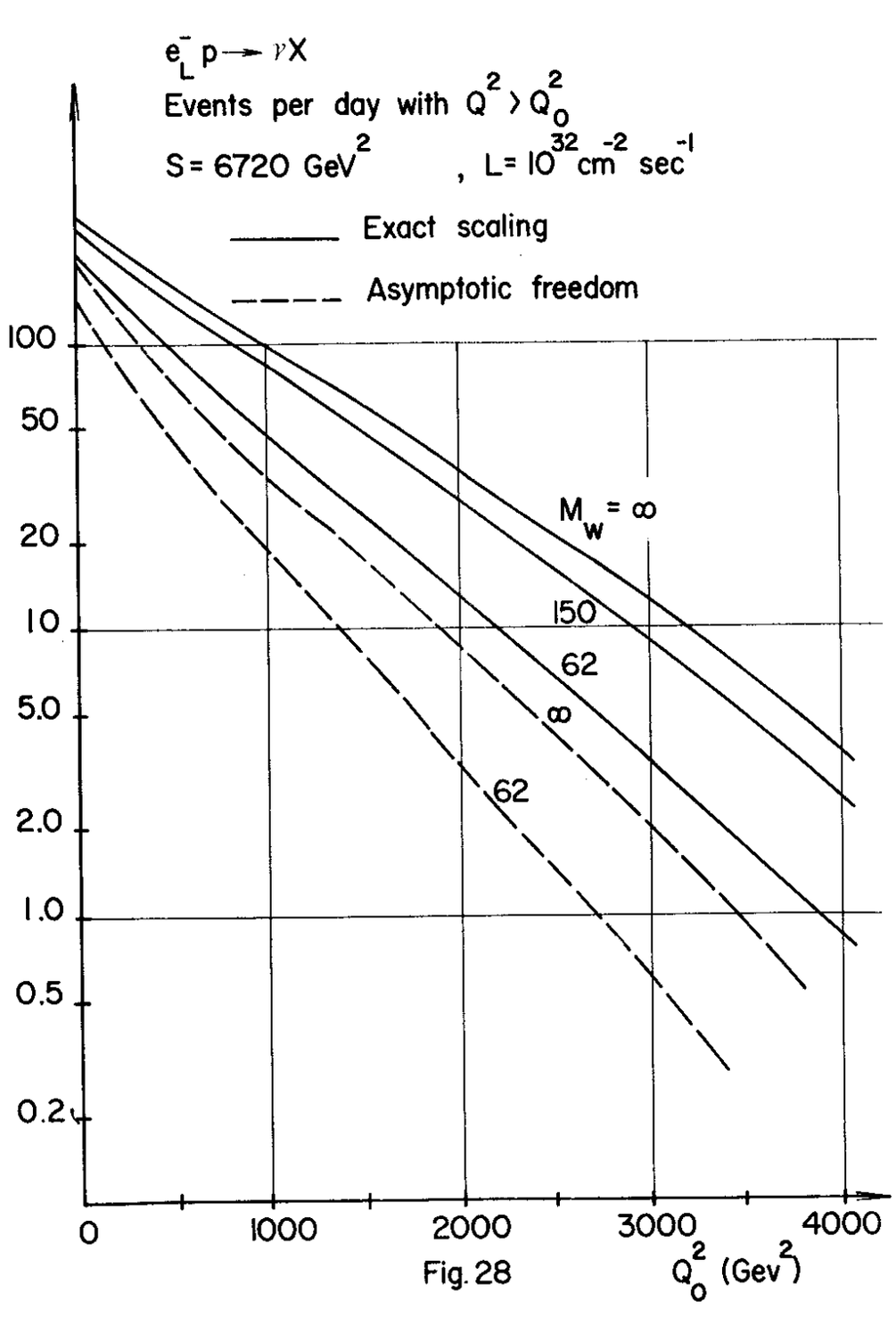
$e^-_L p \to \nu X$
Events per day with $Q^2 > Q_0^2$
$S = 6720\ GeV^2$, $L = 10^{32}\ cm^{-2}\ sec^{-1}$
Exact scaling
Asymptotic freedom
100
50
20
10
5.0
2.0
1.0
0.5
0.2
$M_W = \infty$
150
62
∞
62
0
1000
2000
3000
4000
$Q_0^2\ (Gev^2)$

Fig. 28

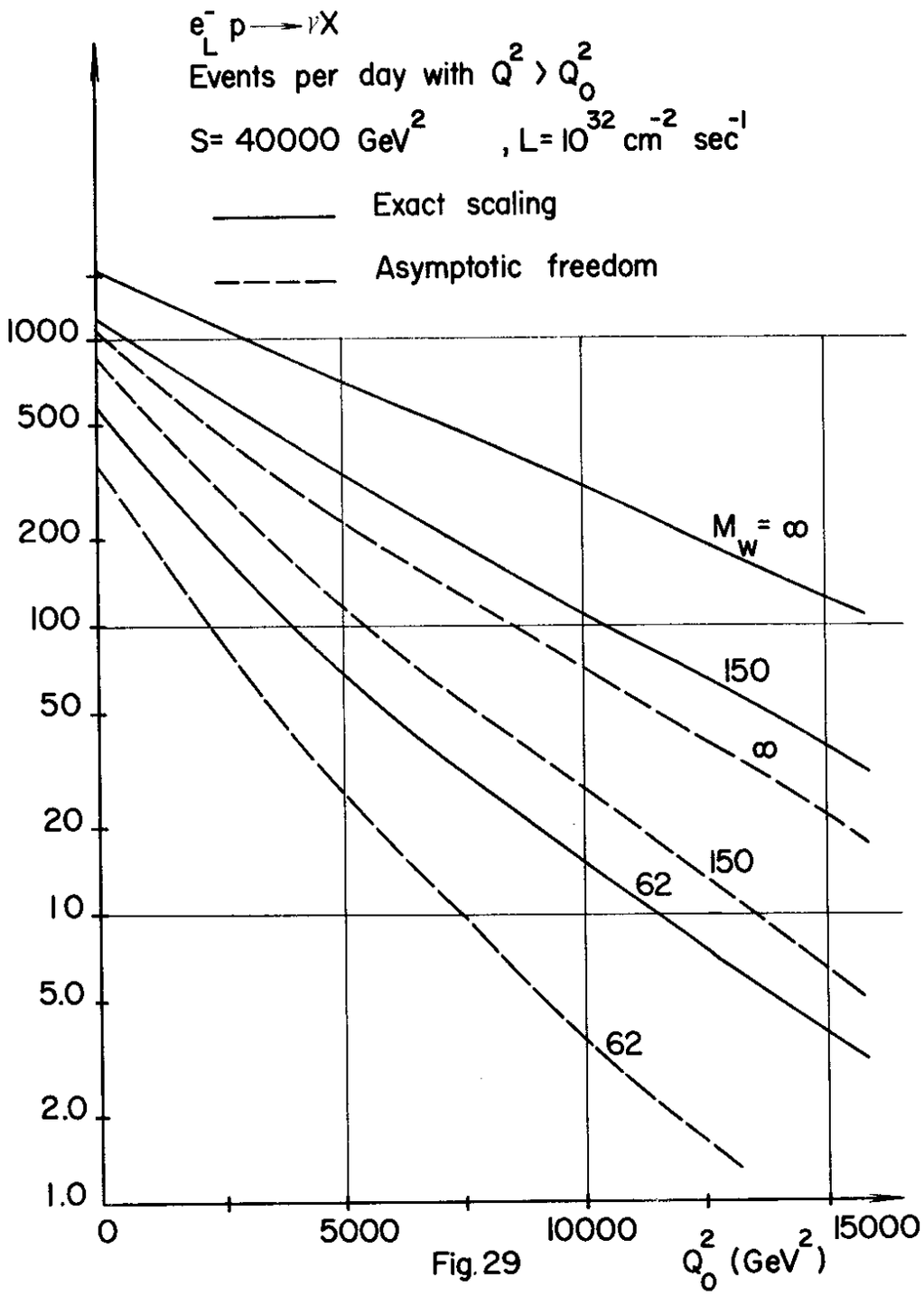
$e^-_L p \to \nu X$
Events per day with $Q^2 > Q_0^2$
$S = 40000\ GeV^2$, $L = 10^{32}\ cm^{-2}\ sec^{-1}$
Exact scaling
Asymptotic freedom
1000
500
200
100
50
20
10
5.0
2.0
1.0
$M_W = \infty$
150
∞
150
62
62
0
5000
10000
15000
$Q_0^2\ (GeV^2)$

Fig. 29

neutrino. The remainder of the proton results in a jet of hadrons which travel along the direction of the incident proton. A charged current event will therefore lead to a hadron final state with a large transverse momentum imbalance and this feature can be used to tag the reaction. Furthermore, the outgoing lepton has high energy and it will be well separated from the hadrons. It should therefore be easy to decide whether the transverse momentum is balanced by an electron or a neutrino and hence to separate the electromagnetic and the weak interactions. Note that the electromagnetic and the weak interaction are expected to yield similar rates (Figs. 3 and 4, and 22 - 25) at large values of Q^2.

In fig. 30 curves of constant momentum are plotted in a Q^2, ν diagram for 25 GeV electrons on 270 GeV protons. Note that by selecting events with a hadron momentum imbalance of $p_\perp$ > 20 GeV the weak rate is not appreciably reduced whereas the electromagnetic rate is. Beam-gas collisions will lead to a completely negligible rate with such a large $p_\perp$ imbalance (caused by not observed hadrons). We would therefore expect a measurement of the total weak cross section to be reasonable straight forward.

However, in order to plot the events as a function of Q^2, ν (x, y) these quantities must be reconstructed from measurements of the hadron final state. If the parton model is taken literally then x and y can be obtained from a measurement of the energy and the angle of the current jet only. The kinematics of the current jet are plotted in Fig. 11 as a function of $p_{//}$ and $p_\perp$. It is clear that the information contained in this graph is complementary to the information contained in the lepton kinematics plotted in Fig. 2. Note that the validity of reconstructing x and y from a measurement of the current jet can be tested in the e + p → e + X collisions. If this model is proven to be wrong, then Q^2, ν can only be reconstructed from a measurement of all the hadrons in the final state. It seems feasible for such experiments to cover angles down to 5 mrad with respect to the proton direction. A more detailed discussion of such a detector can be found elsewhere [8].

The physics interest of studying e + p → ν + X will be discussed next in more detail.

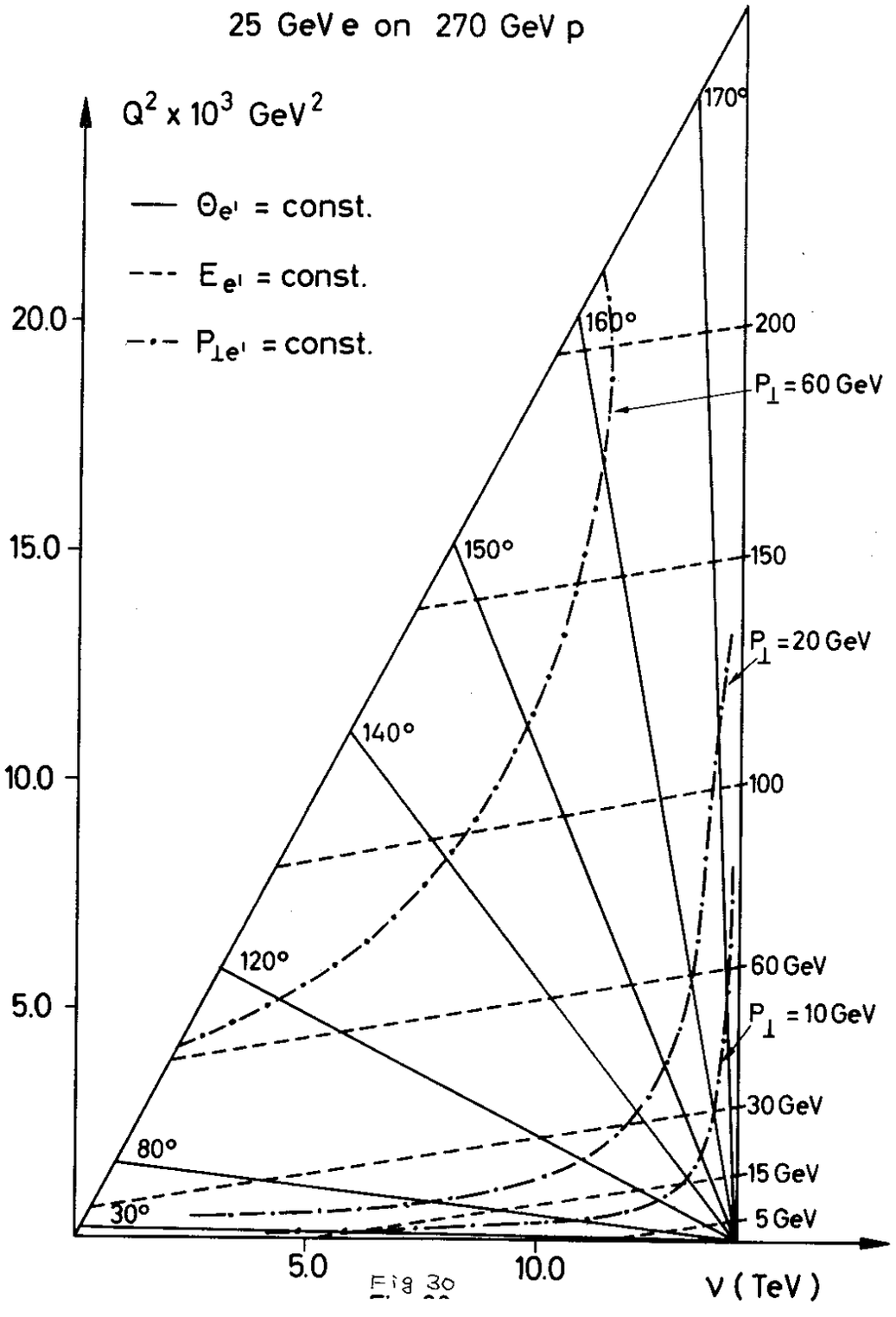

Fig 30

1) It is widely believed that the weak interactions are mediated by a $W^{\pm}$ boson with a mass of about 60 GeV. Whether this is true or, if not, what other mechanism will eventually damp the rising weak cross section is perhaps the outstanding open question in particle physics today. In Figs. 31 und 32 the total cross section for $e_L^- + p$ and $e_R^+ + p$ divided by s is plotted as a function of s for various values of M_W assuming both scaling and scaling violations as expected in asymptotically free theories [12]. These plots show that the scaling violations predicted in asymptotically free gauge theories lead to large changes in the cross section at relatively small values of s. However, the deviations from a linear s dependence are only a few per cent between s = 1000 GeV^2 and 40'000 GeV^2. An intermediate vector boson with a mass of 62 GeV (150 GeV) will change the value of σ_o/s by a factor of 2 (30%) in the same range of s values. More violent scale breaking than that predicted in asymptotically free theories might tend to mask the effect; however, it would also be expected to show up in $e + p \to e + X$. A simultaneous measurement of electromagnetic and weak interactions should therefore make it possible to detect the W independent of scaling violations even in the total cross section. The sensitivity of the experiment to propagator effects is much improved by considering events at large values of Q^2. The existance of an intermediate vector boson with a mass M_W will reduce the rates listed in Figs. 22 – 25 by a characteristic factor $\left(\frac{M_W^2}{M_W^2 + s \times y}\right)^2$. Such measurements with option II are sensitive to an intermediate vector boson with a mass even beyond 150 GeV.

2) Measurement of $e_L^- + p$ and $e_R^+ + p$ are sensitive to new pieces of the weak current at the hadron vertex. For example, suppose that there exists a top quark t which partners a down quark d in a right-handed doublet:

$$\begin{pmatrix} t \\ d \end{pmatrix}_R$$

Well above threshold the production of t quarks would increase $\sigma(e^+ + p \to \nu + X)$ by a factor of four in a valence quark approximation. (a right-handed u quark paired with a quark of charge 5/3 would increase $\sigma(e^+ + p \to \bar{\nu} + X)$ by a factor 7 in this approximation). As indicated in Fig. 32 such spectacular effects would be very easy to see even in the total cross section. The weak interaction makes it possible to liberate new flavours up to quite high masses. Note that these new flavours might be produced off valence quarks and sea quarks.

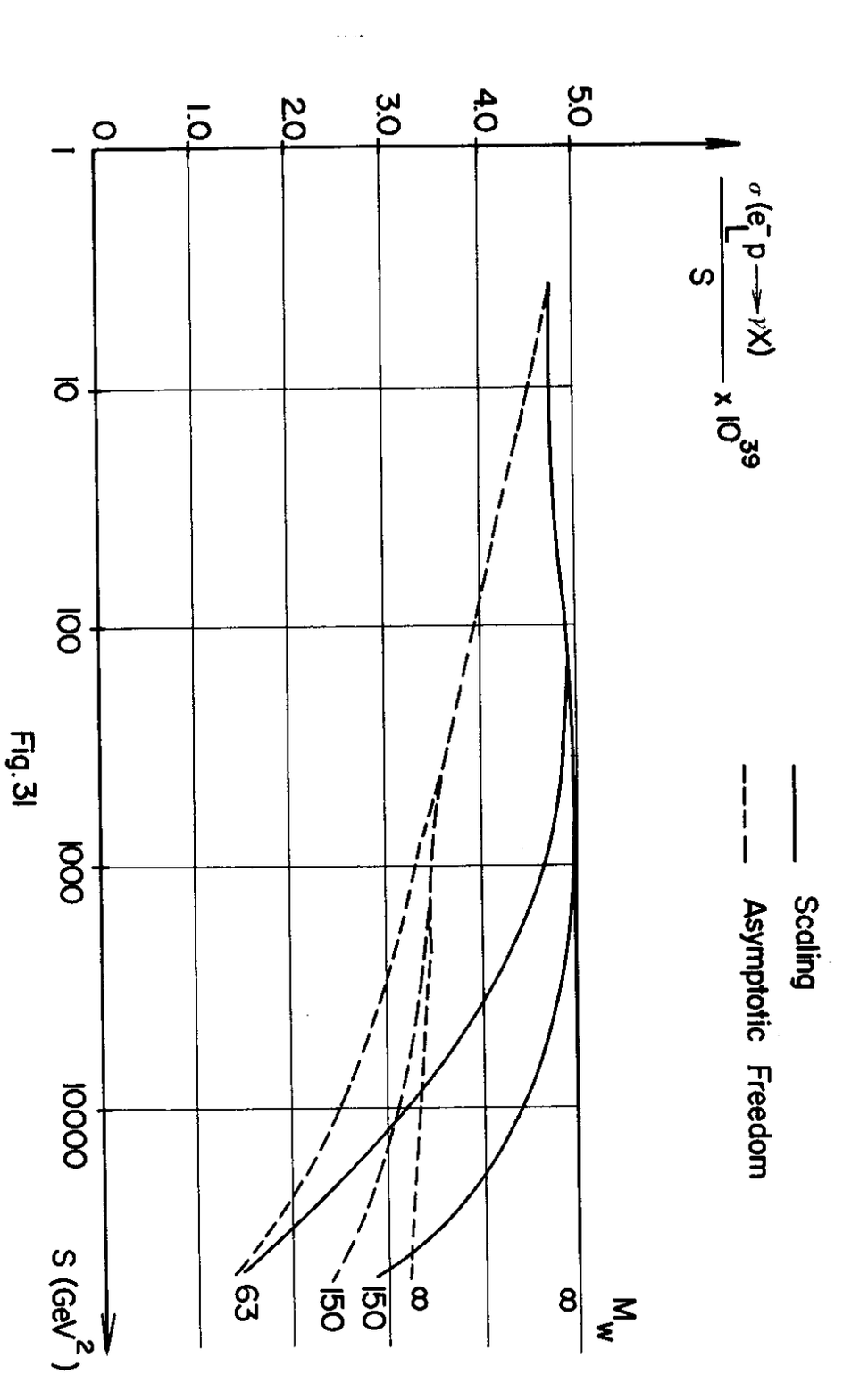

Fig. 31

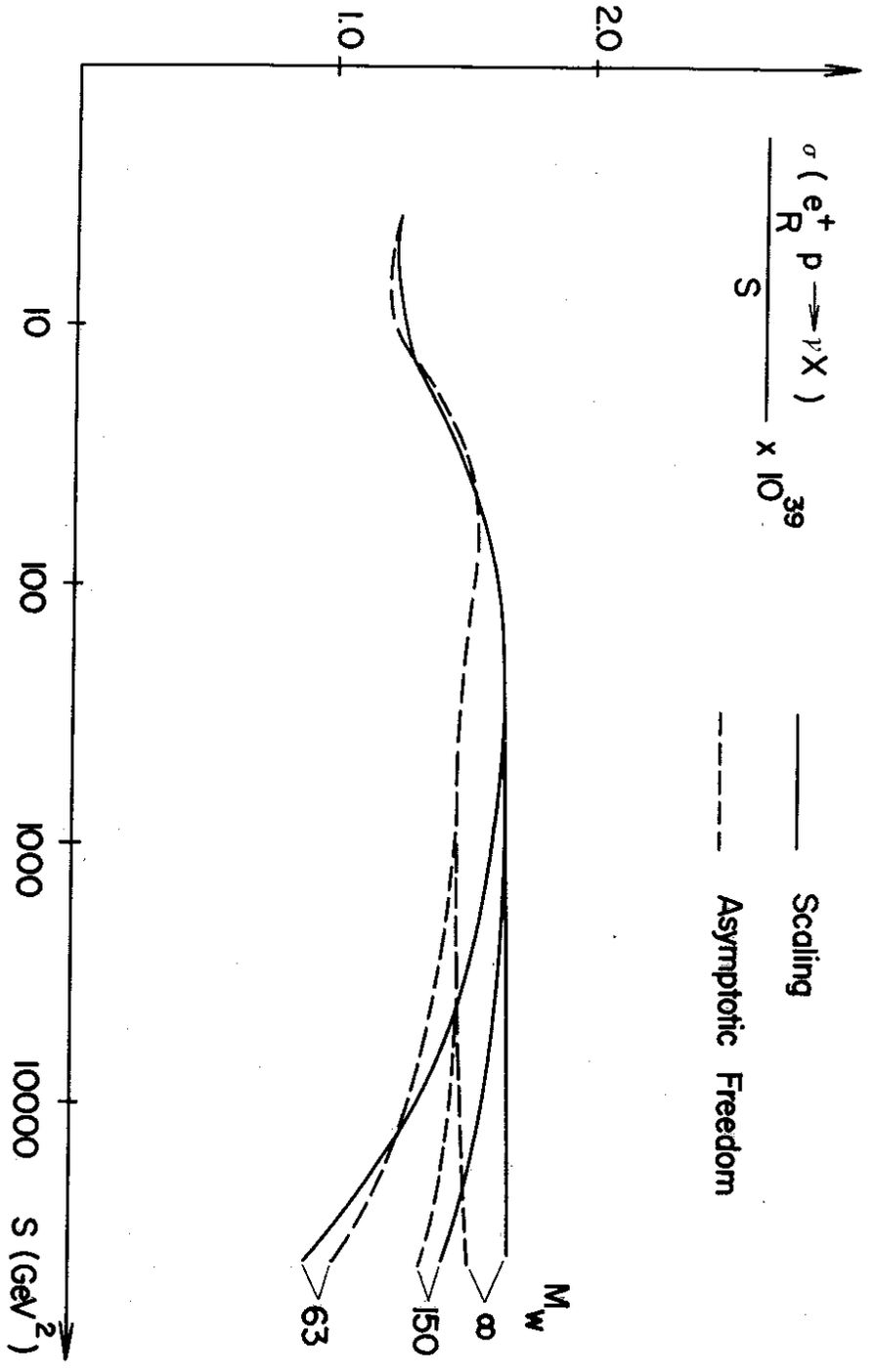

Fig. 32

3) Measurements of $\sigma(e_R^- + p \to \nu + X)$ and $\sigma(e_L^+ + p \to \bar{\nu} + X)$ provide very sensitive tests of the structure of the weak interaction at the lepton vertex. For example, it is possible that there exists an $e_R^- \to \nu_R^e$ and $e_L^+ \to \bar{\nu}_L^e$ coupling to a new current or vector boson W'. To be compatible with existing data this current could only couple μ to ν_μ. It would be very interesting indeed to search for this process.

4. PHOTOPRODUCTION

One of the most remarkable facts to emerge from the study [22] of various photoproduction processes is that, to a surprising degree of accuracy, the photon behaves like a strongly interacting boson with quantum numbers $J^{PC} = 1^{--}$ and an effective coupling strength roughly $1/\sqrt{250}$ of the normal coupling strength of a hadron. This can be understood if one assumes that the photon consists of pairs of quarks and antiquarks written symbolically as $|\text{photon}> = \Sigma\, g_i\, q_i \bar{q}_i$ where g_i is the coupling constant between the photon and the quark-antiquark pair and the sum is extended over all flavours. This is essentially equivalent to decomposing the photon into vector mesons, i.e. $|\text{photon}> = \sum_i g_i' V_i$.

This immediately leads to two interesting classes of experiments:

1) A photon beam is a copious source of vector mesons. From the mass, the width and the decay properties of these vector mesons one might infere the existence of quarks with new flavours.

2) Since, to a good approximation, the photon behaves like a hadron, all the concepts and theories used to describe reactions involving only hadrons should also describe the results obtained with an incident photon beam. In fact, photoproduction experiments might provide particularly sensitive tests of strong interaction theories since:

   a) the photon has spin 1 and in general the photon beam will be polarized; spin correlations can therefore be used to disentangle various reaction mechanism;

   b) the mass of the photon can be varied in a well defined manner. The theory must be able to describe this new degree of freedom.

Hadrons with even charge conjugation and spin different from one can be produced by one photon exchange. This mechanism will become increasingly important at high energies since it yields a cross section which increases logarithmically with energy.

In addition to these experiments where the photon is primarily used as a probe of the strong interaction, there is a large class of experiments which search for properties unique to photons. Such properties might be more easily found at high energies.

4. 1 The Beam

Electroproduction in the limit of $Q^2 \to 0$, can be described as the radiation of an almost real photon followed by the interaction of the photon with the proton. Since the probability of radiating an almost real photon is known, the electron beam is equivalent to a well collimated bremsstrahlungbeam with equivalent laboratory end point energies of 3580 GeV (12 GeV electron on 140 GeV proton) or 21'300 GeV (25 GeV electron on 400 GeV proton). The intensity of the beam, i.e. the number of photons with energies between k and k + Δk per incident electron is given by the well-known Weizäcker-Williams formula

$$N(k)dk = \frac{\alpha}{2\pi}\left(\frac{E^2 + E'^2}{E^2}\right) \ln\frac{|Q^2_{max}|}{|Q^2_{min}|}\,\frac{dk}{k}$$

The nomenclature is defined below

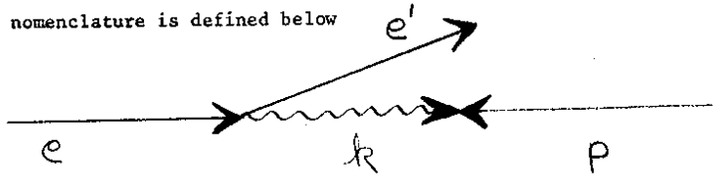

$$k = (E - E')$$
$$Q^2 \simeq - EE'\,\theta^2$$

Not tagging the scattered electrons yields the highest photon luminosity at the price of not knowing the energy of the photon. This is acceptable for those experiments in which the photon energy can be determined from a measurement of the final state. The effective photon spectrum for such a beam is

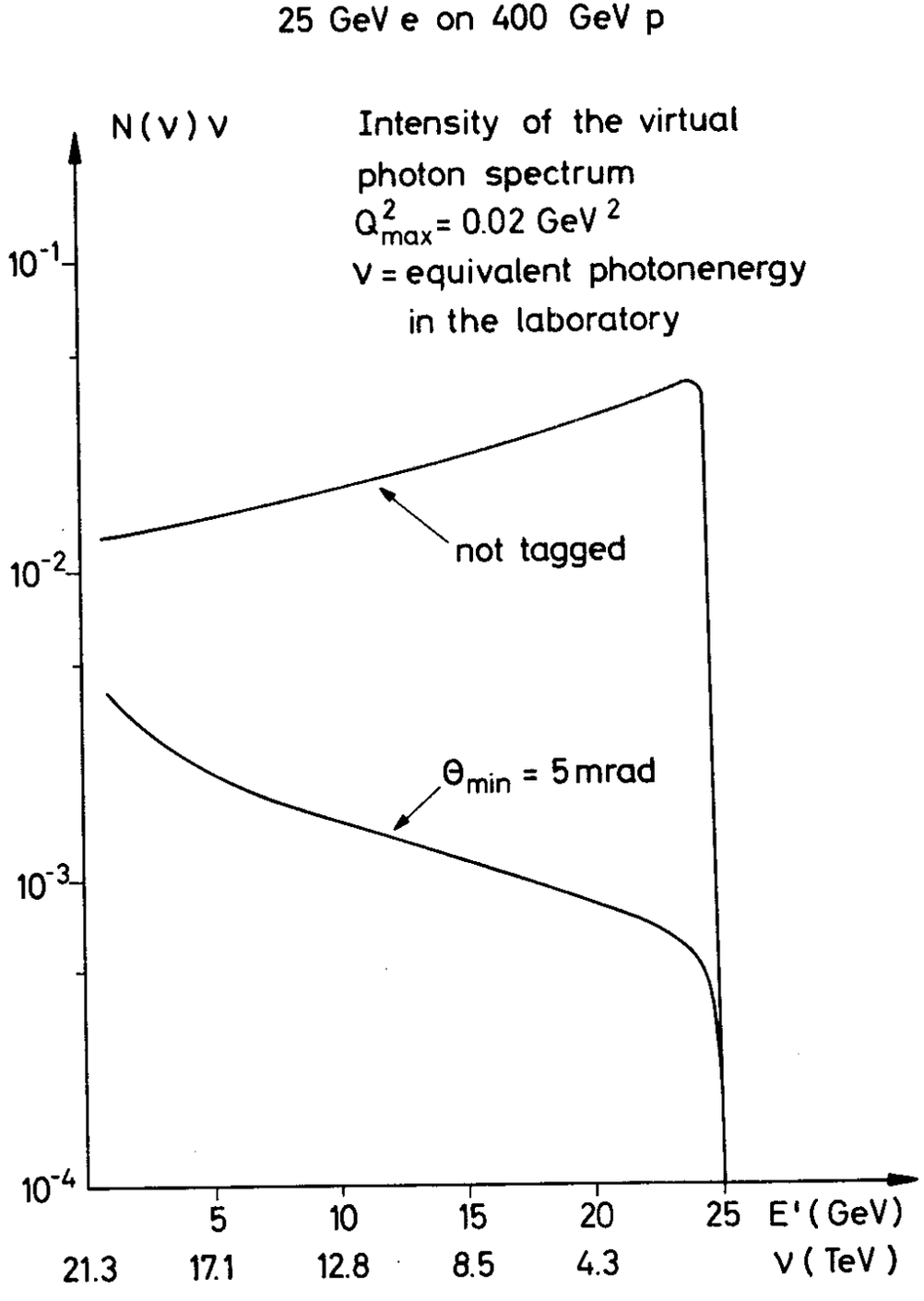

Fig. 33

plotted in Fig. 33 and it yields an effective luminosity $L(\gamma p) \sim 0.1\ L(p)$ for photons with equivalent laboratory energies above, say, 500 GeV (option II). The photons will be circularely polarized if the incident electron beam has a well defined helicity.

A measurement of the energy and angle of the scattered electron offers important advantages. Firstly, it determines the energy of the photon within some error. For example by using a liquid Argon calorimeter ($dE'/E' = \pm 0.05/\ E'(GeV)$) the photon energy is known with an error $d\nu/\nu = \pm 2.5 \times 10^{-3}$ at $\nu = 20'000$ GeV and $\pm 4.5 \times 10^{-2}$ at $\nu = 4200$ GeV.

Secondly, a measurement of the direction of the scattered electron determines the polarization of the photon with respect to the production plane. (Defined by the incident proton and some outgoing hadron). However, these nice features are obtained at a considerable loss of intensity since Q^2_{min} is now given by $EE' \theta^2_{min}$, where θ_{min} is the minimum angle permitted between the tagging counter and the electron beam. The photon spectrum corresponding to $\theta_{min} = 5$ mrad is also plotted in Fig. 33.

The properties of the photon beams are summarized below:

1) 12 GeV electrons on 140 GeV protons
   $\nu_{max} = 3582$ GeV
   Tagging counters: $\Delta\phi = 2\pi$, $5 \times 10^{-3} \leq \theta \leq (m_\pi^2/EE')^{1/2}$
   $L_{\gamma p} \simeq 7 \times 10^{-3}\ L_{ep}$ for 300 GeV > ν > 3300 GeV.

2) 25 GeV electrons on 400 GeV protons
   $\nu_{max} = 21'300$ GeV
   Tagging counters: $\Delta\phi = 2\pi$, $5 \times 10^{-3} \leq \theta \leq (m_\pi^2/EE')^{1/2}$
   $L_{\gamma p} \simeq 3 \times 10^{-3}\ L_{ep}$ for 1000 GeV > ν > 21'000 GeV^2

Next, the rates of some typical photoproduction experiments will be given. A discussion of suitable detectors can be found elsewhere[8].

4. 2 Experiments

The cross section for $\gamma + p \to$ hadrons has been measured [22] for photons with energies between threshold and 100 GeV. Above the resonance region the cross section was found to decrease with energy as $a + b/\sqrt{\nu(GeV)}$, a decrease similar to the one observed in hadronic reactions. However, at higher energies

the hadron-hadron cross section flattens out and starts to increase like $(\ln s)^2$ - the fastest increase permitted by the Froissart bound. In so far as a photon behaves like a hadron, a similar increase is also expected [+] to occur in $\gamma + p \to$ hadrons. A deviation from this behaviour would signal the presence of a non-hadronic piece of the photon. With option II the present data can be extended from a 100 GeV to 21'000 GeV - into a new energy region not yet explored with hadron beams. At such high energies new phenomena materializing as a step in the total cross section may occur. The relative shape of the cross section can be measured very accurately without an absolute normalization, since data are collected simultaneously at all energies and the shape of the bremsspectrum is well known. With a tagged photon beam more than 10^6 events/day are expected for photon energies between a few hundred and 21'000 GeV.

4. 3 Compton Scattering

Compton scattering is one of the most fundamental processes which can be investigated with an incident photon beam, in particular a measurement of this reaction might reveal properties unique to the photon. For example, the amplitudes may contain fixed poles which are not allowed to occur in purely hadronic reactions. The fixed pole contribution is expected[23] to dominate at high energies and large values of t, resulting in an almost real amplitude. This would lead to a large difference in the cross section for photons with the polarization vector either in or normal to the scattering plane.

At low values of t the scattered electron and the scattered photon must be measured in coincidence. Such a set-up yields about 3300 events/day with 120 events/day above $|t| = 0.5$ GeV^2. However, it might be feasible to dispense with the tagging and measure only the recoil proton in coincidence with the scattered photon for $|t| > 0.5$ GeV^2. This would increase the rate by more than an order of magnitude.

A measurement of deep inelastic Compton scattering $e + p \to e' + \gamma + X$ offers the intriguing possibility of determining [24] the charge of the quarks directly.

+) Note that the Froissart bound does not directly apply for an incident photon beam.

4, 4 Photoproduction

Vector mesons have the same quantum numbers as photons and therefore, on general grounds, one might expect them to be diffractively produced. This is expressed in the vector dominance model where the photoproduction cross section is proportional to the elastic vector meson proton cross section as shown in Fig. 34A. Photoproduction of vector mesons can therefore be used to obtain information on elastic meson-proton scattering at very high energies. In fact, these experiments can be made rather sensitive by using polarized photons and by determining the helicity of the produced vector meson. The ϕ and the J/ψ are largely decoupled from the u and the d quark in the proton, and the photoproduction of these particles can therefore be used to provide particularly clean tests of the Pomeron.

The rates for ρ, ω, ϕ and J/ψ production using a tagged photon beam (option II) are listed in Table IV. In principle, a non-tagged beam will suffice, leading to an increase in rate by a factor of 20.

Table IV – Photoproduction of the light vector mesons

Process	σ_{tot}	Events/day tagged	Events/day no tag
$\gamma + p \to \rho + p$	13 μb	5.6×10^5	1.1×10^6
$\gamma + p \to \omega + p$	1.4μb	6×10^4	1.2×10^6
$\gamma + p \to \phi + p$	0.5μb	2.2×10^4	4.4×10^5
$\gamma + p \to J/\psi + p$	30 nb	1.3×10^3	2.6×10^4

A photon beam is also a copious source of new vector mesons. If $|t_{min}| = (m_V^2\, m_p/s)^2$ is limited to 0.2 GeV^2, then vector mesons with a mass of 60 GeV (140 GeV) can be produced in option I (II). However, the cross section for producing a vector meson with hidden new flavours is expected to decrease with increasing mass as $1/M_V^4$. Scaling the J/ψ rate as $1/M_V^4$ yields 1 event/day for M_V = 40 GeV. Such a low rate might be acceptable since their decay produces a clean signature: most of the decays will either yield lepton pairs or two hadron jets well separated in space. The decay products of a heavy mass particle appear at large angles where they can be easily detected.

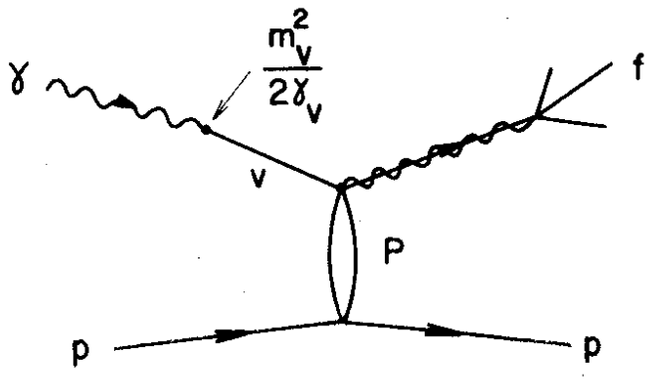

$$\frac{d\sigma}{dt}(\gamma + p \to V + p) = \left(\frac{\alpha\pi}{\gamma_V^2}\right) \cdot \frac{d\sigma}{dt}(V + p \to V + p)$$

Fig. 34A

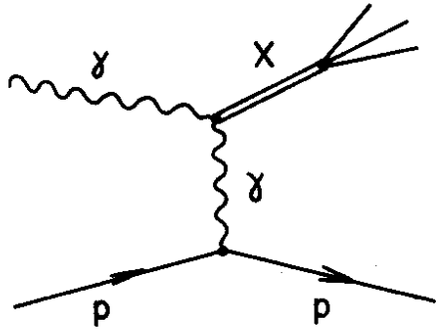

X : $J \neq 1$
$C = +$

$$\frac{d\sigma}{dt}(\gamma + p \to X + p) = \frac{8\pi\alpha}{m^2} \cdot \frac{\Gamma_{\gamma\gamma}}{m} \cdot \left(\frac{t - t_m}{t^2}\right) \cdot \left[F_p(t)\right]^2$$

$$t_m = \left(\frac{m_X^2 \cdot m_p}{S}\right)^2$$

Fig. 34B

4. 5 Primakoff effect

An incident photon can interact with the Coulomb field of the proton to produce hadrons with spin different from one and positive charge conjugation. This process [25], shown in Fig. 34B, leads to a differential cross section of the form

$$\frac{d\sigma}{dt} = \frac{8\pi\,\alpha}{m^2}\left(\Gamma_{\gamma\gamma}/m\right)(t - t_{min})/t^2 \quad |F(t)|^2$$

In this formula, m is the mass of the produced particle, $\Gamma_{\gamma\gamma}$ the partial width of the resonance to decay to a pair of photons, t_{min} the minimum momentum transfer to the proton ($t_{min} \approx (m^2/2k)^2$) and F the proton form factor. Since the proton form factor is near to one, this yields a total cross section:

$$\sigma = (8\pi\,\alpha/m^2)\,(\Gamma_{\gamma\gamma}/m)\,(\ln t_{max}/t_{min} + 1)$$

which increases logarithmically with energy. The rates for some particles with a large value of $\Gamma_{\gamma\gamma}$ are listed in the table below.

Table V

Particle	$\Gamma_{\gamma\gamma}$ (MeV)	σ (nb)	Events/day
π^o	8×10^{-6}	1.4	1082
η	3.8×10^{-4}	0.99	557
X^o	2×10^{-2}	9.8	4704
f	$\sim 4 \times 10^{-3}$	0.84	366
η_c	$\sim 20 \times 10^{-3}$	0.39	94

This process makes it possible to determine radiative widths $\Gamma_{\gamma\gamma}$ for a series of resonances directly. The reaction is also well suited to search for the pseudoscalar partners of vector mesons with new hidden flavours. The rates are also sufficiently large to measure the cross section as a function of q^2. This is related to the structure of the particle.

4. 6 Experiments at finite values of Q^2

A unique advantage of an incident lepton beam is the possibility of varying the mass of the exchanged particle in a well defined manner. The experimental

set-up is the same as the one used in the photoproduction experiments – the only difference is that the electron is now tagged at a larger angle. With a luminosity of 10^{32} cm^{-2} s^{-1} one expects +) 2.2×10^6 events/day with Q^2 greater than 2 GeV^2, 1.8×10^5 events/day with Q^2 above 20 GeV^2 and 2.6×10^4 events/day with Q^2 above 100 GeV^2. These rates are sufficient to carry out a detailed study of most of the channels discussed above.

5. PRODUCTION OF NEW PARTICLES

We have already discussed the production of new flavours in e + p → e + X and e + p → ν + X. The production of vector mesons with hidden new flavours is discussed in the section on photoproduction. Here we discuss the production of intermediate vector bosons ($W^\pm$ and Z^o) and heavy leptons, for which we can make plausible cross section estimates, leaving aside exotica such as quarks, monopoles and Higgs bosons, which one might also hope to find.

5. 1 The Production of $W^\pm$ and Z^o

It turns out that the cross sections for $W^\pm$ and Z^o production by many of the possible mechanisms can be estimated in terms of $\sigma(\nu+p \to \mu+W+X)$ and $\sigma(\nu+p \to \nu+W+X)$ for which numerical evaluations are available. The relevant Feynman diagrams are shown in Figs. 35A and 35B. It is necessary to make the following points about these processes:

1) If we define

$$\xi = \frac{\sigma(\nu+p \to \mu+W+X)}{\sigma(\mu+p \to \nu+W+X)}$$

then truly asymptotically $\xi = 2$ (for an unpolarized muon beam; 1 for left-handed μ^-'s). However, this requires

$$\ln\left(\frac{s}{M_W^2}\right) \gg \ln\left(\frac{M_W^2}{M_\mu^2}\right)$$

so it is not relevant for practical purposes. In fact, at the energies of interest $\xi \gg 1$ [26,27]. The reason is that the μ meson in Fig. 35A can get very close to its mass-shell, which gives rise to a logarithmic divergance as $m_\mu \to 0$. In contrast, the virtual μ or W propagator in all the other diagrams

+) Asymptotic freedom will increase these rates substantially.

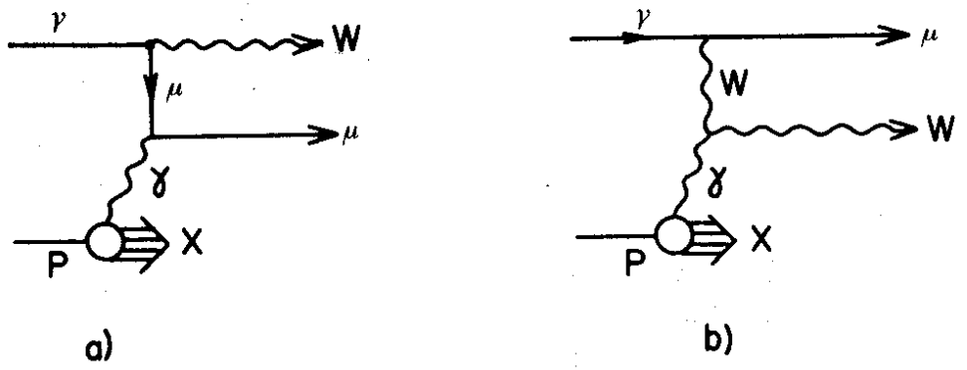

Fig. 35 A

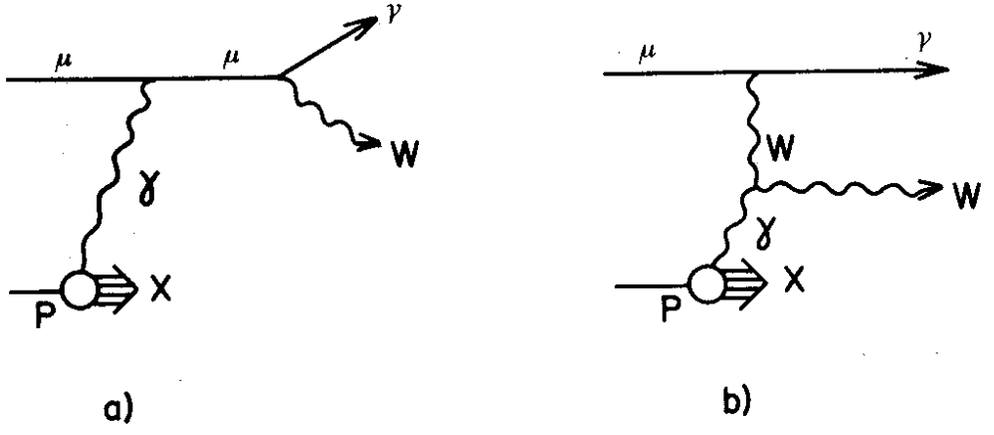

Fig. 35 B

introduce a factor of order $1/M_W^2$, which accounts for the large value of ξ. (There is an instructive discussion of this effect in a simplified model in Ref. 27).

2) In the diagrams in Fig. 35B it is quite safe to set $m_\mu = 0$. In the case of deep inelastic production of a final state X, the cross section can then only depend on M_W and s for $M_W >> M_p$ if we assume scaling. Hence

$$\sigma(\mu+p \to \nu+W+X)_{\text{inelastic}} \sim \frac{\alpha^2 g_W^2}{M_W^2} f(s/M_W^2) \sim \alpha^2 G_F f(s/M_W^2)$$

since $g_W^2 \sim M_W^2 G_F$. This cross section has been calculated for M_W = 5, 10, 15 GeV [26]. It is plotted against s/M_W^2 in Fig. 36. Presumably the values for M_W = 5 GeV do not lie on the same curve as the M_W = 10 and 15 GeV results, because M_p is not negligible in this case. It should be safe to use the curve through the M_W = 10 GeV and 15 GeV points at higher energies+). In the case $\mu+p \to \nu+W+p$ the nucleon form factors provide another parameter with dimensions of a mass, so scaling is not necessarily expected. In fact, however, the calculated values [26], which are available for M_W = 25, 50, 75 and 100 GeV also in this case, seem to exhibit almost exact scaling as can be seen from Fig. 37. These curves can therefore be used for any value of M_W.

3) In $\nu+p \to \mu+W+X$ the muon mass cannot be neglected and this introduces a dependence on $\ln(s/M_\mu^2)$ and $\ln(M_W^2/M_\mu^2)$ as well as on s/M_W^2. Using the analytic results obtained with the simplified model of Ref. 27 we guess a dependence

$$\sigma(\nu+p \to \mu+W+X) \sim \ln\left(\frac{M_W}{a\, m_\mu}\left[\frac{s}{M_W^2} - 1\right]\right) f(s/M_W^2)$$

We find in fact that with a = 35 this formula gives an excellent description of the results of numerical calculations [26] of $\sigma(\nu+p \to \mu+W+p)$ (which are available for a large range of M_W), as can be seen from Fig. 38. The value a = 35 corresponds to

+) Scaling violations will not change this result much since the cross section involves relatively modest values of Q^2. (They might give a small increase as low x presumably dominates).

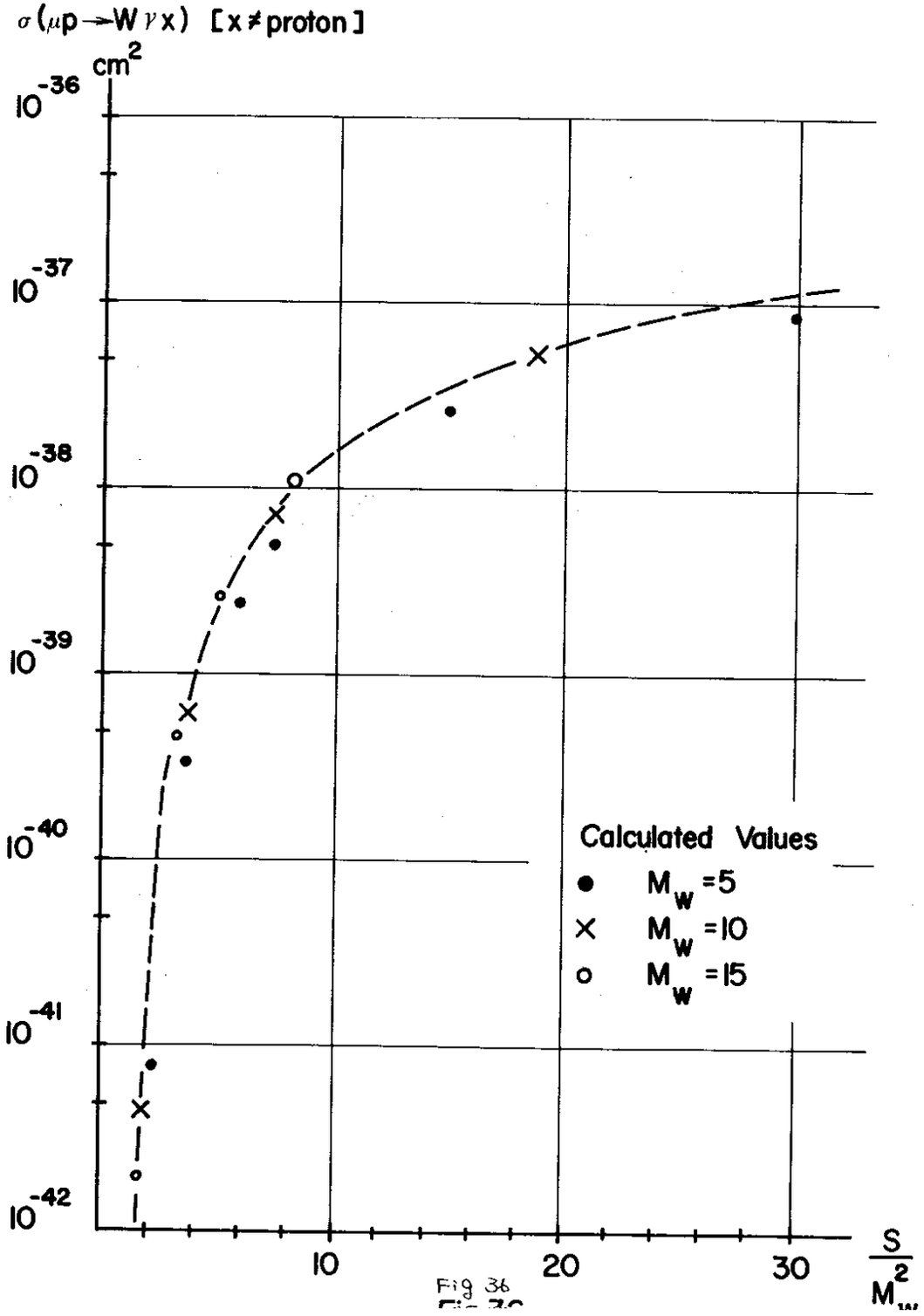
σ(μp→Wνx) [x≠proton]
cm²
10⁻³⁶
10⁻³⁷
10⁻³⁸
10⁻³⁹
10⁻⁴⁰
10⁻⁴¹
10⁻⁴²
Calculated Values
M_W = 5
M_W = 10
M_W = 15
10
20
30
S/M²_W

Fig 36

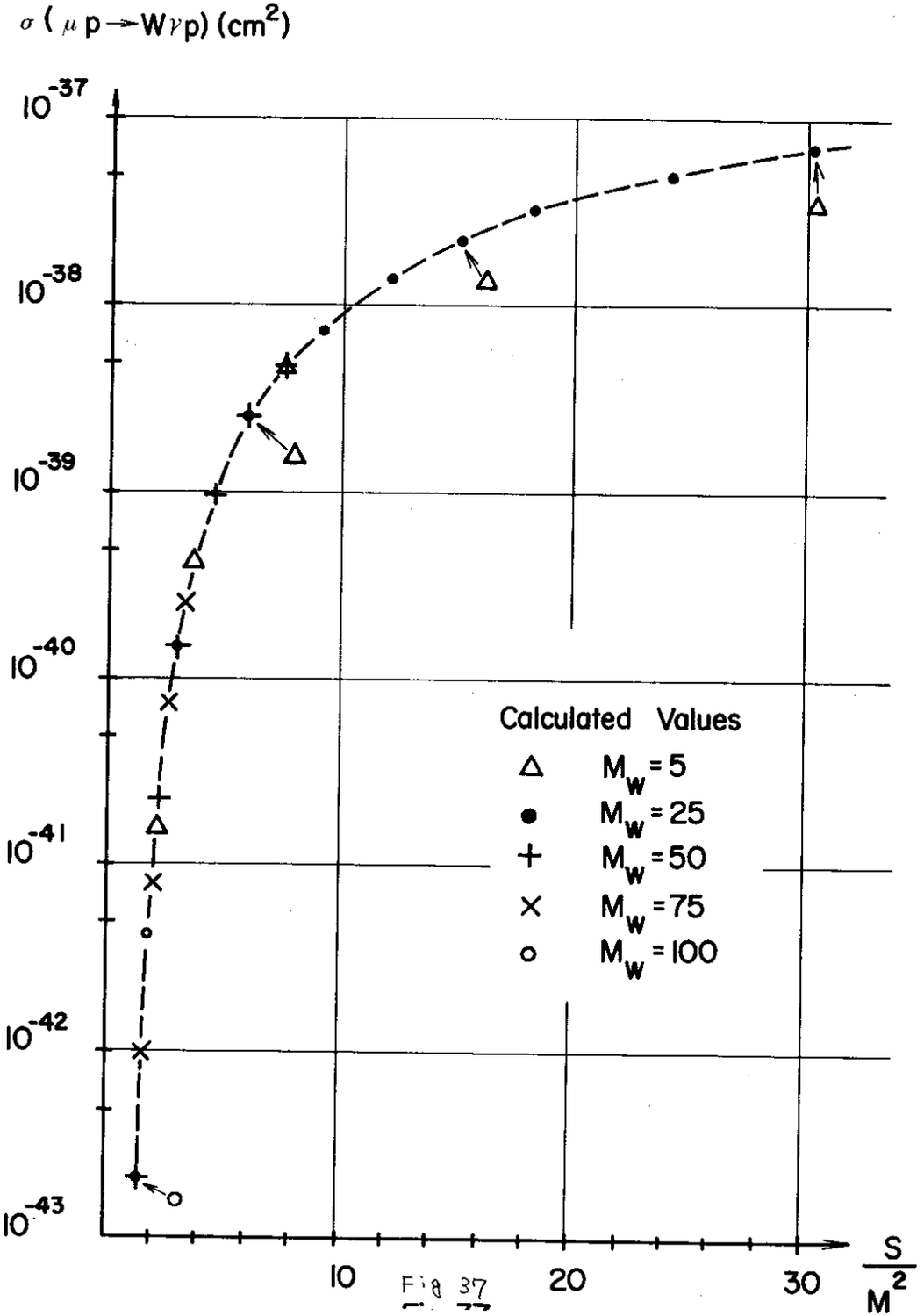
σ(μp→Wνp) (cm²)
10⁻³⁷
10⁻³⁸
10⁻³⁹
10⁻⁴⁰
10⁻⁴¹
10⁻⁴²
10⁻⁴³
Calculated Values
M_W = 5
M_W = 25
M_W = 50
M_W = 75
M_W = 100
10
20
30
S/M²

Fig 37

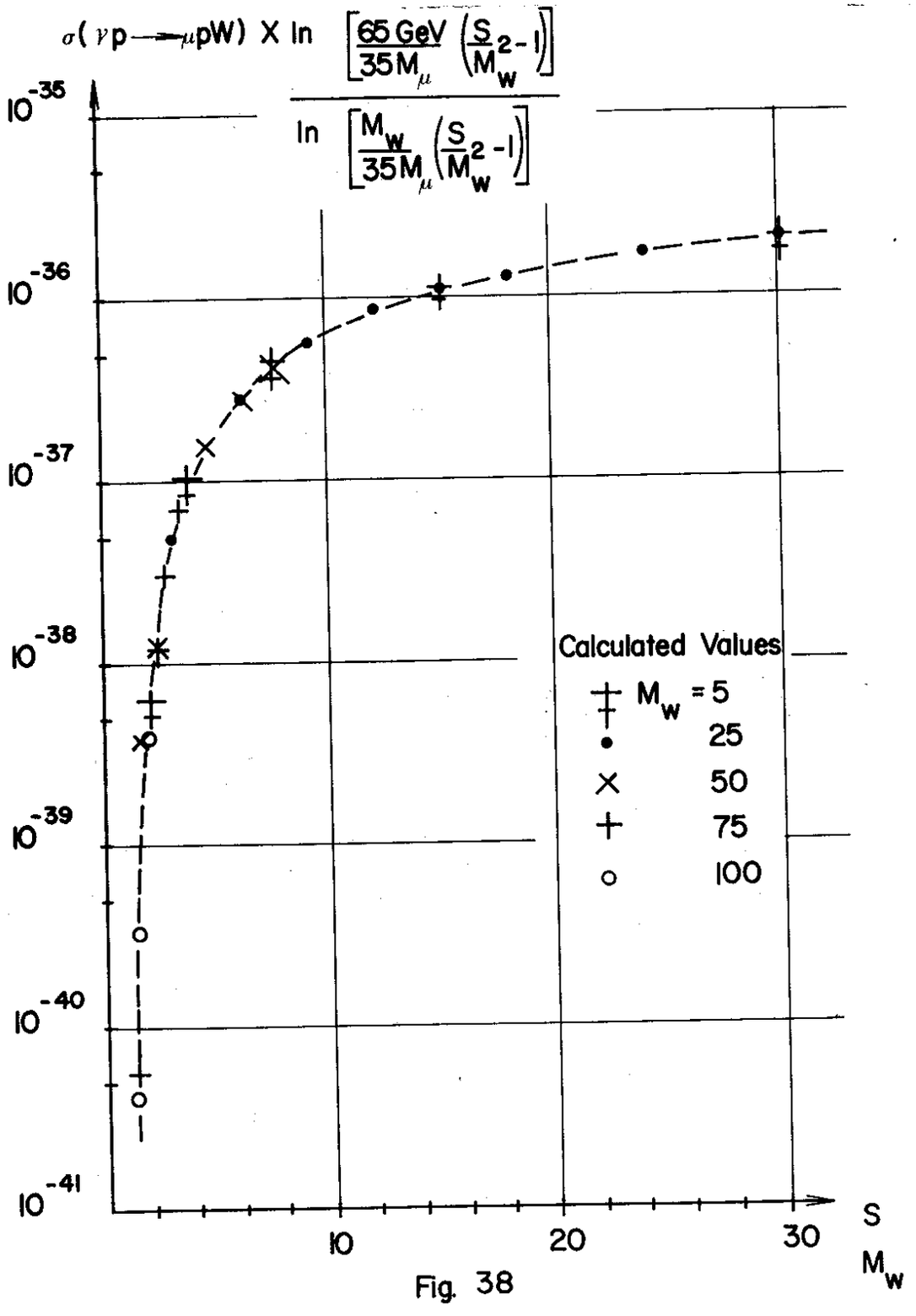

Fig. 38

$$\sqrt{\frac{s_{\gamma^*\nu}}{M_W^2} - 1} = \sqrt{\frac{e}{a}\left(\frac{s}{M_W^2} - 1\right)} = 0{,}3\sqrt{\frac{s}{M_W^2} - 1}\,.$$

in terms of the model of Ref. 27, which does not seem unreasonable. The same scaling law is tried for the case X ≠ proton in Fig. 39; it seems to work as well as the scaling law for μ+p → μ+W+X (Fig. 36) (which was supposed to be exact for $M_W \gg M_p$) and presumably it can be used for higher M_W with reasonable confidence.

After these preliminaries, we turn to the various mechanisms for $W^{\pm}$ and Z^0 production in e-p collisions. The relevant diagrams and the cross sections for the various mechanisms have been collected in Table VI.

5. 2 Production at the Leptonic Vertex

We expect that σ(e+p → W+ν+X) = σ(μ+p → W+ν+X). These cross sections have already been plotted in Figs. 36 and 37 (which are for unpolarized incident leptons; for μ_L^+ and μ_R^- they are zero). Turning to e+p → Z^0+e+X we see that the second diagram, which dominates because the exchanged electron can get near its mass-shell, is kinematically identical to the dominant diagram (Fig. 35Aa) in ν+p → μ+X+X. In fact, defining couplings by

$$Z^{\lambda}\bar{e}\,\gamma_\lambda(g_V + \gamma_5\, g_A)\, e$$

it is found [28] that for an unpolarized beam +)

$$\sigma(\mu+p \to \mu+Z+X)^e = \varepsilon\,\sigma(\nu+p \to \mu+W+X)$$

$$\sigma(e+p \to e+Z+X)^e = \varepsilon\,\sigma(\nu+p \to e+W+X)$$

to within ten percent, where

$$\varepsilon = \frac{g_V^2 + g_A^2}{2\sqrt{2}\,G\,M_Z^2}$$

+) We use the superscripts e and h to indicate production at the hadronic and leptonic vertices respectively.

Table VI (Cross sections in cm^2 for M_W = 65 GeV, M_Z = 75 GeV and assumptions in text)

	Diagrams	Cross Section			Comments
Production at the Lepton Vertex	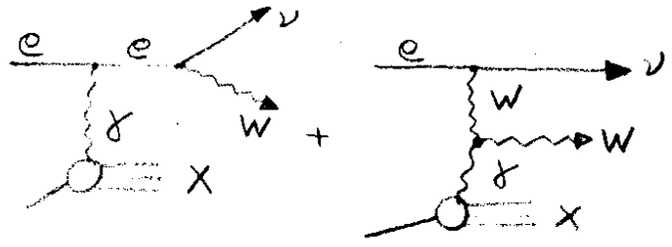	s = 6720	27000	40000	
		X = p 10^{-42}	3×10^{-39}	8×10^{-39}	Small Q^2 clean event
		X ≠ p 10^{-42}	5×10^{-39}	1×10^{-38}	
	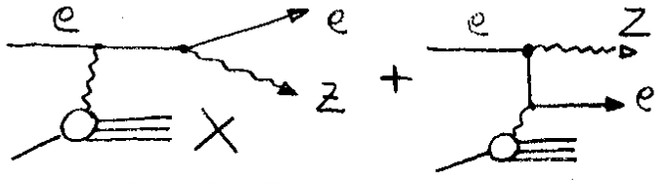	X = p 10^{-41}	8×10^{-38}	2×10^{-37}	Small Q^2 clean event
		X ≠ p < 10^{-41}	6×10^{-38}	1.3×10^{-37}	
Production at the Hadronic Vertex	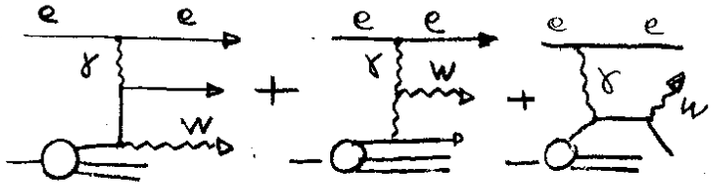	→ W^- ∿ 10^{-41}	5×10^{-38}	1×10^{-37}	Small t in virtual quark line in first (dominant) diagram → "quiet" events
		→ W^+ 10^{-41}	2×10^{-38}	6×10^{-38}	
	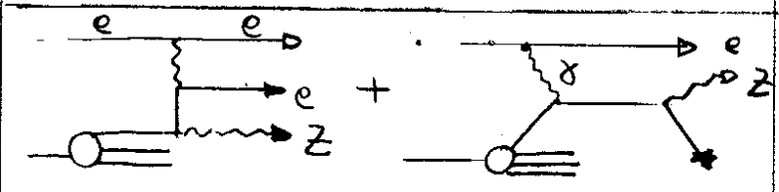	< 10^{-41}	2×10^{-38}	5×10^{-38}	Small t in virtual quark line in first (dominant) diagram → "quiet" events
Photo-Production	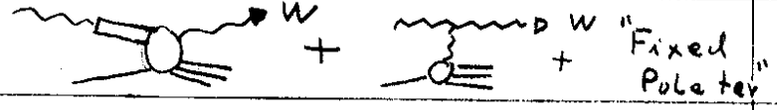	1×10^{-38} $\sigma \to W^+ + W^-$	1.6×10^{-36} $\sigma \to W^+ + W^-$	2.6×10^{-36} $\sigma \to W^+ + W^-$	Estimate uses Drell Yan = hadrons in jets along beams: clean events
	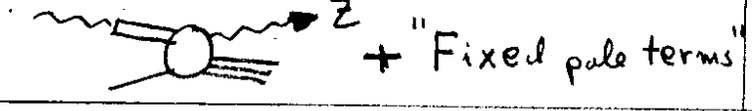	∿ 10^{-37}	5×10^{-37}	8×10^{-37}	Estimate uses Drell Yan = hadrons in jets along beams: clean events
Diffractive Production	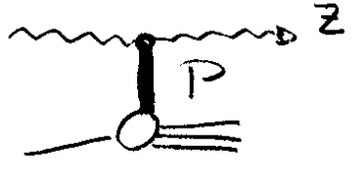		≲ 6×10^{-37}	≲ 6×10^{-37}	Small t → hadrons → clean event

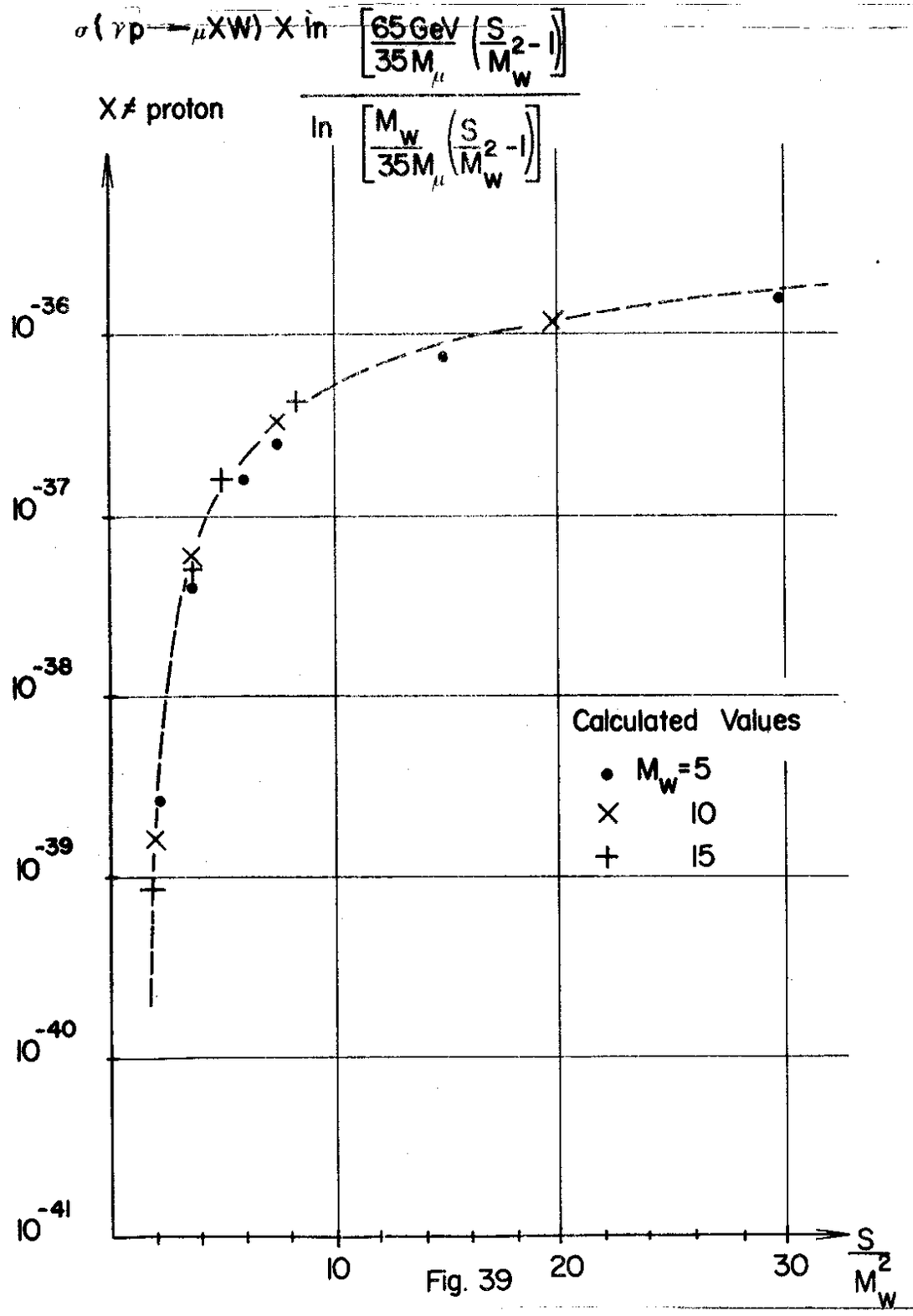

Fig. 39

(The relation would be exact if only the dominant diagram was taken into account). The factor ε represents the ratio of the squares of neutral and charged current couplings and is constrained by neutral current data. We take the Weinberg model value ε ≈ 0.2 (which is not necessarily correct). We assume that the m_μ scaling law above allows us to relate ν_μ and ν_e cross sections thus

$$\sigma(\nu_e+p \to e+W+X) = \frac{\ln\left[\frac{M_W}{35m_e}\left(s/M_W^2-1\right)\right]}{\ln\left[\frac{M_W}{35m_\mu}\left(s/M_W^2-1\right)\right]}\,\sigma(\nu_\mu+p \to \mu+W+X)$$

There is obviously some uncertainty in this estimate. Putting everything together, $\sigma(\mu+p \to \mu+Z^o+X)^e$ is expected to be ε r times the quantity plotted in Figs. 38 and 39, where r = 5.5, 2.3 and 2.2 for s = 6720, 27'000 and 40'000 GeV^2 respectively if M_Z = 75 GeV.

5. 3 Production at the Hadronic Vertex

We employ the parton model as shown in the diagrams in the table. For both $W^\pm$ and Z^o production there is one diagram which is kinematically enhanced (like Fig. 35Aa) because the virtual quark can get near its mass-shell. In fact, for scattering on a bare unpolarized quark, taking the quark mass equal to the mass of the muon and considering only the dominant diagram

$$\sigma(e+d \to e+W^-+u) = \frac{4}{9} \cdot 9 \cdot \frac{1}{2}\,\sigma(\nu_\mu+d \to \mu+W+d)$$

$$\sigma(e+u \to e+W^++d) = \frac{1}{9} \cdot \frac{9}{4} \cdot \frac{1}{2}\,\sigma(\nu_\mu+u \to \mu+W+u)$$

where the factors $\left(\frac{4}{9}\right)^{\pm 1}$ and $\left(\frac{1}{9}\right)^{\pm 1}$ are quark charges squared and the factor $\frac{1}{2}$ is a polarization averaging factor. Folding both sides with a quark distribution factor and assuming that the proton is made of just three valence quarks which are identically distributed we get

$$\sigma(e+p \to e+W^-+X)^h \approx \frac{2}{9}\,\sigma(\nu_\mu+p \to \mu+W+X)$$

$$\sigma(e+p \to e+W^++X)^h \approx \frac{1}{9}\,\sigma(\nu_\mu+p \to \mu+W+X)$$

A similar calculation for Z^o production, using the Weinberg model with $\sin^2\theta_w = 0.38$ gives

$$\frac{\sigma(e+p \to e+Z^o+X)^h}{\sigma(\nu_\mu+p \to \mu+W+X)} = 0.15$$

5. 4 Photoproduction

There are two contributions to photoproduction: a "hadronic" piece, which might be estimated using vector dominance, and a "fixed pole type" piece which may be said to represent pointlike interactions of the photon. (The necessity for such terms is particularly obvious in the case of $W^\pm$ production where they are needed to ensure the gauge invariance of the diagram in which the photon couples directly to the W). We ignore the fixed pole piece which is presumably included in the $Q^2 \to 0$ limit of our parton calculation of electroproduction. Leaving the diffractive contribution to Z^o production for the moment, we set

$$\sigma(\gamma+p \to \begin{Bmatrix} W^\pm \\ Z^o \end{Bmatrix} + X \simeq \frac{1}{250}\,\sigma\left(\rho^o+p \to \begin{Bmatrix} W^\pm \\ Z^o \end{Bmatrix} + X\right)$$

$$\simeq \frac{1}{250}\,\sigma\left(\pi^o+p \to \begin{Bmatrix} W^\pm \\ Z^o \end{Bmatrix} + X\right)$$

and use the Drell-Yan model with the pion and proton structure functions of Altarelli et al. [29] to calculate the latter quantity with the results shown in the table +). (For Z^o production the Weinberg model was used with $\sin^2\theta_w = 0.38$).

The diffractive production of Z^o's is hard to estimate reliably. However, there is a plausible bound obtained by setting $\sigma(\gamma+p \to Z^o+\gamma) \lesssim \sqrt{\sigma(\gamma+p \to \gamma+p)_{forward}\ \sigma(Z^o+p \to Z^o+p)_{forward}}$ where the latter quantity may be estimated if we assume Bjorken scaling for time-like as for space-like neutral current (Z^o) scattering. This gives $\sigma(\gamma+p \to Z^o+p) \lesssim 6 \times 10^{-37}$ cm^2. This might be a gross over-estimate (vector dominance and estimates based on other calculations [30] give much smaller results; this will be discussed further in Ref. 8).

+) Scaling violations [12] may reduce the results substantially at $s = 6720$ GeV^2, slightly at $s = 27'000$ GeV^2 but not at all at $s = 40'000$ GeV^2.

5. 5 Detection of $W^\pm$ and Z^o

The estimated rate for $W^\pm$ and Z^o production is totally negligible with option I and still only marginal with option II where we would expect to produce 4 $W^\pm$ and 4 Z^o's a day. This low rate is somewhat compensated for by the fact that the production process in general is rather clean +) yielding few additional particles which tend to travel along the proton direction and are well separated from the decay products of the $W^\pm$ and Z^o. These will in general emerge at large angles with respect to the proton beam.

The W has the following decay modes: $W \to e+\nu$, $\mu+\nu$ and $W \to$ hadrons. In particular the leptonic decay modes lead to a striking and unique signature; a single lepton at large angles with a well defined hadron jet (or a single proton) travelling along the proton direction resulting in a final state with a large momentum imbalance. The hadronic decay modes will yield two jets of hadrons at large angles well separated in space in addition to the proton fragmentation jet. Measuring the angle and the energy of the two jets will enable us to reconstruct the mass of the W to an accuracy of about 10%.

The relative ratio between these decay modes depends on what new leptons and flavours exist since they provide new decay channels. With N_q weak doublets of quarks and N_e doublets of leptons we expect

$$\frac{\Gamma(W \to \mu+\nu)}{\Gamma_w} = \frac{\Gamma(W \to e+\nu)}{\Gamma_w} = \frac{1}{3N_q + N_e}$$

i.e. a total lepton branching ratio on the order of 20% or less.

The Z^o events are also likely to provide a very clean signature. The following decay modes are expected:

$$Z_o \to e^+e^-,\ \mu^+\mu^-$$

$$Z_o \to \nu+\bar{\nu}$$

$$Z_o \to \text{hadrons}$$

+) In particular Z^o production will yield very clean events. The production of $W^\pm$ needs further study.

The branching ratio for these various channels is rather model dependent. In the Weinberg model with $\sin^2\theta_w = 3/8$ one expects a branching ratio to $e^+ + e^-$ and $\mu^+ + \mu^-$ on the order of a few per cent [31] with the bulk of the events leading to two jets of hadrons. The signature of these events would therefore be either two leptons or two hadron jets at large angle with either only a proton or a jet of hadrons along the incident proton direction.

It therefore seems that these events will be rather clean with the background resulting from diffractive production of vector mesons. The production of vector mesons with hidden new flavours is expected to decrease with mass as $1/M_V^6$ leading to a small rate at large masses. Vector mesons made of "old quarks" might decrease as $1/M_V^2$ leading to a larger background at masses around 60 - 100 GeV. However, these states should be very wide resulting in a continuum and not give a peak in the invariant mass spectrum.

5. 6 Heavy Lepton Production

Suppose there exist heavy neutral and charged leptons coupled to electrons by the known weak current. Then for $s \gg M_L^2$

$$\frac{\sigma(e_L^- + p \to E^o + X)}{\sigma(e_L^- + p \to \nu + X)} = \left(\frac{g_{e_L E^o}}{g_{e_L \nu}}\right)^2 = \frac{\sigma(e_R^+ + p \to \bar{E}^o + X)}{\sigma(e_R^+ + p \to \bar{\nu} + X)}$$

$$\frac{\sigma(e_R^- + p \to E^o + X)}{\sigma(e_L^- + p \to \nu + X)} \approx \frac{1}{3}\left(\frac{g_{e_R E^o}}{g_{e_L \nu}}\right)^2$$

$$\frac{\sigma(e_L^+ + p \to \bar{E}^o + X)}{\sigma(e_R^+ + p \to \bar{E}^o + X)} \approx 3\left(\frac{g_{e_R E^o}}{g_{e_L \nu}}\right)^2$$

$$\frac{\sigma(e_L^- + p \to E^- + X)}{\sigma(\nu + p \to \nu + X)} = \frac{\sigma(e_R^+ + p \to E^+ + X)}{\sigma(\bar{\nu} + p \to \bar{\nu} + X)} = \left(\frac{g_{e_L E^-}}{g_{\nu\nu}}\right)^2$$

$$\frac{\sigma(e_R^- + p \to E^- + X)}{\sigma(\bar{\nu} + p \to \bar{\nu} + X)} = \frac{\sigma(e_L^+ + p \to E^+ + X)}{\sigma(\nu + p \to \nu + X)} = 1\left(\frac{g_{e_R E^-}}{g_{\nu\nu}}\right)^2$$

where the approximate equalities hold in a valence parton model. These asymptotic ratios are approached fairly rapidly, e.g. according to the model of Ref. 32 the ratios have risen to half their final value for $\sqrt{s} > 4\ M_L$. Hence with $g_{e_L E^o} = g_{e_L \nu}$ and the most pessimistic neutrino rates in Figs. 28 and 29 (obtained with $M_W = 62$ and scaling violations), we get > 70 events per day for $M_L \lesssim 20$ GeV at $s = 6720\ \text{GeV}^2$ and > 190 events per day for $M_L \lesssim 50$ GeV at $s = 40'000\ \text{GeV}^2$. Even for a very heavy lepton with a mass around 100 GeV several events a day are expected with option II. Therefore we can expect substantial rates for the production of neutral and charged heavy leptons if they exist and couple to e^-. Theoretically, coupling to the known (neutral) current is perhaps not so likely for charged leptons but of course there may be an $e^- \to E^-$ coupling to new currents, which might perhaps be associated with the production of new flavours, which would give rise to very interesting events; we can even speculate on the possible existence of doubly charged currents coupling e^- to E^+ and to exotically charged quarks.

Heavy leptons may have such decays as:

$$\begin{aligned}
E^o &\to e^- + \text{hadrons} \\
&\to e^- + \mu^+ + \nu_\mu \\
&\to e^- + e^+ + \nu_e \\
&\to \nu_e + \text{hadrons} \\
&\to \nu_e + e^+ + e^- \\
&\to \nu_e + \mu^+ + \mu^- \\
&\to \nu_e + \nu + \bar{\nu} \\
&\to E^- + \text{hadrons} \\
&\to E^- + \mu^+ + \mu_\nu \\
&\to E^- + e^+ + \nu_e \\
E^- &\to e^- + \text{hadrons} \\
&\to e^- + e^+ + e^- \\
&\to e^- + \mu^+ + \mu^- \\
&\to e^- + \nu + \bar{\nu}
\end{aligned}$$

$$E^- \rightarrow \nu_e + \text{hadrons}$$
$$\rightarrow \nu_e + e^- + \bar{\nu}_e$$
$$\rightarrow \nu_e + \mu^- + \bar{\nu}_\mu$$
$$\rightarrow E^0 + \text{hadrons}$$
$$\rightarrow E^0 + e^- + \bar{\nu}_e$$
$$\rightarrow E^0 + \mu^- + \bar{\nu}_\mu$$

These decays give rise to such spectacular signatures as multilepton events and apparent lepton non-conservation (if E^0 and $E^\pm$ exist with well separated masses so that one decays frequently into the other, such striking events as $e^- + p \rightarrow \mu^+ + e^- + \mu\ \mu^{+\ -} + \ldots$ are possible).

The kinematics for heavy lepton production is very similar to the kinematics encountered in deep inelastic electron scattering and will lead to events with a three-jet structure [+)] with the jet from the decay of the heavy lepton well separated from the current jet and the proton fragmentation jet. The existence of a neutral lepton can be inferred from the occurence of events of this type with one jet consisting of two charged leptons only - i.e. $e^- + \mu^+$, $e^- + e^+$ or $\mu^+ + \mu^-$. The mass of the neutral lepton can be determined from the decay to e^- + hadrons [++)]. The existence of a new charged lepton can be inferred and its mass determined by observing jets consisting of three charged leptons ($e^- + e^+ + e^-$ or $e^- + \mu^+ + \mu^-$).

The signatures for both neutral and charged leptons are both spectacular and unique. It therefore seems entirely feasible to identify leptons with production rates of one or more a day, corresponding to $m_L \leq 100$ GeV with option II.

Clearly, the case with which heavy leptons may be found provides a major attraction of large electron-proton colliding rings.

+) This is true for "light" new leptons. The decay products from a heavy new lepton will be more isotropically[8)] distributed.

++) New lepton production can easily be separated from the electroproduction of new flavours - since in the former case the transverse momentum of the current jet is balanced not by the scattered electron but by a jet of particles from the decay of the heavy lepton.

Acknowledgements

We are very grateful to K.H.Mess who collaborated in much of the computation of the results reported here and to I.Hincliffe who collaborated with one of us in the calculations based on asymptotic freedom. One of us acknowledges the hospitality of DESY in January 1975. We are very grateful to CERN for the extended hospitality during the period January to April 1977 when this paper was completed.

References

1) The Physics Interest of a 10 TeV Proton Synchrotron, 400 x 400 GeV^2 Proton Storage Rings and Electron-Proton Storage Rings, CERN Yellow Report 76-12

2) Physics with Very High Energy e^+e^- Colliding Beams, CERN Yellow Report 76-18

3) Proposal for Construction of a Proton-Proton Storage Ring - Isabelle, Brookhaven Report BNL 20161, 1975

4) Anti-Protons in the SPS, CERN/DG-2, 1977

5) Particle Physics with Positron-Electron-Proton Colliding Beams, SLAC-146/LBL-750, 1972
PEP Proposal, LBL-2688/SLAC-171, 1974

6) A Feasibility Report for Colliding Beam Facility - EPIC, Rutherford Laboratory Report RL-74-124, 1976

7) An e-p Facility in the SPS, CERN ISR-ES-GE-GS/76-50

8) Report of ECFA Working Parties on e-p Physics (in preparation).

9) V.G.Gorslikov et al., Sov. J.Nucl.Phys. 6, 361, 1967.
J.Bartels, Nucl.Phys. B82, 172, 1974, and private communication.

10) V.Barger and R.J.N.Phillips, Nucl.Phys. B73, 269, 1974

11) The theoretical literature may be traced from:
V.Zakharov, Proc. 1976 Tblisi Conference.
C.H.Llewellyn Smith, Proc. 1975 Stanford Conference.

12) Detailed Treatment of Scaling Violations in Aymptotically Free Gauge Theories, I.Hincliffe and C.H.Llewellyn Smith, Oxford Preprint 1977

13) H.L.Anderson et al., Phys.Rev.Lett. 37, 4, 1976
C.Cheng et al., Phys.Rev.Lett. 35, 961, 1975
V.K.Bharadwaj, Oxford D.Phil.Thesis (1976)
T.W.Quirk, private communication

14) E.M.Riordan et al., SLAC-PUB 1634 (1975)
R.E.Taylor in Proc. 1975 Stanford Conference

15) C.Zettler, private communication

16) L.W.Mo, K.W.Hanson, R.F. Mozley, G.Wolf in Proc. 1975 Stanford Conference, and references therein

17) J.D.Bjorken, Phys.Rev. D7, 282, 1973

18) E.G.Floratos, CERN TH-2661, 1976

19) The calculations were done by I.Hincliffe and C.H.Llewellyn Smith using the methods described in ref.12).

20) C.H.Llewellyn Smith and D.V.Nanopoulos, Nucl. Phys. B78, 205, 1974 (E: B83, 544, 1974). References to earlier work on parity violation in ep→ex may be found in this paper

21) This is a slight extension of the results in ref.19).

22) **Invited papers on photoproduction in:**
1971 International Symposium on
Electron and Photon Interactions at High Energies, Cornell University, Ithaca, New York, August 23-27, 1971,
Sixth International Symposium on Electron and Photon Interactions at High Energies, Bonn University, FRG, August 27-31, 1973
1975 International Symposium on Lepton and Photon Interactions at High Energies
Stanford University, U.S., August 21-27, 1975

23) S.J.Brodsky, F.E.Close and J.F.Gunion,
Phys.Rev. D6, 2487, 1972

24) J.D.Bjorken and E.A.Paschos, Phys.Rev. 185, 1975, 1969
S.J.Brodsky, R.L.Jaffe and J.F.Gunion, Phys.Rev.D6, 2487, 1972

25) H.Primakoff, Phys.Rev. 81, 899 (1951)

26) R.W.Brown and J.Smith, Phys.Rev. D3, 207, 1971
J.Smith, private communication

27) F.A.Berends and G.B.West, Phys.Rev. D3, 262, 1971

28) R.N.Brown, L.B.Gordon and K.O.Mikaelian, Phys.Rev.Lett. 33, 1119, 1972

29) G.Altarelli, N.Cabibbo, L.Maiani and R.Petronzio,
Nucl.Phys. B92, 413, 1975

30) R.F.Cahalan and K.O.Mikaelian, Phys.Rev. D10, 3769, 1974

31) J.R.Ellis and M.K.Gaillard, in ref.2),

32) J.D.Bjorken and C.H.Llewellyn Smith, Phys.Rev. D7, 887, 1973.